Ph.D. DISSERTATION

# Multi-Functional Optical Elements by Imprinting Technique for Mobile Display Applications

# 휴대형 디스플레이 응용을 위한 임프린팅 기술 기반의 다기능 광학 소자에 관한 연구

BY

LIM, YONG-WOON

FEBRUARY 2009

SCHOOL OF ELECTRICAL ENGINEERING AND
COMPUTER SCIENCE
COLLEGE OF ENGINEERING
SEOUL NATIONAL UNIVERSITY

# 휴대형 디스플레이 응용을 위한 임프린팅 기술 기반의 다기능 광학 소자에 관한 연구

Multi-Functional Optical Elements by Imprinting Technique for Mobile Display Applications

지 도 교 수 이 신 두

이 본문을 공학박사 학위논문으로 제출함

2008년 10월


서울대학교 대학원

전기 컴퓨터 공학부

임 용 운


임 용 운의 공학박사 학위논문을 인준함

2008년 12월

위 원 장 이 병 호 (인)

부 위원장 이 신 두 (인)

위 원 홍 용 택 (인)

위 원 최 종 선 (인)

위 원 김 재 훈 (인)

# Abstract

Organic and polymeric materials have attracted great interest for a long time since their excellent performances in the optical and electronic devices and fundamental success of molecular engineering in creating a new class of materials with appropriate physical and optical properties. Particularly, liquid crystals (LCs) and liquid crystalline polymers (LCPs) are very useful in several key areas of electronic and optical devices. Moreover, the multi-ordered LC systems have attracted great interest and have been widely studied because of the importance of the fundamental research and their potential for device applications to the optical systems including displays. Recently, organic functional materials, offering far greater fabrication flexibility and processing simplicity than current inorganic materials, have extensively studied for the use as electrically active layers having the properties of conductivity or light-emission. With increasing the demands of mobile devices in the digital multimedia broadcasting environments, all

organic displays where all the elements consisting of the display are made of the organic materials have attracted much attention since several advantages such as low-power consumption and simple fabrication processes. In addition, optical elements, such as optical retardation plates, color filters, polarization converters, and interference filters, based on LCPs are one of the classes that have been widely used for the advancement of LC displays (LCDs) that provide improved optical performances such as high light efficiency, wider viewing angle properties, and complicated optical functions. In such cases, it is not only necessary to produce the LCP into an optically anisotropic film structure being divided into multi-domains. Thus, the employment of these structures as alignment layers is in need of ordering and patterning for organic materials.

For fabricating anisotropic structures with multi-optic axes in order to align and pattern the optical film with multi-domain, a rubbed surface or photo-treated surfaces have been used previously. However, the rubbing process inevitably involves the mechanical damage and dust particles on the alignment surface and the multi-ordered pattern size is limited to a few hundred micrometers on the double rubbing process. Photoalignment is an alternative process to rubbing. Although the photoalignment process could be patterned with micro-size domains, the process suffers from the weak

anchorage on the surface of the photo-treated surface. Moreover, in above mentioned processes, supplemental alignment layer onto the optical films is needed to order LC molecules for LC based optical elements and/or LCDs.

In this thesis, we have investigated the mechanism of imprinting technique and proposed to fabricate functional optical elements and/or non-display and/or display applications having the functional optical elements. In addition, nano- or microstructures on the surface of functional optical elements induce self-aligning capability of introduced LC molecules. Also, the novel optical element concepts of the in-cell dye-polarizer using an imprinting technique and display applications with the novel optical elements for high device performances are proposed and demonstrated.

In theoretical aspect, the controlling of liquid crystalline order has been investigated focused on the induced imprinted system. The subjects of research are divided into two categories. One is the concept of the imprinting technique and the other is optical characteristics of the imprinted LCP structures such as birefringence, physical properties, surface anchoring energy and anisotropic wettability. Furthermore, well-defined nano-structures were fabricated by a nano-imprinting lithography with fluorine-based self-assembled monolayer. Novel imprinting technique provides a functional optical elements such as a patterned retarder (A-plate) and a C-plate, which

can be used electrically tunable retarder and wide-viewing angle enhancement film inside devices (in-cell). Also, thin film polarizers such as dye-doped polarizer can be fabricated by using an above mentioned imprinting technique. Next, as the in-cell functional optical elements with imprinted surface structures, three types of display application such as the transflective LCDs are described.

First, we demonstrate a novel design of a transflective LC cell using an inverse twisted nematic (ITN) mode and embedded optical layers in a single gap configuration. To overcome several disadvantages in the twisted nematic (TN) and electrically controlled birefringence modes, the ITN mode based on a homeotropic to twisted planar transition is proposed for our transflective LC cell. The embedded films in the LC cell were aligned and patterned by an imprinting technique using silane treated polymer mold. The imprinted optical films (IOFs) can be used function as an in-cell patterned retarder or a viewing angle enhancement film. In addition, the geometrically generated microstructures of the surface of IOFs have a self-aligning capability of LCs due to Berreman effect and thus, the inverse nematic LC layer undergoes a vertical to 90°-TN state in the transmissive (T) part and a vertical to 45°-TN state in the reflective (R) part during operation. Moreover, it achieves compensation of optical path difference (OPD) between

both parts and possesses higher transmission, wider viewing, and achromatic characteristics. This device is expected to have high transmittance and high reflectance simultaneously. Moreover, an imprinting technique, using a photopolymerizable LCP material, is a a simple and versatile technique for fabricating micro-patterned optical films with multi-array.

Second, we proposed a single cell gap transflective LCD using multi-TN based LC cell and embedded patterned dye-polarizer which functions as a polarization direction dependent polarizer to avoid the need of any patterned retarder. For fabricating multi-TN LC mode, the LC cell is composed of both a patterned dye-polarization film and an imprinted quarter wavepalte (QWP) with unique alignment direction inside glass substrates. In addition, the geometrically generated microstructures of the surface of two in-cell functional films have a self-aligning capability of LCs due to Berreman effect. This device is expected to have high transmittance and high reflectance simultaneously. Moreover, an imprinting technique, using a photopolymerizable LCP material without and with dichroic dye, is a simple and versatile technique for fabricating micro-patterned optical films with multi-array and unique alignment direction.

Third, we demonstrate a new design of a single LC mode transflective LCD having a wire grid polarizer (WGP) and an inner patterned retarder in

a single gap configuration. The WGP is served as a polarizer in the T-part and a reflector in the R-part. This device is expected to have high transmittance and high reflectance simultaneously. Moreover, the patterned retarder has two domains, i.e., an anisotropic part and an isotropic part, that are placed in the T and the R parts, respectively. The patterned retarder based on LCP material can be fabricated on the inner side of lower glass substrate. Due to different liquid crystalline phases of the patterned LCP layer between the two parts, two induced optical properties of the LCP layer in the T-part and the R-part were different in dielectric constant, respectively. As well be discussed later, the appearance of the different dielectric constants is essential to significantly reduce the electro-optic disparity between the T and the R parts.

In conclusion, throughout this thesis, patterning and aligning the organic functional materials by imprinting technique with self-aligning capability of imprinted surface structures for injected LC molecules has been extensively explored from the viewpoints of scientific researches and device applications. Basically, almost optical and electronic elements and/or applications can be practically realized in the functional organic passive and active systems produced and may be a foundation for the future scientific researches and novel applications.

Keywords: imprinting technique, liquid crystal alignment, liquid crystalline polymer alignment, functional optical elements, transflective liquid crystal device.

Student number: 2002-23542

# Contents

# List of Figures

# List of Tables

# Chapter 1

# Introduction

Liquid crystals (LCs) have found wide commercial application over the last three decades in electro-optical (EO) flat panel display (FPD) devices for consumer audiovisual and office equipment, such as watches, clocks, stereos, calculators, portable telephones, personal organizers, notebooks, and laptop computers. There are many other applications for LC displays (LCDs), such as information displays in technical instruments and in vehicle clocks, speedometers, navigation, and positional aids. They are also used in low-volume, niche products, such as spatial light modulators and generally as very fast light shutter. More importantly, they have come to dominate the displays market in portable instruments due to their slim shape, low weight, low-voltage operation, and low power consumption. LCDs are now

starting to win market shares from cathode ray tubes (CRTs) in the computer monitor market. The market share of LCDs in the total market for displays is expected to significantly increase over the next decade. There are a number of existing competing FPD technologies, such as plasma displays (PDs), vacuum fluorescence displays (VFDs), inorganic light-emitting diodes (OLEDs), light-emitting polymers (LEPs), and field emission displays (FEDs). The first production lines for LEP technology were recently commissioned. However, the value of LCDs is still expected to exceed that of the CRT tube in the near future. Manufacturing facilities for FPDs are very capital intensive. For example, a plant for twisted nematic LCDs with active matrix addressing can cost upward of $1 billion. As consequence of the capital already invested in LCD plants, it will take many years for competing technologies to gain a significant market share in the displays market in general. In particular, LCDs can be expected to maintain a dominant position in portable applications.

The successful development of LCD technology was dependent on parallel developments and progress in an unusual combination of scientific disciplines such as synthetic organic chemistry, physics, electronics, and device engineering. These include improvements in batteries, polarizers, electrodes, complementary metal-oxide semiconductor (CMOS) drivers, spac-

ers, alignment layers, and nematic liquid crystals (NLCs). These developments were made in response to a clear market requirement for a low-voltage, low-power-consuming FPD screen for portable, battery-operated instruments to display graphic and digital information of ever increasing volume, speed, and complexity. In this chapter, we attempt to illustrate this development using the three most important types of LCDs currently in large-scale manufacture. We also describe ferroelectric LCDs, which have the potential to become a major commercial product, to illustrate the problems to be overcome before an LCD tchnology can be successfully established in the displays market. All of these technologies can be incorporated in gels and polymer-dispersed LCDs. Therefore, they will not be dealt with here in any detail, because the general principles of operation are essentially the same.

In this thesis, organic device configurations with multi-ordered interfaces produced by the imprinted optical films and/or alignment layer are studied in the viewpoints of the scientific researches and device applications. By using imprinting technique, the surface-induced ordering effects of the organic materials on the device performances and self-aligning capability of injected LC molecules are numerically and analytically investigated. Also, the novel optical component concepts of the patterned retarder or patterned

polarizer on the inside of the cell and novel LC devices embedded these optical components are proposed and demonstrated. First, in this chapter, the importance of the necessary of an imprinted optical film and/or alignment layer, which produce the imprinting technique, is briefly introduced.

## 1.1 Liquid Crystalline Materials

The LCs are extremely important in several key areas of FPDs and fiber-optic communications since their large optical anisotropy are electrically and/or geometrically controlled in a simple fabrication process. The basis of the majority of specific LC EO effects, anisotropy of the electrical and optical properties of the LCs, is found in the reorientation of the LC director, described as the average axis of preferred orientation of the LC molecules, in the macroscopic volume of the material under the influence of an externally applied field [1].

LCs are novel mesophases whose mechanical and symmetrical properties are intermediate between features of a liquid and those of a crystal [2]. Molecules of a specific shape form liquid crystalline phases. The most typical are rod-like molecules or rod-like molecular aggregates, which have orientational order (like crystals), but lack positional order (like liquids) [1]. This

orientational order results in strong electrical and optical anisotropy. Depending on the degree of order of the medium, various intermediate phases (mesophases) may exist.

Typically, the LC phases are classified in to two types: lyotropic and thermotropic. Lyotropic LCs, where the control parameter for the mesophase is the concentration of the compounds, are of great interest in biological researches naturally appearing in living systems [3]. Thermotropic LCs, where the control parameter is the temperature, are widely studied in both scientific researches and the engineering applications such as information display and optical elements [4].

Thermotropic LCs with rod-like molecular shape are categorized into the nematic, the cholesteric, and the smectic phases as shown in Fig. 1.1. The NLCs are anisotropic liquids with a lowest degree of order having an only long-range orientational order with no positional one (Fig. 1.1(a)). The orientational order of the LCs produces large anisotropy of the optical and electrical properties. The cholesteric LCs are the NLCs with a helical structure on a macroscopic scale (Fig. 1.1(b)). In the smectic LCs, the molecules are parallel to each other, but their centers are stacked in parallel layers within which they have random positions, so that they have positional order in one direction (Fig. 1.1(c) and (d)). In the smectic A phase (Fig.

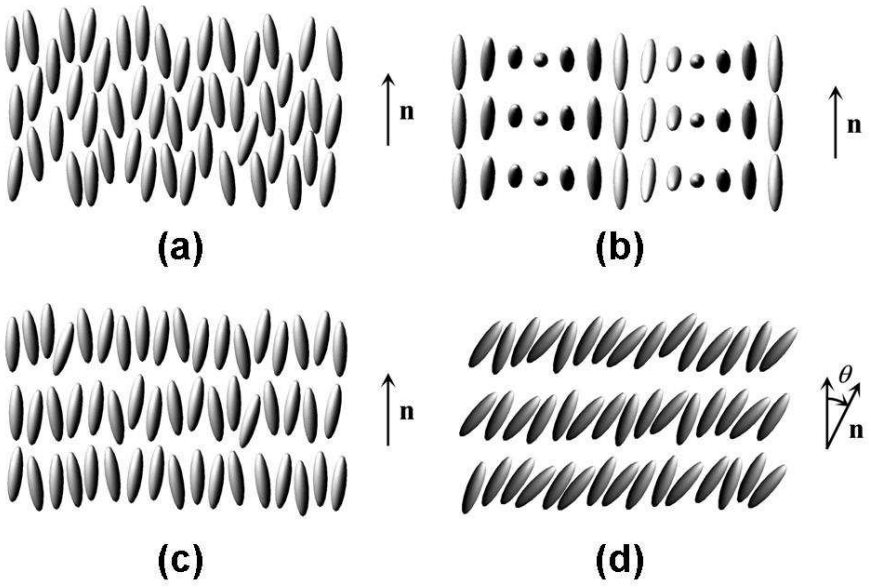


LC phases: (a) nematic, (b) cholesteric, (c) smectic A, and (d) smectic C phases. Here, **n** depicts the LC director which is the average axis of preferred orientation of the LC molecules.

1.1(c)), the LC director is parallel to the layer normal direction whereas in the smectic C phase, the LC director is tilted with respect to the smectic layer (Fig. 1.1(d)).

For examining the intrinsic properties of the LCs and adopting a variety of the practical applications, sandwich-type cells consisting of two treated substrates and the LCs between them are generally used. In those LC cells, the ideal conformation, in which the molecules are aligned along a common direction, will not be compatible with the constraints that are

imposed by the limiting surfaces of the device and by external fields acting on the molecules. Thus, there will be some degree of deformations in the alignment of LC molecules, resulting in the change of the electrical and the optical properties.

For LC devices including LCDs, particularly, the interaction of the LC molecules with a treated substrate predominantly governs their EO properties since a surface alignment layer strongly influences the collective reorientation of the LC molecules. For the fundamental researches as well as device applications, the surface anchoring energy is one of the important factors used to characterize the surface orientation of the LC molecules. Through the modification of the surface layer governing the LC molecular configuration, a variety of practical devices, such as the LCDs with improved viewing characteristics [5, 6], optical filters in fiber-optic communications [7, 8], diffractive devices used for optical information processing [9,10], and biosensors for recognition of biomolecular reaction [11, 12], are developed with the improved performances.

Liquid crystalline polymers (LCPs) are the polymers having liquid crystalline ordering. The structures, a main chain and a side chain, of LCPs are illustrated in Fig. 1.1. The LCPs [13–16] combine the self organization of the mesogenic gropus into the ordered structure of LC phases with some

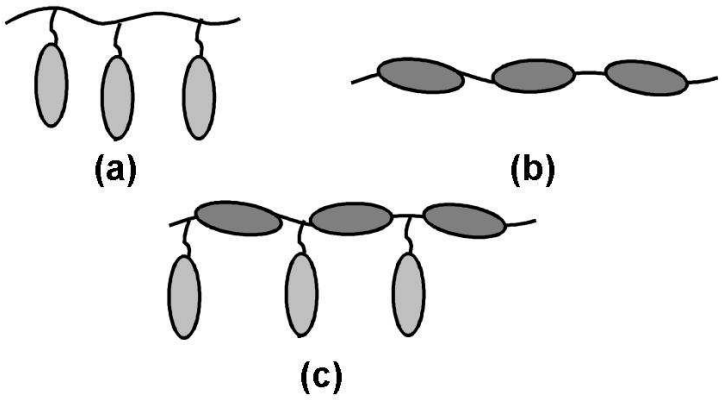


Figure 1.1: Different types of LCPs. The nematic phases formed by rigid and flexible linear chain polymers [15, 16].

typical polymer properties, such as the freezing of the disorder of the polymer chain at the glass transition temperature. Thus, in most cases, the LC phases also freeze glassy on cooling. In addition, an induced orientation can be frozen-in. LCPs can be prepared by incorporating the anisotropic mesogenic gropus into polymeric systems. Three different ways as shown in Fig. 1.1 to do this will be discussed, the first two of which are most commonly used. First, the mesogenic groups can be linked to the polymer chain as side groups, to produce LC side group polymers (Fig. 1.1.(a)). Second, they can be incorporated into the polymer chain, to obtain LC main chain polymers (Fig. 1.1.(b)) Third, both structural principles can be combined, to prepare combined main chain/side group polymers (combined LCPs) (Fig. 1.1.(c))

[15, 16].

### Mesogen

As shown in Fig. 1.2, mesogen is the fundamental unit of a liquid crystal that induces structural order in the crystals. Typically, a liquid-crystalline molecule consists of a rigid moiety and one or more flexible parts. The rigid part aligns molecules in one direction, whereas the flexible parts induce fluidity in the liquid crystal. This rigid part is referred to as mesogen, and it plays a crucial role in the molecule. The optimum balance of these two parts is essential to form liquid-crystalline materials. In a calamitic liquid crystal, the mesogen is a rod-like structure composed of two or more aromatic and aliphatic rings connected in one direction as shown in Fig. 1.2(a). In a discotic liquid crystal, the flat-shaped aromatic core that makes molecules

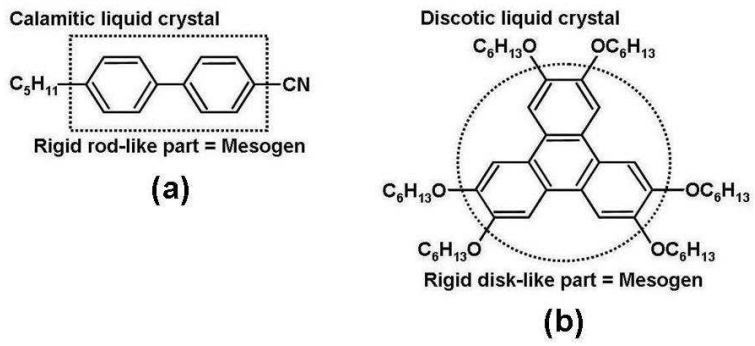


Figure 1.2: The example of Mesogenic Structures [17].

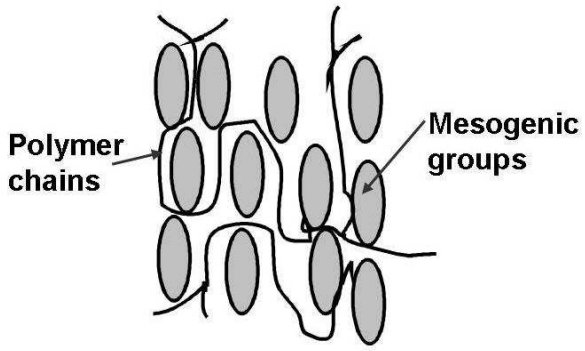


Figure 1.3: The schematic representation of a crosslinked LCP. The linkage between polymeric chains and mesogenic groups is not yet specified.

stack in one direction is defined as the mesogen as shown in Fig. 1.2(b).

These rod-like and disk-like structures are formed not only by covalent bonds, but also by non-covalent interactions, such as hydrogen bonds, ionic interactions, and metal coordination. In such cases, key structures which define the macromolecular shapes of the assembled molecules are called mesogens or mesogenic parts.

The structure of polymeric mesophase is largely influenced by a shape of the mesogenic groups, the rigidity of the main chain and the length of the flexible spacers separating mesogenic groups [18]. Polymer molecules shown in Fig. 1.3 form thermotropic and photopolymerizable LCPs. Among them, all the types of mesophases known for low-moleculear weight compounds are virtually revealed. Figure 1.3 combined the properties already discussed,

with rubber elasticity. In these systems a macroscopic deformation of the crosslinked sample leads to a corresponding equilibrium deformation of the polymer chains. Different degrees of orientation of the polymer chains can be achieved by stretching the macroscopic sample to different degrees. Afterwards an orientation of the mesogenic groups, which results due to interactions of polymer chains and mesogenic groups, can be determined under equilibrium conditions. However, in uncrosslinked LCPs, non equilibrium orientations resulting from flow above the glass transition temperature have to be frozen-in below $T_g$. Therefore the LCP seems to be ideal systems in which to investigate the interaction of the orientation of the polymer chains (induced by mechanical fields) and that of the mesogenic groups (induced by electric fields). As polymer networks, which are not liquid crystalline, cannot be swollen with mesogenic groups in the LC phase due to incompatibility, the mesogenic grups must be linked covalently to the polymer chains to prevent a demixing. The importance of LCP has been increased in connection with patterned retarder which will be discussed in the later part of thesis.

## 1.2 Importance of the Liquid Crystalline Ordering at Surface Structures

During the last decade, the technical progress in LCD industry have triggered a considerable scientific interest in the microscopic origin of surface alignment. The alignment of LC is closely connected with the contacting surface properties, and many researches have been reported on the boundary effects on the LC alignment [19–21]. In other words, to orient LC, a solid substrate is treated by applying some kind of actions. Figure 1.4 and table 1.1 show classification [22] and characteristics [23] of various LC

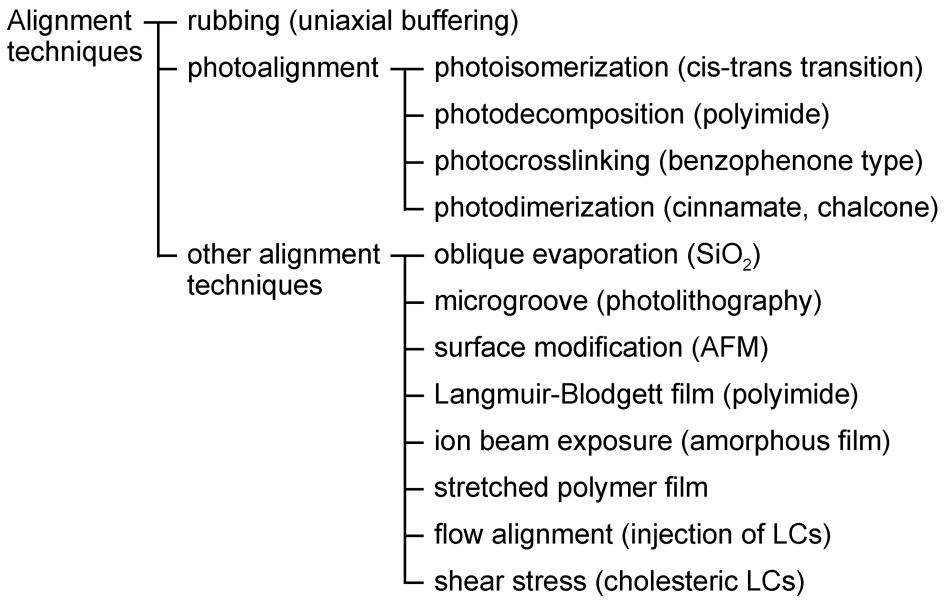


Figure 1.4: Classification of various LC alignment techniques [22].

alignment techniques, respectively. The surface treatment, a rubbing process [24], is the most widely used in display industry, but has some disadvantages coming from the mechanical contact. As an alternative of the rubbing, many methods modifying surfaces have been reported to align LC, such as $SiO_2$ evaporation [25], ion-beam alignment [26], and surface modification using atomic force modulation (AFM) [27, 28], and the photoalignment technique [29, 30]. In such cases, it is not only necessary to produce the LCP into an optically anisotropic film structure being divided into multi-domains. Thus, the employment of these structures as alignment layers is in need of ordering and patterning for LCP molecules. For fabricating anisotropic structures with multi-optic axes in order to align and pattern the LCP optical film with multi-domain, for aligning and patterning the LCP optical films with multi-domain, a rubbed surface [31] or photo-treated surfaces [32, 33] have been used previously. However, the rubbing process inevitably involves the mechanical damage and dust particles on the alignment surface and the multi-ordered pattern size is limited to a few hundred micrometers on the double rubbing process. Photoalignment is an alternative process to rubbing. Although the photoalignment process could be patterned with micro-size domains, the process suffers from the weak anchorage on the surface of the photo-treated surface [34]. Moreover,

in above mentioned processes, supplemental alignment layer onto the LCP optical films is needed to order LC molecules for LC based optical elements and/or LCDs.

For modification of the drawbacks among the listed methods, we have focused on the surface treatment by soft lithography, imprinting technique. The technique offers a unique possibility of a more complex structuring and patterning of the interfacial order. Moreover, new studies on the imprinted alignment, including the gliding of easy axis, are reported which requires scientific approach to understand the microscopic mechanism. The motivation of this thesis is divided into two parts: The detailed study on imprinted alignment itself and the new application of imprinting technique.

In the first part of thesis, we investigate the control of easy axis in both polar and azimuthal directions. Since the first development of the imprinting technique, most of researches have been focused on the phenomenological aspects.

## 1.3 Outline of Thesis

This thesis contains six chapters. **Chapter 1** introduces liquid crystalline materials such as LC and LCP and the importance of the surface

Table 1.1: Characteristics of various LC alignment techniques [23].

| Alignment Method | Alignment Material | Large-size Uniformity | Display Quality | Industrial Feasibility |
|---|---|---|---|---|
| **Rubbing** | Uniaxial buffering | Good | Good | Good |
| **Photoisomerization** | Cis-trans transition | Fair | Good | Fair |
| **Photodecomposition** | Polyimide | Good | Good | Fine |
| **Photocrosslinking** | Benzophenone type | Good | Good | Fine |
| **Photodimerization** | Cinnamate, chalcone | Good | Good | Fine |
| **Oblique evaporation** | SiO2 | Poor | Good | Poor |
| **Microgroove** | Photolithography | Poor | Fair | Poor |
| **Surface modification** | AFM | Poor | Fair | Poor |
| **Langmuir-Blodgett film** | Polyimide | Fair | Good | Fair |
| **Ion-beam exposure** | Amorphous film | Good | Good | Poor |
| **Stretched polymer film** | PVA | Poor | Poor | Fair |
| **Flow alignment** | Injection of LCs | Poor | Poor | Poor |
| **Shear stress** | Cholesteric LCs | Poor | Poor | Poor |

structures for aligning liquid crystalline materials. The novel alignment layer, imprinting technique, of the research is also included in this chapter. **Chapter 2** provides the detail information of imprinting technique. The optical properties such as optical anisotropy, dichroism, and dielectric anisotropy and the surface phenomena and anchoring energy for self-aligning capability of the introduced LC molecules on the imprinted polymeric alignment layers. In the end of this chapter, the experiments of the polymeric alignment layers using the imprinting technique. In **Chapter 3**, novel imprinting technique provides a functional optical elements, which are in-cell patterned optical films, in-cell polarizer such as dye-doped polarizer and wire gird polarizer. **Chapter 4** contains the display applications of the organic molecules such as the LC and imprinted LCP layer. The new transflective LCD in the single gap configuration having an imprinted patterned retarder, in-cell patterned polarizer, and wire grid polarizer for high efficient optical performances. Finally, some concluding remarks are made and further studies are suggested in **Chapter 5**.

# Chapter 2

# Imprinting Process for Patterning and Self-Aligning Capability

## 2.1 Aligning Properties on Imprinted Surface Structures

The interaction of LCs with neighbor phases (gas, liquid, solid) is a very interesting problem relevant to their EO behavior. The structure of liquid crystalline phases close to an interface is different from that in the bulk,

and this "surface structure" changes boundary conditions and influences the behavior of a LC in bulky samples. The nematic phase is of great importance from the point of view of applications in EO devices; thus, in this section we shall concentrate mainly on the surface properties of nematics.

### 2.1.1 Typical types of alignments and the methods of their implementation

In most practical applications and when examining LCs, sandwich type cells are used. A flat capillary with a thickness of 1-10 microns and above is formed from two glass plates with transparent electrodes. The separation between the plates is fixed by means of an insulating spacer (mica, polyethylene, etc.). To fix a very narrow gap (about 1 micron), glass balls or pieces glass thread of proper diameter are put between glasses. In sandwich cells, light is incident along the direction of the electric field or, if required, at a specified angle to it.

Tin dioxide ($SnO_2$) or indium oxide ($In_2O_3$) are most often used as transparent conducting coating. Layers of $SnO_2$ with a resistance of 20 $\Omega/m^2$ and less are obtained. This method can produce layers of varying thickness, depending on which is more important things such as the optical

transparency or the electrical resistance. Fine wires can be attached to the layers of $SnO_2$ using a very diluted ethanol solution of the glue based on polyvinylbutyral resin. Layers of $In_2O_3$ are produced by cathodic sputtering of the indium in a vacuum of $10^{-5}$ torr. This method is more efficient, and the properties of the coating (mechanical strength, optical transparency, electrical resistance) are approximately the same as with $SnO_2$.

In order to investigate the anisotropy of the properties of LCs and the character of their EO behavior, it is necessary to make a definite orientation of their molecules at the boundary walls of the cell. Molecules in the successive layer "attach" themselves to the molecules on the surface layer and the whole sample will become a monocrystal, either ideal or deformed, depending on the orientation of these surfaces. The orientation of the molecules on the surface is characterized by two parameters: the average angle of the molecules to the plane of the surface $\theta_0$ (preferred direction at the surface) and the anchoring energy $W$. Using the angle $\theta_0$, we can distinguish various orientation: homeotropic ($\theta_0 = 0$), planar ($\theta_0 = \pi/2$), and tilted ($0 < \theta_0 < \pi/2$).

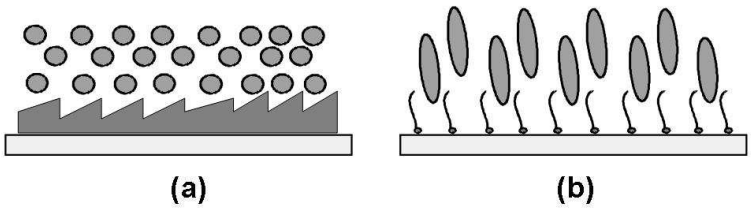


Figure 2.1: Illustration of the mechanism for: (a) planar orientation and (b) homeotropic orientation [1].

### A. Planar (homogeneous) orientation

Most commonly, a planar orientation is produced by a mechanical rubbing of the surface of the glass with paper or cloth (Chatelain's method). The rubbing creates a microrelief in the electrode coating or glass in the form of ridges and troughs, which promotes the orientation of the molecules along these formations. It is very simple, but unfortunately it does not always provide a sufficiently strong anchoring of the director to the surface. Better results are given by the evaporation of metals or oxides (e.g., SiO) onto the surface at oblique incidence [25]. The mechanism of planar orientation of NLCs by means of an obliquely evaporated thin film of metal is illustrated in Fig 2.1 (a).

In order to explain why longitudinal ridges and troughs on the surface of the glass promote a planar orientation of a NLCs, it is important to

study the interaction of a NLC with such surfaces from the viewpoint of a minimum elastic energy [24]. For convenience, the shape of the cross-section perpendicular to the ridges and troughs is taken as sinusoidal:

$$\phi(z = 0) = A \sin qx \tag{2.1}$$

where $x$ is the direction perpendicular to the rubbing of the surface of the substrate, $q$ is the wave vector of the surface structure, and $A$ is its amplitude By comparing Fig. 2.1 (a) and Fig. 2.1 (b), it can be seen that orientation of the director perpendicular to the surface (a) requires elastic energy for deformation of the medium, whereas positioning the director along the troughs in surface (b) is not accompanied by such a deformation.

The extra energy in the case of (a) can be calculated once the azimuthal $\phi(x, z)$ of the deviation of the director from the x-axis has been determined.

The excess of the elastic energy between the two configurations of the LC molecules parallel and perpendicular to the grooves can be calculated by minimizing the NLC elastic energy $F = W_\phi$ in the half-plane ($z > 0$) with the boundary conditions in the form

$$F = \int_0^\infty q(z)dz = \frac{1}{4} K A^2 q^3 \tag{2.2}$$

where $K$ is elastic constant of the LC and $q(z)$ is defined from Eq. 2.1. Thus, the additional elastic energy is quadratic, dependent on the depth of

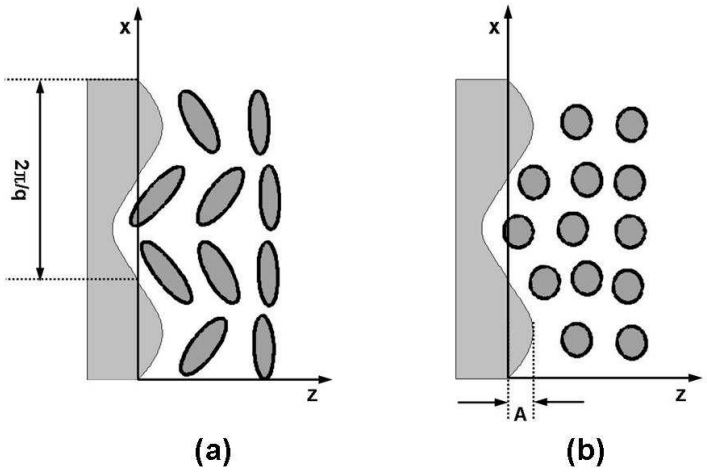


Figure 2.2: Illustration of Berreman's model [1,24]. (a) Deformation of the molecular distribution when the director is oriented perpendicular to the ridges on the surface. (b) No deformation is present with an orientation of the molecules parallel to the ridges and throughs on the surface.

the relief (amplitude $A$) and inversely proportional to the cube of the period of the relief $q$.

Thus, the orientation of the director, shown in Fig. 2.2(a) ($\phi_0 = \pi/2$) has an excess energy (when compared with the orientation in Fig. 2.2(b), $\phi_0 = 0$).

### B. Homeotropic orientation

As was already mentioned, etched glass surfaces promote a homeotropic orientation. Some crystalline cleavages ($Al_2O_3$, $LiNbO_3$) also orient nematics homeotropically. However, the most popular technique for the homeotropic orientation is utilization of surfactants.

The mechanism of homeotropic orientation by a monomolecular layer of a surfactant is demonstrated in Fig. 2.1(b). An orienting monolayer can be achieved by withdrawing the substrate from the solution by polymerization of the organosilicon films directly onto the substrate, and, in particular, by using a plasma discharge. Moreover, surface-active impurities can be introduced directly into the LC (e.g., lecithin or alkoxybenzoic acids). Using this method, different types of LC can be oriented (nematic, cholesteric, and smectic). Treatment of the walls with organometallic complexes also produces a stable homeotropic orientation in NLCs.

Homeotropic orientation can be also produced by a UV aligning technique [35,36]. In this case, the sample with a photosensitive layer is illuminated by a normally incident nonpolarized light. The LC molecules tend to orient perpendicular to the light polarization vector, and consequently the only "allowed" preferred direction remains along the light propagation.

### C. Tilted orientation

Orientation of molecules at a given angle to the surface is achieved using layers of SiO produced by oblique evaporation at a very large angle (80 - 90°) between the normal to the surface and the direction to the source [37]. In this case, quasi-one-dimensional surface structure is achieved that is oriented at an angle to the surface. This induces a tilt of the NLC molecules in the same direction [38].

Another method of the pretilt angle generation includes a proper rubbing of polymer (polyimide) films. In this case, the chemical structure of the oriented NLCs must be taken into consideration [39]. A very important thing is the presence of alkyl-branches in a rubbed polyimide film [36]. The absence of the alkyl-branches results in a low pretilt ($\approx 2°$), polyimide films with a low density of the alkyl-branches leads to a medium pretilt ($\approx 5°$), while a high pretilt angle ($\approx 20°$) may be achieved for the high density of the alkyl-branches. The physical reason for this is evident. The presence of the alkyl-branches increases the tendency for a homeotropic orientation, because they work similar to surfactants on the polyimide surface. Tilted orientation of the NLC molecules can also be achieved by using surfactants [38]. The pretilt angle irreversibly increases with temperature due to the

increase of the flexibility of the polymer side chains. The effect is more pronounced for the larger dielectric constants of LCs [40].

The angle of tilt of the molecules to the surface can be determined by optical methods, by studying the birefringence of the layer of the crystal with a change of angle of incidence of the light onto the cell [37]. The UV aligning technique is also capable of generating tilt angles on the photosensitive surface. One of the most attractive possibilities includes the application of the two subsequent illuminations [39, 41]. The director tilt angles of more than 4° on the surface can be produced, which is highly important for the applications in supertwist liquid crystal display cells [42, 43].

### 2.1.2 Surface parameters

#### A. Easy axis and anchoring energy

The macroscopic behavior of NLCs depends on the boundary conditions for the orientation of the direction $\overrightarrow{n}$. For this reason, the proper description of physical properties of alignment layer is important to investigate LC-interface systems. The major surface parameters of alignment layer are easy axis, pretilt angle and anchoring energy. We first describe the definition and expression of anchoring energy.

The director orientation at the interface between a NLC ($z > 0$) and alignment medium ($z < 0$) is characterized by two angles: the surface polar angle $\theta_S$ and the surface azimuthal angle $\phi_S$. At equilibrium and in the absence of external torques, the surface free energy is minimized if the director is aligned along one direction (easy axis) characterized by the two angles $\theta_0$ and $\phi_0$. Depending on the nature of the interface, several kinds of easy director orientations can be obtained. If the substrate is an isotropic medium without preferential direction on the surface plane, the easy axis is characterized only by a well-defined polar angle $\theta_0$. If the substrate is an anisotropic medium (solid crystal, isotropic substrate rubbed along a given direction) the easy axes are characterized by well-defined polar and azimuthal angles. Depending on the values of the easy polar angle, the director configuration is divided into homeotropic, tilted and planar configuration.

Let us consider the interface between a semi-infinite NLC ($z > 0$) and another semi-infinite medium ($z < 0$). At large distance from the interface the system exhibits a translational symmetry and thus the local physical parameters of the NLC do not depend on the position in space. Near the interface, the translational symmetry is broken and the local parameters depend on the distance z from the interface and one easy direction exists

for the director at the interface. The free energy per unit area contributed from an interface $\gamma$ is given by [44]

$$\gamma = \int_0^\infty [F_{LC}(z) - F_{LC}(\infty)]dz + \int_{-\infty}^0 [F_{sub}(z) - F_{sub}(\infty)]dz \qquad (2.3)$$

where $F_{LC}(z)$ is the free energy density of the NLC per unit volume at the distance z from the interface and $F_{LC}(\infty)$ is its asymptotic value in the bulk ($z \to -\infty$).

$\gamma$ is assumed that a function of the two surface angles $\theta$ and $\phi$ of the director. At equilibrium and in the absence of external forces, the director at the surface is aligned along the easy axis, $\theta_0$ and $\phi_0$. The free energy $\gamma$ can be written as

$$\gamma(\theta, \phi) = \gamma(\theta_0, \phi_0) + W(\theta, \phi) \qquad (2.4)$$

where $\gamma(\theta_0, \phi_0)$ is the equilibrium value $\gamma(\theta, \phi)$ and $W(\theta, \phi)$ corresponds to the work needed to deviate the director from the equilibrium position $(\theta_0, \phi_0)$, the anchoring energy function.

For the small deformation,

$$W(\theta, \phi_0) = \frac{1}{2} {W_p}^2 (\theta - \theta_0) \qquad (2.5)$$

and

$$W(\theta_0, \phi) = \frac{1}{2} {W_a}^2 (\phi - \phi_0) \qquad (2.6)$$

where $W_p$ and $W_a$ are the polar and azimuthal anchoring strength, respectively. They have dimensions of a surface tension and give a direct measure of the strength of the orientational interactions between the LC and the substrate. However, to describe the large deformation from the equilibrium, modifications are needed. The most commonly used analytical approximation for the surface free energy of a NLC is Rapini Papoular formula.

$$W(\alpha) = \frac{W_\alpha}{2} \sin^2 \alpha \tag{2.7}$$

Furthermore, other approximations are more productive in describing some other phenomena. The expression of $W$ in Legrendre polynomials was proposed.

$$W(\alpha) = \sum_i W_i \sin^{2i} \alpha \tag{2.8}$$

**B. Polar anchoring energy**

The polar anchoring strength is related to the energy required to deviate the polar angle of LC director from the easy axis. Many kind of methods are proposed to measure the polar anchoring strength. The anchoring strength deduced from the distorted LC director in wedge cell [45], surface disclination [46], the Freedericksz transition [47], and the distortion induced by applying high field [48, 49]. In this thesis, we adopted Yokoyama's high

field method [48] to measure the polar anchoring energy.

Let us consider the NLC layer with thickness $d$ assuming that both substrates at $z = 0$ and $z = d$ are identically treated. The free energy of NLC is written as

$$F = \frac{1}{2}\int_0^d [(K_1 \cos^2\Theta + K_3 \sin^2\Theta)(\frac{d\Theta}{dz})^2 + \frac{D^2}{(\varepsilon_1 \sin^2\Theta + \varepsilon_2 \cos^2\Theta)}]dz + 2f(\theta) \tag{2.9}$$

where $\Theta$, $f(\theta)$, and D denote the angle between the director and the substrate, anchoring energy, and electric displacement, respectively. The angle $\theta$ is related to $\Theta$ as $\theta = \Theta(0) = \Theta(d)$. Here $K_1$ and $K_3$ are the Frank elastic constants for splay and bend deformation, and $\varepsilon_1$ and $\varepsilon_2$ are the dielectric constants parallel and perpendicular to the director, respectively.

After minimizing the elastic free energy by the Euler-Lagrange approach and combining the torque balance equation at the interface between the substrate and LC, the equation can be obtained as,

$$\frac{d\Theta}{dz} = \frac{\Delta\varepsilon D_z^2}{K_1 {\varepsilon_1}^2} \frac{\cos^2\Theta - \cos^2\Theta_m}{(1 + \gamma \sin^2\Theta)(1 - \alpha\cos^2\Theta)(1 - \alpha\cos^2\Theta_m)} \tag{2.10}$$

where $\Delta\varepsilon = \varepsilon_1 - \varepsilon_2$, $\alpha = \Delta\varepsilon/\varepsilon_1$, and $\gamma = (K_3 - K_1)/K_1$. And $\Theta_m$ is the angle at $z = d/2$.

For a normally incident light of wavelength $\lambda$, linearly polarized, the

retardation R can be expressed as,

$$R = \frac{2\pi}{\lambda}\int_0^d (n_{eff}(\phi) - n_o)dz \tag{2.11}$$

$$n_{eff}(\phi) = \frac{n_o}{\sqrt{1-\nu\cos^2\phi}}$$

$$\nu = \frac{{n_e}^2 - {n_o}^2}{{n_e}^2}$$

where $n_e$, $n_o$, and $\phi$ are the extraordinary, ordinary refractive index, and the angle between the director and the substrate, respectively. By inserting Eq. (2.10) into Eq. (2.11), a simple relation between $R/R_0$ and $1/CV$ can be obtained as

$$\frac{R}{R_0} = \frac{\xi}{CV} I(\alpha, \gamma, \nu, \theta) \tag{2.12}$$

$$I(\alpha,\gamma,\nu,\theta) = \frac{2}{\pi}\int_\theta^{\pi/2} \frac{1-\nu+(1-\nu)^{1/2}}{1-\nu\cos^2\Theta+(1-\nu\cos^2\Theta)^{1/2}} \times(1+\gamma\sin^2\Theta)^{1/2}(1-\alpha\cos^2\Theta)^{1/2}\cos\Theta d\Theta \tag{2.13}$$

where $\xi = (\pi CV/d)(K_1/\Delta\varepsilon)^{1/2}$, $R_0 = 2\pi d(n_e - n_o)/\lambda$.

For simplicity, $f(\theta)$ can be approximated by the Rapini-Papoular form and rewritten as $W_\theta \sin^2(\theta-\theta_0)/2 \sim W_\theta^2(\theta-\theta_0)/2$, where $\theta_0$ is the pretilt angle. After some simplification [48] of Eq. (2.14), the relation between $R/R_0$ and $1/CV$ is obtained as

$$\frac{R}{R_0} = \frac{\xi}{CV} I(\alpha,\gamma,\nu,\theta) - \frac{2(K_1\cos^2\theta_0 + K_3\sin^2\theta_0)}{W_\theta d} \tag{2.14}$$

The measurements of the optical retardation and capacitance of a homogneously aligned NLC cell, as a function of applied voltage, can produce the polar anchoring strength using Eq. 2.14.

### C. Azimuthal anchoring energy

For the measurement of azimuthal anchoring energy, the torque balance method in a twisted-nematic (TN) cell has been proposed using a single wavelength [50] or spectral distribution of light [51, 52]. In this thesis, the azimuthal anchoring strength was evaluated by using a twist angle of TN cell which was fabricated with an imprinted alignment (IA) substrate and a rubbed polyimide (PI) substrate. According to continuum theory, the free energy per unit area can be written as a sum of the energies as follows.

$$F = F_{bulk} + F_{IA} + F_{PI} \tag{2.15}$$

where $F_{bulk}$, $F_{IA}$, and $F_{PI}$ are the bulk elastic energy, the surface anchoring energy of IA and the anchoring energy for PI, respectively. The bulk elastic energy and the surface anchoring energy of photopolymer are written as

$$F_{bulk}(\phi) = \frac{K_2}{2d}(\phi - 2\pi\frac{d}{p})^2 \tag{2.16}$$

$$F_{IA} = \frac{W}{2}\sin^2\Delta\phi \tag{2.17}$$

where $K_2$, $\phi$, and $d$ denote the elastic constant, the twist angle and the cell gap, respectively. We assume the strong anchoring for the polyimide. If $\Phi$ is the angle between two aligned directions, the deviation of the surface LC director from the aligning direction is denoted as $\Delta\phi$ as

$$\phi = \Phi - \Delta\phi \tag{2.18}$$

By minimizing F or $\delta F/\delta\Delta\phi = 0$, the surface anchoring strength W is express as

$$W_\phi = \frac{2K_2(\phi - 2\pi d/p)}{d\sin(2\Phi - 2\phi)} \tag{2.19}$$

and evaluated from the twist angle $\phi$ of the TN cell.

## 2.2 Imprinted Surface Structures

LCs and LCPs are very useful in several key areas of electronic and optical devices. Moreover, the multi-ordered LC systems have attracted great interest and have been widely studied because of the importance of the fundamental research and their potential for device applications to the optical systems including displays. In addition, optical elements, such as optical retardation plates, color filters, polarization converters, and interference filters, based on polymers, including LCPs, are one of the classes that have

been widely used for the advancement of LCDs that provide improved optical performances such as high light efficiency, wider viewing angle properties, and complicated optical functions. In such cases, it is not only necessary to produce the LCP into an optically anisotropic film structure being divided into multi-domains. Thus, the employment of these structures as alignment layers is in need of ordering and patterning for organic materials.

For fabricating anisotropic structures with multi-optic axes in order to align and pattern the optical film with multi-domain, a rubbed surface or photo-treated surfaces have been used previously. However, the rubbing process inevitably involves the mechanical damage and dust particles on the alignment surface and the multi-ordered pattern size is limited to a few hundred micrometers on the double rubbing process. Photoalignment is an alternative process to rubbing. Although the photoalignment process could be patterned with micro-size domains, the process suffers from the weak anchorage on the surface of the photo-treated surface.

In this chapter, we have investigated the mechanism of imprinting technique and proposed the application to functional optical elements. In addition, display and/or non-display applications with the novel optical elements for high device performances are proposed and demonstrated.

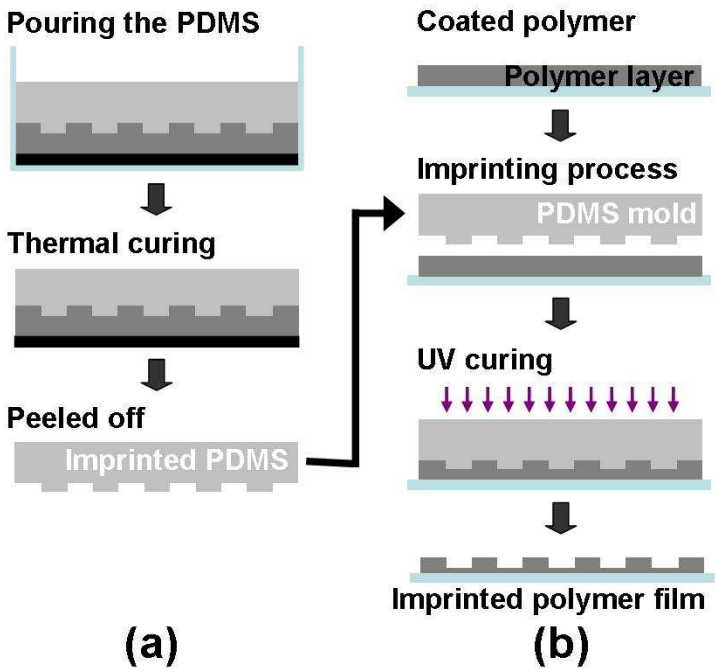


Figure 2.3: The schematic diagram showing the fabrication of an imprinted polymeric patterns. (a) Fabrication of the polymer (PDMS) mold. (b) Patterned structure transferred from a PDMS mold to a polymer-coated substrate using imprinting technique.

### 2.2.1 Imprint lithography

The formation of patterned structures on micro- or nanometer length scales is essential for the fabrication of many electronic, optics, microfluidics, and biological devices. Patterning technologies are well established for semiconductors and metals, but are relatively undeveloped for organic polymers with the notable exception of the specialized polymers used in photolithography.

The limitations of the conventional photolithography such as their high costs and the resolution limit due to diffraction, motivate the exploration and development of unconventional nanofabrication techniques. These unconventional approaches, of course, have limitations of their own. Unconventional routes may offer alternatives to photolithography in manufacturing. These techniques create opportunities for fabrication on non-planar surfaces (particularly smooth, curved surfaces) and over large areas and may offer competition in nanofabrication where cost and materials make photolithography difficult. Unconventional techniques have the potential to be the ultimate, low-cost method for nanomanufacturing. They are also operationally much simpler to use than are conventional techniques and thus help to open nanoscience and nanotechnology.

**1. Mold (master) preparation**

Silicon elastomers are resistant to ozone and ultraviolet (UV) degradation, have good chemical stability and are available in a variety of useful forms as conformal coatings, encapsulants and adhesives. We used polydimethylsiloxane (PDMS, Sylgard 184, Dow Corning) as an elastomeric mold, which was supplied as two part liquid component kits comprised of

Table 2.1: The mixing ratio of two part liquid component kits.

| Mixing ratio (by weight or volume) | Components (as supplied) |
|---|---|
| 10 : 1 | Base/curing agent |

When liquid components are thoroughly mixed, the mixture cures to a

Table 2.2: Physical properties of the PDMS (Sylgard 184) used in our experiment.

| Color | Viscosity (cP) | Specific gravity | Thermal conductivity (Watt-m-deg.) |
|---|---|---|---|
| Clear | 3900 | 1.03 | 0.18 |

flexible elastomer. Physical properties of the PDMS used in our experiment are shown in Table 2.1. We fabricated a PDMS master that has a planar surface with recessed or protruding patterns by casting PDMS against a complementary relief structure prepared by photolithography or electron-beam method.

As shown as Fig. 2.3(a), the PDMS was first poured on the master to give the polymer mold thickness of 5 cm. It was then cured on a hot plate at about 70°C, at which the adhesion between the PDMS mold and the master is relatively small, for 5 hours. The PDMS mold was finally peeled off from the master.

**2. Film coating and placement of the mold**

For the polymer, we used commercial UV curable photo-polymer, NOA65 (Norland Products Inc.), and polyurethane (PU, Minuta Tech.). Typically, glass was used as the substrate, which can readily be expanded to other kinds of organic or inorganic substrate if the surface is planar enough to allow a conformal contact with the PDMS mold. The glass substrates were cleaned by ultrasonic treatment in acetone solvent for 30 minutes and dried at 80° for 30 minutes in air atmosphere. As shown upper part in Fig. 2.3(b), polymer films were spin-coated onto the glass substrate to 300 nm to 1.5

$\mu$m thickness, which was measured by the alphastep and the PDMS mold was placed on the polymer surface. In spite of the spontaneous wetting property of the PDMS mold, care should be taken to avoid small gaps or bubbles between the mold and the polymer surface. The film was then annealed at a temperature above the glass transition temperature, $T_g$.

As is well known, the difference in the thermal expansion coefficient between the PDMS mold and the substrate is considerably large. As a result, the mold tends to separate from the polymer surface when the annealing temperature is high. In order to prevent the separation, the mold can be made soft (curing agent ($\sim$ 6 %) and the annealing can be carried out gradually from room temperature to the setting temperature. In this case, no weight or pressure is needed to keep the mold in contact with the surface. However, repeated annealing causes cross-linking of the mold, thereby leading to poorer wetting properties. We found that the same mold can be used about 15 times but a weak pressure ($\sim$ 100 g/cm$^2$) is need for further use of the mold.

### 3. Curing and characterizations

Typically, polymer films of NOA65 and PU were cured for 5 minutes and 2 hours using a UV exposure to make the polymer chain sufficiently pho-

topolymerized as shown lower part in Fig. 2.3(b). PDMS has a very low reactivity toward the polymers and its elasticity is sufficient to allow its separation from the polymeric structure. After curing and cooling to ambient temperature, the mold was removed from the surface and the remaining polymer structure was examined by AFM and scanning electron microscopy (SEM).

### 4. Mechanism of imprinted LCP optical films

Figure 2.4 shows the mechanism of fabrication of imprinted LCP optical films. By taking the Berreman's effect, micro- or nanostructure of PDMS mold induces orientation of LCP molecules. During the imprinting process,

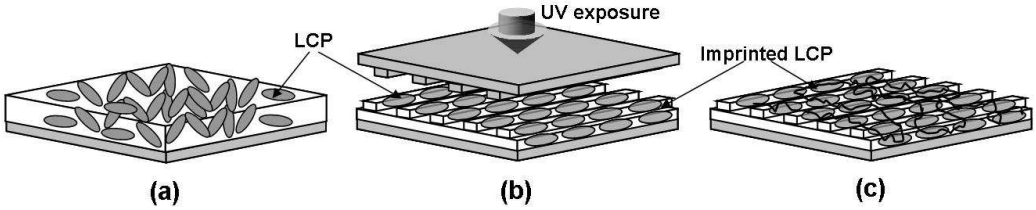


Figure 2.4: The mechanism of imprinted optical films based on LCP. (a) Spin-coating of LCP materials onto ITO glass substrate. (b) UV exposure during imprinting using a PDMS mold. (c) Imprinted LCP optical films with surface microstructure.

mesogenic groups of coated LCP materials were oriented by surface structure of PDMS mold (Fig. 2.4(b)) and polymer chains were crosslinked by exposure of UV light under a nitrogen atmosphere (Fig. 2.4(c)). Thus, the imprinted LCP optical film was fabricated.

### 2.2.2 Anisotropic wettability

Surface wettability is an important property of materials, which is generally characterized by measuring the contact angle of a liquid droplet sitting on the surface. When water is used, a contact angle less than 90° is indicative of a hydrophilic surface while a contact angle greater than 90° is indicative of a hydrophobic surface. If a surface show identical contact angles when measured from different directions, the surface is said to be isotropic in wettability, otherwise it is anisotropic. Modification of surface wettability is achieved through either chemical or physical means or through both. Chemical means such as silanization [53, 54], fluorination [55–57], plasma treatment [58–61], and photolytic treatment [62–64] have been widely used; some of these, however, suffer the drawback of a short-lived effect. Physical means of modifying surface wettability are typically achieved through surface roughening, which results in either ordered or disordered surface structures. Very often, surface roughening or patterning works together

with chemical treatments to alter surface wettability [65, 66].

Meanwhile, the natural world has provided some inspirations for surface wettability modifications. For example, the hierarchical surface texture is responsible for the superhydrophobic and self-cleaning properties of the lotus leaf [67]; the hierarchical structure in a gecko's foot gives rise to its ability to adhere to the wall and ceiling [68]; and the heterogeneous surface on a Stenocara beetle's back consisting of hydrophilic spots on a hydrophobic background endows the beetle with a unique water harvesting capability in the desert [69]. These inspirations have led to a lot of efforts to mimic these biological structures, in particular the hierarchical structure of the lotus leaf and thus the remarkable superhydrophobic property [70–74]. Most of these examples reported isotropic hierarchical structures with the aim to achieve superhydrophobicity on different materials such as on silicon and polymer substrates.

Anisotropic wettability has attracted much interest more recently. Similar to the approaches taken on tuning the surface wettability, anisotropic wettability is also achieved either through chemical patterning [75–77] or surface roughening [78, 79]. Surfaces with controlled anisotropic wettability have the advantage of restricting liquid flow to a desired direction, which has potential applications in microfluidic devices [80]. For example, Sommers

et al. reported enhancement with the aid of wetting drainage enhancement with the aid of wetting anisotropy on an aluminum (Al) surface [81]. In nature, anisotropic wettability has been observed on the surface of the rice leaf, and it has been mimicked by growing aligned carbon nanotubes on a substrate [82]. Anisotropic wettability was also reported on parallel PDMS grooves [83]. While most literature addressed anisotropic wetting behavior on single level parallel line structures, there are relatively few papers on the study of anisotropic wettability of surface with fabricated micro- or nanoscale structures and none reported the combined effects of wettability of imprinted surface patterns, which is based on conventional nanoimprint lithography (NIL) [84]. These structures allow the anisotropic wettability on polymeric films without the use of chemical treatment.

### 2.2.3 Fluorine-based self-assembled monolayer (SAM)

Conventional process such as photolithography has been a dominant technology for nanostructure fabrication. However, as the cost of short wavelength light source systems and photosensitive polymers increases significantly and the required feature size is reduced, photolithographic technol-

ogy will eventually reach its limit. For these reasons, extensive efforts have been made to replace photolithography with simple techniques employing a replica mold for patterning nanometer scale features.

Simple techniques such as imprint lithography, soft lithography, capillary force lithography, polymer transfer printing, and others have been developed for patterning nanoscale features, and displayed substantial results. Particularly, NIL based on a soft polymer mold has been utilized successfully as an alternative for nanostructure fabrication applicable for electron and/or optical devices.

In NIL, soft polymer, such as a PDMS, mold with fine features is pressed on a polymeric optical film. After the PDMS mold is released, the fine pattern on the mold is transferred to the polymer layer. Each type of happened problems was unsuccessful in imprinting process according to procedures illustrated in Fig. 2.5 [85]. As shown in Figs. 2.5 (a) and (b), polymer layer was separated from substrate due to adhesion between polymer layer and PDMS mold and polymer layer was irregularly broken because adhesion energy between polymer layer and substrate is similar to that between polymer layer and PDMS mold. In all cases, the fatal defects were occurred due to adhesion energy of interaction of layers. Moreover, in NIL, it should be more significantly considered when the high resolution patterns with sub-

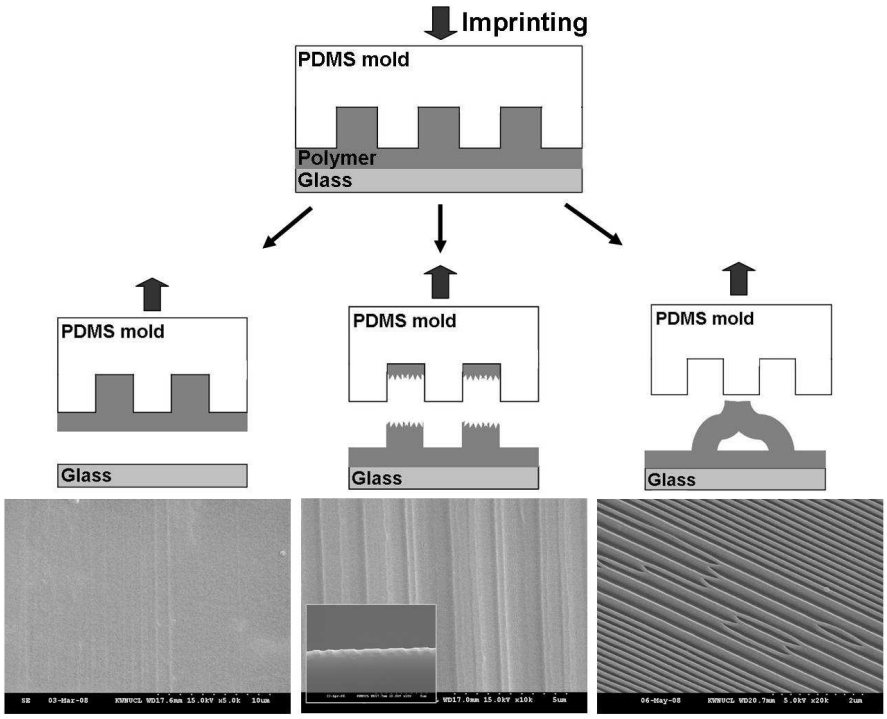


Figure 2.5: Illustration of failure types in NIL: (a) failed patterning by the lift-up of polymer layer, (b) failed patterning by the fracture of polymer layer, (c) failed pairing patterning by the elongation of polymer layer [85].

nanometers would be fabricated by NIL because the pattern aspect ratio gets larger as a pattern width is small. Therefore, the failure such as pairing in forming patterns with sub-nanometer was frequently observed as shown in Fig. 2.5 (c). To overcome the adhesion problem, mold surface treatment by a fluorine-based self-assembled monolayer (SAM) [53–57] is introduced to decrease the energy of the mold. Consequently, the surface treatment

may be successful for high resolution patterns transfer.

# Chapter 3

# Functional Optical Elements by an Imprinting Technique

## 3.1 Introduction

Many polymer based optical films are currently used in both active matrix and passive matrix LCDs [86]. For a long time the classical absorption based polarizer was the only optical films in a LCD. More recently other films with new functionalities have been introduced in LCDs. Brightness enhancement films and reflective polarizers are used to improve the light efficiency of LCDs. Compensation films and retarders are used to improve the angular and spectral dependence of the viewing angle properties. Front

scattering films and holographic films are components that are attracting interest for application in reflective displays. A common feature of these films is that they have to perform complicated optical functions. A dedicated production technology is usually required to obtain films with the desired properties.

At this moment, all of these optical films have uniform optical properties across the surface area. For some applications, however, it is useful to locally tailor the optical properties. Examples of such applications are patterned polarization rotators for stereoscopic displays, polarization sensitive gratings, reflective color filters and patterned polarizers. Recently, a number of new technologies based on the manipulation of the organization of LCs have become available that allow the preparation of such structured films. Some of the most promising technologies are based on manipulation of the orientation of LCs by light.

In this chapter, novel imprinting technique provides a functional optical elements, which are in-cell patterned optical films, in-cell polarizer such as dye-doped polarizer.

### A. Optical waveplates

Traditional optical waveplates are made of crystalline materials, such as calcite, mica, quartz, and potassium dihydrogen phosphate (KDP), that exhibit anisotropic optical properties. These solid crystals have relatively low birefringence ($\leq 0.01$). Therefore, waveplates fabricated using these materials are generally quite thick ($50 \sim 100$ $\mu$m), hence are not suitable for applications requiring thin waveplates, such as passive waveplates incorporated within a Fabry-Perot etalon. Furthermore, zero-order solid crystal waveplates are fragile, and their manufacture difficult and labor-intensive due to the need for precision cleaving and polishing of the optical elements. Thus, such waveplates are impractical for large aperture applications.

The advent of stretched polymer retardation sheets, designed for applications such as LCDs, has expanded the application realm of passive waveplates to large aperture devices. These polymer sheets are flexible films that can be attached directly to a substrate using adhesives. However, stretched polymer sheets exhibit low birefringence. Hence even zero order waveplates made of these sheets are thick (on the order of 100 $\mu$m), and their transmittance characteristics are temperature- and humidity-dependent.

Conventional LC monomers used in devices such as variable retarders,

light valves, and tunable wavelength filters are well documented [87, 88]. LC monomers are advantageous in terms of low cost and high birefringence, and devices made with these LC materials are active devices whose optical characteristics can be varied by application of an electric field across the LC layer. However, the LC material must be confined between two substrates. Incorporation of these materials into a compact, single unit device with multiple components is problematic.

LCP materials also exhibit high birefringence, therefore can be used to achieve thin (on the order of a few microns in thickness), zero order quarter waveplates (QWPs) in the visible wavelengths. High quality optical films can be processed easily on a single substrate, and are therefore suitable for use as a part of a compact, multiple component device.

### B. Polarizers

Now that we have some idea of what polarized light is, the next logical step is to develop an understanding of the techniques used to generate, change, and manipulate it to fit our needs. An optical device whose input is natural light and whose output is some form of polarized light is a polarizer. For example, recall that one possible representation of unpolarized light is the superposition of two equal-amplitude, incoherent, orthogonal P-states. An

instrument that separates these two components, discarding one and passing on the other, is known as a linear polarizer. Depending on the form of the output, we could also have circular or elliptical polarizers. All these devices vary in effectiveness down to what might be called leaky or partial polarizers.

Polarizers come in many different configurations, but they are all based on one of four fundamental physical mechanisms: dichroism, or selective absorption, reflection, scattering, and birefringence or double refraction. There is, however, one underlying property that they all share, there must be some form of asymmetry associated with the process. This is certainly understandable, since the polarizer must somehow select a particular polarization state and discard all others. In truth, the asymmetry may be a subtle one related to the incident or viewing angle, but usually it is an obvious anisotropy in the material of the polarizer itself.

By definition, if natural light is incident on an ideal linear polarizer only light in a P-state will be transmitted. That P-state will have an orientation parallel to a specific direction called the transmission axis of the polarizer. Only the component of the optical field parallel to the transmission axis will pass through the device essentially unaffected. If the polarizer is rotated about the z-axis, the reading of the detector will be unchanged because of the complete symmetry of unpolarized light. Keep in mind that we are

dealing with waves, but because of the very high frequency of light, our detector will measure only the incident irradiance. Since the irradiance is proportional to the square of the amplitude of the electric field, we need only concern ourselves with that amplitude.

Now suppose that we introduce a second identical ideal polarizer, or analyzer, whose transmission axis is vertical. If the amplitude of the electric field transmitted by the polarizer is $E_0$, only its component, $E_0\cos\theta$, parallel to the transmission axis of the analyzer will be passed on to the detector (assuming no absorption). The irradiance reaching the detector is then given by

$$I(\theta) = \frac{c\varepsilon_0}{2} {E_0}^2 \cos^2\theta \tag{3.1}$$

The maximum irradiance, $I(0) = c\varepsilon_0 {E_0}^2/2$, occurs when the angle $\theta$ between the transmission axes of the analyzer and polarizer is zero. Equation 3.1 can be rewritten as

$$I(\theta) = I(0)\cos^2\theta \tag{3.2}$$

This is known as Malus's Law, having first been published in 1809 by Etienne Malus, military engineer and captain in the army of Napoleon.

Observe that $I(90^\circ) = 0$. This arises from the fact that the electric field that passed through the polarizer is perpendicular to the transmission axis

of the analyzer (the two devices so arranged are said to be crossed). The field is therefore parallel to what is called the extinction axis of the analyzer and has no component along the transmission axis.

### C. Wire-grid polarizer (WGP)

The simplest device of this sort is a grid of parallel conductiong wires, as shown in Fig. 3.1. Imagine that an unpolarized electromagnetic wave impinges on the grid from the right. The electric field can be resolved into the usual two orthogonal components, in this case, one chosen to be parallel to the wires and the other perpendicular to them. The y-component of the field drives the conduction electron along the length of each wire, thus generating a current. The electrons in turn collide with lattice atoms, imparting energy

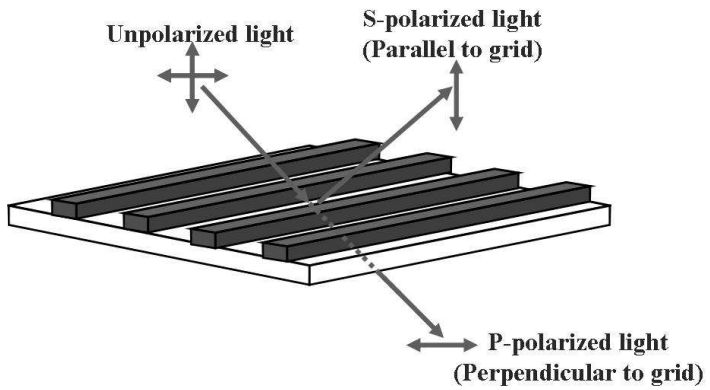


Figure 3.1: Optical principles of the WGP.

to them and thereby heating the wires (joule heat). In this manner energy is transferred from the field to the grid. In addition, electrons accelerating along the y-axis radiate in both the forward and backward directions. As should be expected, the incident wave tends to be canceled by the wave reradiated in the forward direction, resulting in little or no transmission of the y-component of the field. The radiation propagating in the backward direction simply appears as reflected wave. In contrast, the electrons are not free to move very far in the x-direction, and the corresponding field component of the wave is essentially unaltered as it propagates through the grid. The transmission axis of the grid is perpendicular to the wires. It is a common error to assume naively that the y-component of the field somehow slips through the spaces between the wires.

One can easily confirm our conclusions using microwaves and a grid made of ordinary electrical wire. It is not so easy a matter, however, to fabricate a grid that will polarized light, but it has been done. In 1960 George R. Bird and Maxfield Parish, Jr., constructed a grid having an incredible 2160 wires per mm [89]. Their feat was accomplished by evaporating a stream of gold (or at other times aluminum) atoms at nearly grazing incidence onto a plastic diffraction grating replica. The metal accumulated along the edges of each step in the grating to form thin microscopic "wires" whose width

and spacing were less than one wavelength across.

Although the wire grid is useful, particularly in the infrared, it is mentioned here more for pedagogical than practical reasons. The underlying principle is shared by other, more common, dichroic polarizers.

## 3.2 Optical Properties

The rodlike shape of LCs means that their physical properties [2, 90, 91] also possess a degree of anisotropy; that is, they exhibit different values when measured parallel or perpendicular to the director [90]. Free rotation around the long molecular axis gives an axis of symmetry parallel to the director, so that the values of the physical properties measured perpendicular to the director (i.e., along the y and z axes) are identical; however, they do differ from those measured parallel to the director (i.e., along the x axis). The anisotropic nature of the physical properties of LCs, due to their shape anisotropy, combined with the ability of magnetic and electric fields to influence the bulk spatial orientation of these molecules renders them of such importance to EO display devices. Their fast reorientation under the influence of a moderate electric field is a result of their fluid nature. The physical properties also depend on temperature and pressure, as well as the

type of LC state (e.g., nematic, smectic, columnar) and the degree of ordering in the liquid crystalline state. The anisotropic properties of relevance to LCDs [92, 93] are described in general in the next section.

### A. Optical anisotropy (birefringence)

Aligned calamitic LCs are uniaxial, due to their shape and polarization anisotropy, and are therefore birefringent, exhibiting different properties for light travelling with the electric field propagating parallel and perpendicular to the director or optic axis. Birefringence is a property usually associated with transparent crystals with a noncentrosymmetrical lattice structure (e.g., calcite). The free rotation in liquids averages out any asymmetry of molecular shape and renders the optically isotropic. The electric vector of incident plane polarized light entering a birefringent medium is split into two mutually perpendicular components called the ordinary (o) and extraordinary (e) ray. The electric field of the o-ray is always perpendicular to the optic axis, so its refractive index $n_o$ is a constant independent of propagation direction. The electric field of the e-ray lines in a plane that contains the optic axis, so its refractive index $n_{eff}(\theta)$ varies with the ray propagation angle $\theta$ with respect to the optic axis according to

$$n_{eff}(\theta)^2 = \left(\frac{\cos^2\theta}{n_o^2} + \frac{\sin^2\theta}{n_e^2}\right)^{-1} \tag{3.3}$$

The birefringence of the medium, $\Delta n(\theta)$, depends on the propagation direction and is defined as

$$\Delta n(\theta) = n_{eff}(\theta) - n_o \tag{3.4}$$

The maximum birefringence occurs when $\theta = 90°$ (i.e., when the electric field of the e-ray is parallel to the optic axis) and is given by

$$\Delta n = n_e - n_o \tag{3.5}$$

where $n_e = n_{eff}(\theta = 90°)$. $\Delta n$ is defined as the difference between the refractive indices for the o- and the e-rays of a fully oriented nematic phase [94] propagating parallel and orthogonal, respectively, to the optic axis of the nematic medium. Most NLCs have positive birefringence ($\Delta n > 0$), meaning that the e-ray is delayed with respect to the o-ray on passage through the material.

Birefringence is responsible for the appearance of interference colors in LCDs operating with plane-polarized light. Interference between the e-ray and the o-ray, which have travelled through the medium with different velocities, give rise to the colored appearance of these thin films. For a wave at normal incidence, the phase difference in radians between the o- and e-rays caused by traversing a birefringent film of thickness $d$ and birefringence

$\Delta n$ is referred to as the optical retardation $\delta$ given by

$$\delta = \frac{2\pi \Delta n d}{\lambda_v} \tag{3.6}$$

where $\lambda_v$ is the wavelength of light in a vacuum. The retardation is wavelength dependent, so that positive and destructive interference occur at different wavelengths, resulting in the suppression of some part of the visible spectrum and therefore, a nonwhite color. Moreover, the birefringence is also wavelength and temperature dependent, because the refractive indices also vary with these parameters. Above the nematic clearing point in the isotropic liquid, the material is no longer birefringent ($n_e = n_o$) and an isotropic refractive index $n_i$ is observed.

**Birefringence measurement**

The experimental setup for measuring the birefringence of the cells is shown in Fig.3.2. Assuming that the amplitude and the frequency of the photoelastic modulation (PEM) [95] are $A_0$ and $\Omega$ and the retardation of sample is $B$, respectively the light intensity at the detector in Fig.3.2 is as follows [96].

$$I = 1 - \cos(B) J_0(A_0) + 2 \sin(B) J_1(A_0) \cos(\Omega t) \tag{3.7}$$

$$+2 \cos(B) J_2(A_0) \cos(2\Omega t) + \cdots, \tag{3.8}$$

where $J_k(A_0)$ denotes the $k_{th}$ order coefficient of Bessel function. The dc term, the first harmonic (1f) term, and the second harmonic (2f) term are all identified. If $A_0$ is chosen such that $J_0(A_0) = 0$, then the DC or average signal is independent of the birefringence $B$. The DC signal may be used to normalize the 1f and the 2f signals measured by using the lock-in amplifier. However, the lock-in amplifier presents the root-mean-square (RMS) voltages. Therefore, the ratios can be defined by the equations.

$$R_{1f} = \frac{V_{1f,RMS}}{V_{DC}} = \sqrt{2}\sin(B)J_1(A_0) \tag{3.9}$$

$$R_{2f} = \frac{V_{2f,RMS}}{V_{DC}} = \sqrt{2}\cos(B)J_2(A_0) \tag{3.10}$$

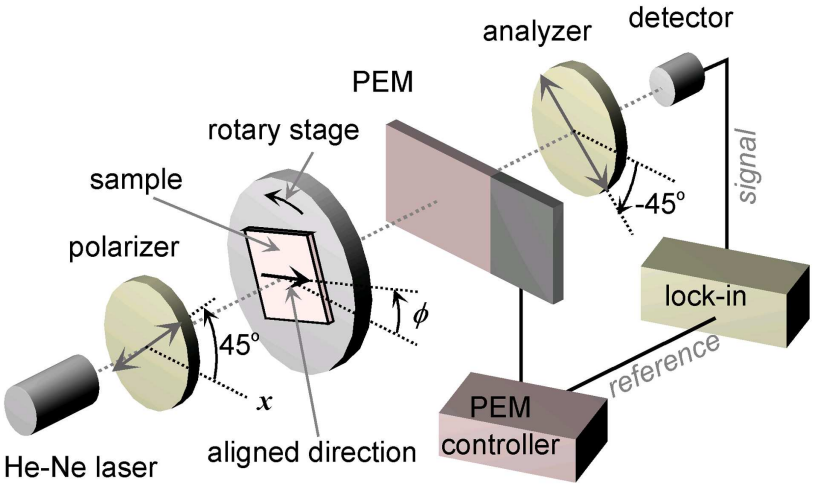


Figure 3.2: Schematic diagram of the birefringence measurement using PEM method [95].

Therefore, the birefringence is

$$B = \sin^{-1}[\frac{R_{1f}}{\sqrt{2}J_1(A_0)}], \tag{3.11}$$

$$= \cos^{-1}[\frac{R_{2f}}{\sqrt{2}J_2(A_0)}] \tag{3.12}$$

$$= \tan^{-1}[\frac{R_{1f}J_2(A_0)}{R_{2f}J_1(A_0)}] + m\pi \tag{3.13}$$

where $m$ is a integer.

### B. Dielectric anisotropy

The interaction between a LC and an electric field is dependent on the magnitude of the dielectric permittivity measured parallel $\varepsilon_{\parallel}$ and perpendicular $\varepsilon_{\perp}$ to the director and to the difference between them, i.e., the dielectric anisotropy $\Delta\varepsilon$. The dielectric permittivity measured along the x axis is unique, whereas the dielectric permittivities measured along the y and z axes are identical. Therefore,

$$\Delta\varepsilon = \varepsilon_{\parallel} - \varepsilon_{\perp} \tag{3.14}$$

where the dielectric permittivity $\varepsilon$ of a material is defined as the ratio of the capacitance $C_m$ of the parallel plate capacitor that contains the material to the capacitance $C_v$, of the same capacitor that contains a vacuum:

$$\frac{C_m}{C_v} = \varepsilon \tag{3.15}$$

The dielectric constants are dependent on the temperature and the frequency of the applied field up to the transition to the isotropic liquid Above the clearing point, the dielectric constants measured along all three axes are equal due to the isotropic nature of a liquid and, therefore, the dielectric anisotropy decreases to zero. The resultant dielectric constant $\varepsilon_i$ is the dielectric constant of the liquid. The sign and magnitude of the dielectric anisotropy are dependent on the anisotropy of the induced polarizability, $\Delta\alpha$, and the anisotropy and direction of the permanent polarization attributable to the resultant of permanent dipole moments.

### C. Dichroism

Absorption anisotropy (dichroism) in LCs takes place either due to the presence of the short wavelength ($< 400$ nm) oscillator, usually coinciding with the direction of its long molecular axis, or due to the impurities, such as dichroic dyes ("guests") dissolved in LCs ("hosts"). We will consider the second case as the most important for practical applications ("guest-host" effect [97]).

Consider a molecule $n_{dye}$ of the "guest" dye whose long molecular axis forms an angle $\theta$ with the director $n_{LC}$ of a LC "host". Let the absorption oscillator O be located at angle $\beta$ with respect to the long molecular axis

of the dye. Then the order parameter of the dichroic dye $S_{dye}$, $\beta$, and the dichroic ratio

$$N = \frac{A_p}{A_c} \tag{3.16}$$

where $A_p$ and $A_c$ are absorption with direction of parallel and perpendicular between dyes and polarizer and thus, the following relationship are known to satisfy [97]:

$$S_{dye} = \frac{N-1}{N+1}[1 - \frac{2}{3}\sin^2\beta]^{-1} \tag{3.17}$$

**D. Polarization efficiency**

The most essential passive optical element in LCDs is the polarizer. Polarizers are indispensable for the displaying of the information content and important front-of-screen performance parameters, such as brightness and contrast, are strongly influenced by the performance of the polarizer. Currently, the most widely used polarizers for LCD applications are derivatives of the H-sheet polarizer as invented by E. H. Land in 1938 [98]. These dichroic polarizers are based on uniaxially stretched poly(vinyl alcohol) that is impregnated with iodine or doped with dichroic dyes. These sheet polarizers show excellent optical performances that can be expressed by the polarization efficiency (PE) in combination with the single-piece transmit-

tance ($T_{sp}$), which means a transmission of unpolarized light through a single polarizer, as

$$PE = \sqrt{\frac{T_p - T_c}{T_p + T_c}} \times 100\% \tag{3.18}$$

where $T_p$ and $T_c$ are defined as the transmission of unpolarized light through two polarizers with their transmission axis parallel and perpendicular, respectively.

$$T_{sp} = \frac{10^{-A_p} + 10^{-A_c}}{2} \tag{3.19}$$

where $A_p$ and $A_c$ are defined as the absorbance parallel and perpendicular to the average orientation of the long axis of the chromophores, respectively. The polarizer performance can also be expressed by a single parameter; the extinction ratio (ER)

$$ER = \frac{T_p}{T_c} \tag{3.20}$$

## 3.3 In-Cell Multi-Functional Optical Films

We developed a novel imprinting technique, based on a soft lithography, in combination with the exposure of UV light to produce a wide range of

anisotropic optical films of the LCP. It is extremely important to produce a patterned LCP film which can be used as both an in-cell retarder and an alignment layer for next-generation LCDs. The anisotropic surface forces of the LCP produced at a nano- or micro-scale level during the imprinting process result in the LC alignment on the patterned LCP film without any surface treatment. The anisotropic LCP film with chain ordering by imprinting was implemented into a LC cell to serve as an alignment layer of the LC as well as an in-cell retarder.

### 3.3.1 Patterning by imprinting technique

#### 1. Fabrication of a polymer (PDMS) mold

The master made of a UV curable photopolymer material (NOA63, Norland Ltd.) was used to fabricate a polymer mold. We used a PDMS (RTV615, GE silicones) [99] as a polymer mold with micro-patterns. As shown as Fig. 3.3(a), the PDMS was first poured on the master to give the polymer mold thickness of 5 cm. It was then cured on a hot plate at about 70°C at which the adhesion between the PDMS mold and the master is relatively small, for 5 hours. The PDMS mold was finally peeled off from the master. The period of the PDMS mold was varied from 3.0 to 8.0 $\mu$m with the

line-to-space (LS) ratio from 0.5 to 2.0, and the depth was fixed as 1.2 $\mu$m. The feature sizes were determined using a SEM and field emission SEM (FESEM) for detailed observation.

## 2. Imprinting technique for fabricating a patterned LCP film

We used a commercial LCP material, RMS 03-001 (E. Merck), to fabricate an anisotropic optical film. Figure 3.3(b) shows a schematic diagram of producing a patterned LCP film through an imprinting process which utilizes our PDMS polymer mold. The LCP material was first spin-coated on a glass substrate at the spinning rate of 2500 rpm for 30 seconds without a pre-coated alignment layer, giving the layer thickness of 1.5 $\mu$m, and baked

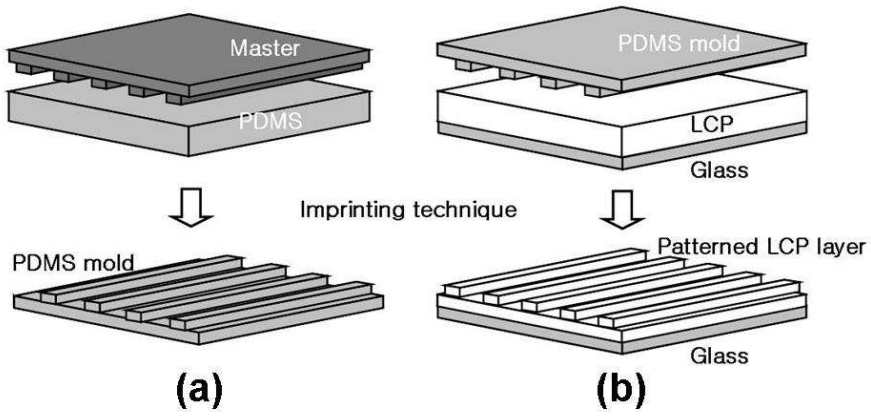


Figure 3.3: Schematic diagram showing the fabrication of a PDMS mold and a patterned LCP film by the imprinting technique [100].

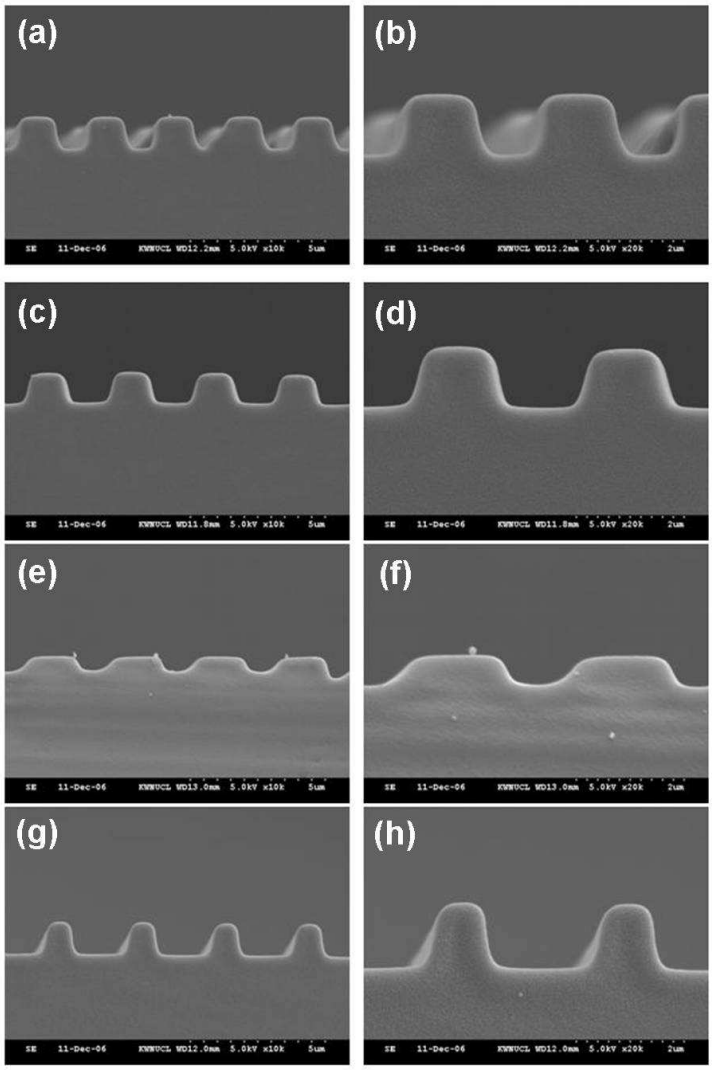


Figure 3.4: The FESEM images of the PDMS molds having different periods with different LS ratios: (a),(b) 3.0 $\mu$m with 0.5, (c),(d) 3.0 $\mu$m with 1, (e),(f) 8.0 $\mu$m with 1, and (g),(h) 3.0 $\mu$m with 2.

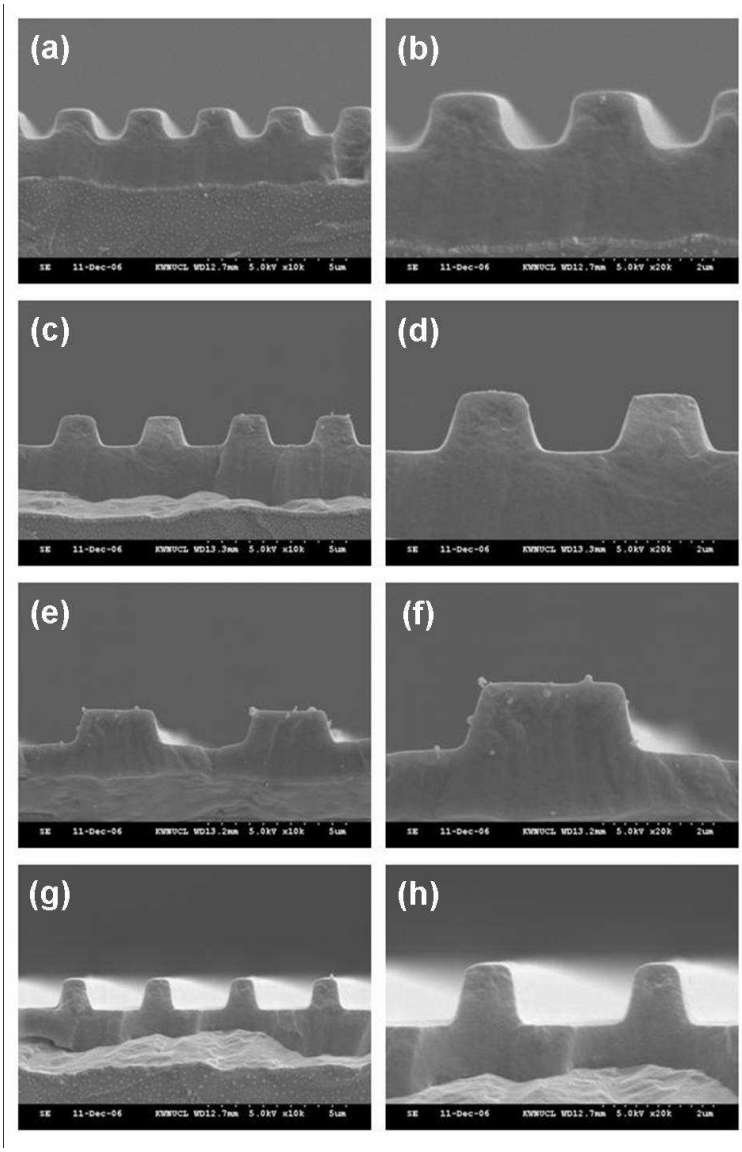


Figure 3.5: The FESEM images of the imprinted LCP layers having different periods with different LS ratios: (a),(b) 3.0 $\mu$m with 2, (c),(d) 3.0 $\mu$m with 1, (e),(f) 8.0 $\mu$m with 1, and (g),(h) 3.0 $\mu$m with 0.5.

subsequently at 65°C for 1 minute. By pressing the PDMS mold onto the prepared LCP layer, micro-patterns of the mold were replicated on the LCP layer. The micro-patterns of the PDMS mold were well transferred to the surface of the LCP layer under an imprinting pressure resulting from just above a gravitational force of the PDMS mold. After the micro-patterns were formed on the LCP layer, the LCP layer was exposed to the UV light at the intensity of 40 mW/cm$^2$ for 5 minutes under a nitrogen ($N_2$) atmosphere so as to preserve the shapes of the micro-patterns. The patterned LCP film was then peeled off from the PDMS mold. During imprinting process, mesogenic groups of coated LCP materials were oriented by microstructure of PDMS mold and polymer chains were crosslinked by expo-

Table 3.1: The material constants of RMS03-001.

| Parameters | Values |
|---|---|
| $n_e$ | $1.629 + 18360/\lambda^2$ †‡ |
| $n_o$ | $1.501 + 10010/\lambda^2$ †‡ |
| Viscosity | 5.8 cPs † |
| Clearing point | 75 ± 1°C |

† The results are measured at 20 ± 1°C.

‡ $\lambda$ is a wavelength of incident light in nm.

Table 3.2: The characteristics of RMS03-001 cured film.

| Parameters | Values |
|---|---|
| $n_e$ | 1.684 ± 0.005 at 589 nm † |
| $n_o$ | 1.529 ± 0.005 at 589 nm † |
| On-axis retardation | 150 ± 10 nm (1 ± 0.1 $\mu$m) |
| Polar surface energy | 5.4 ± 0.5 mN $m^{-2}$ † |
| Disperse surface energy | 30.2 ± 0.5 mN $m^{-2}$ † |
| Total surface energy | 35.6 ± 0.5 mN $m^{-2}$ † |
| Pencil hardness | HB |

† The results are measured at 20 ± 1°C.

sure of UV. Thus, the imprinted optical film based on LCP was fabricated. The optical anisotropy was observed with a polarizing optical microscopy (POM, Optiphot2-Pol, Nikon) and the phase retardation was measured using a PEM method.

### 3.3.2 Results and discussion

#### 1. Microstructures imprinted on the LCP

Figure 3.6 shows the SEM images of microstructures produced on various PDMS molds and those transferred on the LCP films from the PDMS molds.

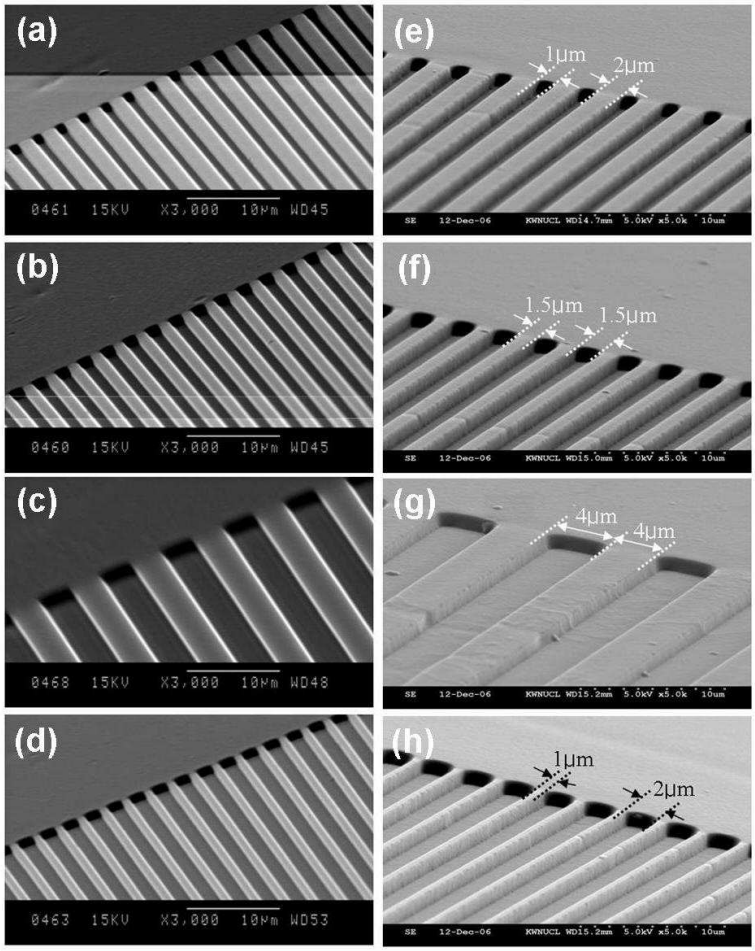


Figure 3.6: The SEM images of the PDMS molds having different periods with different LS ratios: (a) 3.0 $\mu$m with 0.5, (b) 3.0 $\mu$m with 1, (c) 8.0 $\mu$m with 1, and (d) 3.0 $\mu$m with 2. The SEM images of the imprinted LCP layer, the negative patterns of the PDMS molds, having different periods with different LS ratios: (e) 3.0 $\mu$m with 2, (f) 3.0 $\mu$m with 1, (g) 8.0 $\mu$m with 1, and (h) 3.0 $\mu$m with 0.5.

The SEM images shown from Fig. 3.6(a) to Fig. 3.6(d) correspond to the patterns having the periods of 3.0 $\mu$m with the LS ratio of 0.5, 3.0 $\mu$m with the LS ratio of 1.0, 8.0 $\mu$m with the LS ratio of 1.0, and 3.0 $\mu$m with the LS ratio of 2.0. The depth of the mold patterns was about 1.2 $\mu$m. Figures 3.6(e), (f), (g) and (h) show the SEM images of the imprinted LCP films, corresponding to the negative line shapes of the PDMS molds, whose periods are 3.0 $\mu$m with the LS ratio of 2.0, 3.0 $\mu$m with the LS ratio of 1.0, 8.0 $\mu$m with the LS ratio of 1.0, and 3.0 $\mu$m with the LS ratio of 0.5, respectively. Note that the PDMS mold has sufficient rigidity to prevent the collapse of microstructures, and at the same time, it is soft enough to release the LCP film. Using our imprinting process combined with the UV exposure, micro-scale lines will be patterned with high regularity at precisely determined micro-scale intervals, strongly indicating that microstructures can be patterned with high feature density and precision.

**2. The imprinted LCP film as an in-cell patterned retarder**

Figure 3.7 shows microscopic textures of our imprinted LCP films, observed with the POM under crossed polarizers, having different pattern sizes of 3.0 $\mu$m and 8.0 $\mu$m in period and the LS ratio from 0.5 to 2. The depth of each mold pattern is about 1.2 $\mu$m. The dotted lines represent the boundaries

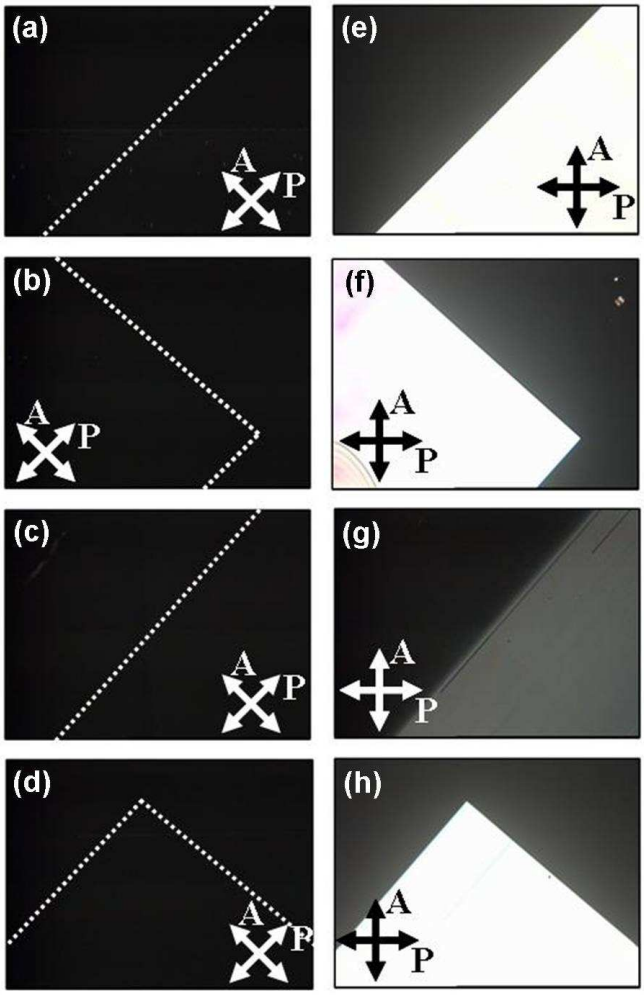


Figure 3.7: Microscopic textures of imprinted LCP films observed with the POM under crossed polarizers. The dotted lines represent the boundaries between the imprinted region with patterns and the bare region with no patterns. The direction of the mold patterns on the imprinted LCP film is parallel (0°) to the optic axis of the polarizer in (a)-(d) while it makes an angle of either 45° or 135° to the optic axis of the polarizer in (e)-(h) [100].

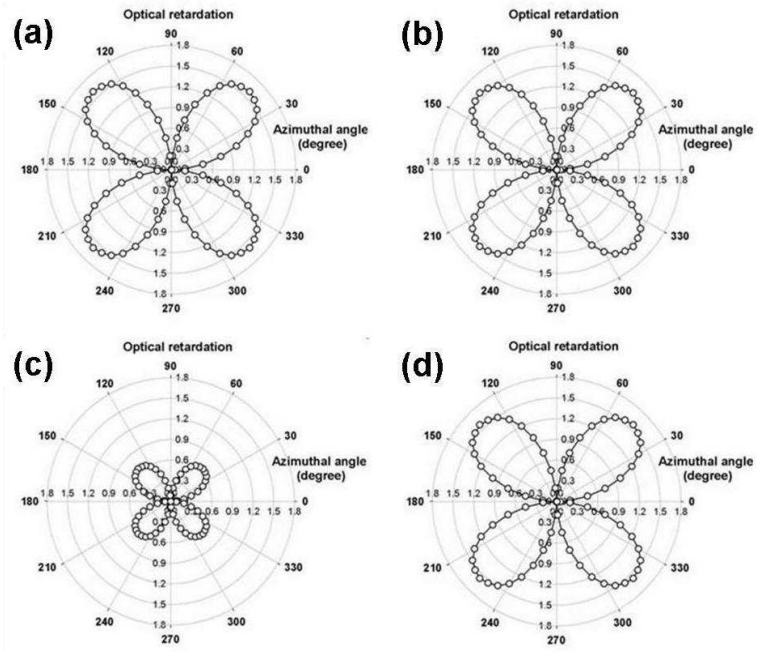


Figure 3.8: The optical retardation of the imprinted LCPs, which different periods with different LS ratios are 3.0 $\mu$m with 2 for (a) and (e), 3.0 $\mu$m with 1 for (b) and (f), 8.0 $\mu$m with 1 for (c) and (g), and 3.0 $\mu$m with 0.5 for (d) and (h), were measured as a function of the azimuthal rotation angle.

between the imprinted region with patterns and the bare region with no patterns. The direction of the mold patterns on the imprinted LCP film is parallel (0°) to the optic axis of the polarizer or that of the analyzer in Figs. 3.7(a), 3.7(b), 3.7(c), and 3.7(d) while it makes an angle of either 45° or 135° to the optic axis of the polarizer in Figs. 3.7(e), 3.7(f), 3.7(g), and 3.7(h). The microscopic textures from Fig. 3.7(a) to Fig. 3.7(d) [or from

Fig. 3.7(e) to Fig. 3.7(h)] correspond to the patterns having the periods of 3.0 $\mu$m with the LS ratio of 2, 3.0 $\mu$m with the LS ratio of 1.0, 8.0 $\mu$m with the LS ratio of 1.0, and 3.0 $\mu$m with the LS ratio of 0.5. Except for the period of 8.0 $\mu$m as shown Fig. 3.7(g), all the cases of 3.0 $\mu$m in period show a completely bright state when the direction of the mold patterns makes an angle of either 45° or 135° to the optic axis of the polarizer. The insufficient phase retardation as the QWP in Fig. 3.7(g) indicates that the LCP molecules did not fully aligned at a nano-scale level during the imprinting process.

We now describe the phase retardation of an imprinted LCP film itself and that of the LC cell with an in-cell LCP film to examine the two-fold functionality of the imprinted LCP film as an alignment layer and an in-cell QWP. Figure 3.8 (a) shows the schematic diagram of our LC cell configuration where the LC layer behaves as another QWP. The planar alignment of the LC molecules was used in our study. As shown in Fig. 3.8(b), the phase retardation of $\pi/2$ through the imprinted LCP film itself, measured using the PEM method as a function of the azimuthal rotation angle at the wavelength of 632.8 nm, corresponds exactly to the QWP. The measured phase retardation of $\pi$ through our LC cell with the in-cell LCP film behaving as a QWP tells us that the LC molecules were well aligned on

the imprinted, in-cell LCP film and the LC layer alone produces the phase retardation of $\pi/2$. The total phase retardation through the LC layer and the in-cell LCP film corresponds to the half-wave plate. In fact, the use of a patterned in-cell retarder such as our imprinted LCP film allows for high transmittance, no parallax, and wide viewing characteristics in a variety of the LC-based optical devices.

### 3. The imprinted LCP film as a C-plate

Another imprinted film was fabricated by a same imprinting process of fabricating the above mentioned C-plate using another LCP with negative dielectric anisotropy such as RMS 03-015 (E. Merck) instead of LCP with positive dielectric anisotropy such as RMS 03-001. As shown in Fig. 3.9, the imprinted, patterned C-plate shows bright and dark states along the LS patterns and small white and gray arrows coincide with the directions of

Table 3.3: The material constants of RMS03-015.

| Parameters | Values |
|---|---|
| Viscosity | 2.7 cPs † |
| Clearing point | 96 ± 1°C |

† The results are measured at 20 ± 1°C.

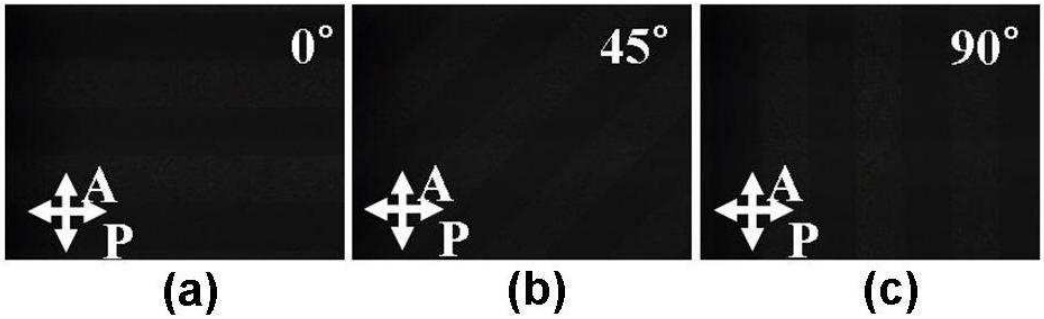


Figure 3.9: Microscopic textures of imprinted C-plate observed with the POM under crossed polarizers between the plate and polarizer at angle of (a) 0°, (b) 45°, and (c) 90°, respectively.

45° and 0° aligned LS multi-domains, respectively. As shown in Fig. 3.9(b), microscopic textures of the imprinted, patterned C-plate was rotated by an angle of 45° with respect to Fig. 3.9(a).

Table 3.4: The characteristics of RMS03-015 cured film.

| Parameters | Values |
|---|---|
| $n_e$ | 1.667 ± 0.005 at 589 nm † |
| $n_o$ | 1.525 ± 0.005 at 589 nm † |
| On-axis retardation | 150 ± 10 nm (1 ± 0.1 $\mu$m) |
| Polar surface energy | 6.7 ± 0.5 mN $m^{-2}$ † |
| Disperse surface energy | 40.3 ± 0.5 mN $m^{-2}$ † |
| Total surface energy | 47.0 ± 0.5 mN $m^{-2}$ † |
| Pencil hardness | 5B |

† The results are measured at 20 ± 1°C.

### 3.3.3 High resolution patterning technique

Conventional process such as photolithography has been a dominant technology for nanostructure fabrication. However, as the cost of short wavelength light source systems and photosensitive polymers increases significantly and the required feature size is reduced, photolithographic technology will eventually reach its limit. For these reasons, extensive efforts have been made to replace photolithography with simple techniques employing a replica mold for patterning nanometer scale features.

Simple techniques such as imprint lithography, soft lithography, capillary force lithography, polymer transfer printing, and others have been developed for patterning nanoscale features, and displayed substantial results. Particularly, NIL based on a soft polymer mold has been utilized successfully as an alternative for nanostructure fabrication applicable for electron and/or optical devices.

#### 1. NIL for fabricating nanoscale optical films

Figure 3.10 illustrates the procedures for NIL using polymer molds derived from master, which was made of ultraviolet (UV) curable photopolymer material, PUA. Preferentially, we used a PDMS mold with nanoscale patterns. The PDMS was poured on the PUA master and eliminate captured

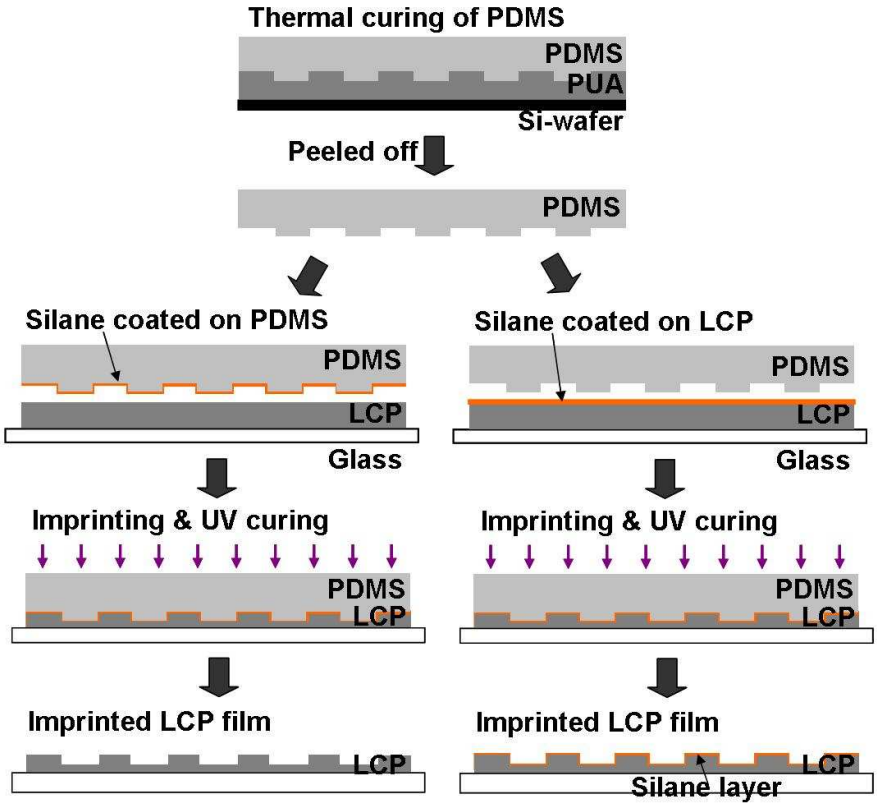


Figure 3.10: Schematic illustrations for the fabrication of PDMS mold and patterned LCP layer by NIL process.

air bubbles of the uncured PDMS in vacuum chamber for about 1 hour. After that, the PDMS cured on a hot plate at about 70°C, at which the adhesion between the PDMS mold and the master is minimized, for 5 hours. The PDMS mold was then peeled off from the master. The different half-pitches of the PDMS molds for the imprinting technique were from 250 nm

to 800 nm with same LS distribution ratio and the depth was fixed 500 nm.

For fabricating polymeric optical films, we used a commercialized LCP material, RMS 03-001C (E. Merck). The LCP material was first spin-coated on a glass substrate at the spinning rate of 2500 rpm for 30 seconds without a pre-coated alignment layer, giving the layer thickness of 1.5 $\mu$m, and baked subsequently at 65°C for 1 minute. Due to get relatively weak adhesion between the LCP layer and the PDMS mold compared to the interaction between the LCP layer and the glass substrate, fluorine based SAM is treated on the surface of the PDMS mold or the non-cured LCP layer as shown in Figs. 3.10 (a) and (b), respectively. By pressing the PDMS mold onto the prepared LCP layer, nano-patterns of the mold were replicated on the LCP layer. Under our standard process condition, we have successfully transferred the pattern of the PDMS mold to the surface of the LCP layer with low imprinting pressure, which is only gravitational force of the PDMS mold. Once the nanostructures of the imprinted LCP layer were formed, they were polymerized by the UV light exposure at 40 mW/cm$^2$ for 5 minutes in a nitrogen atmosphere at room temperature so that the shapes of the nanostructures were preserved. The imprinted LCP optical film was then peeled off from the PDMS mold.

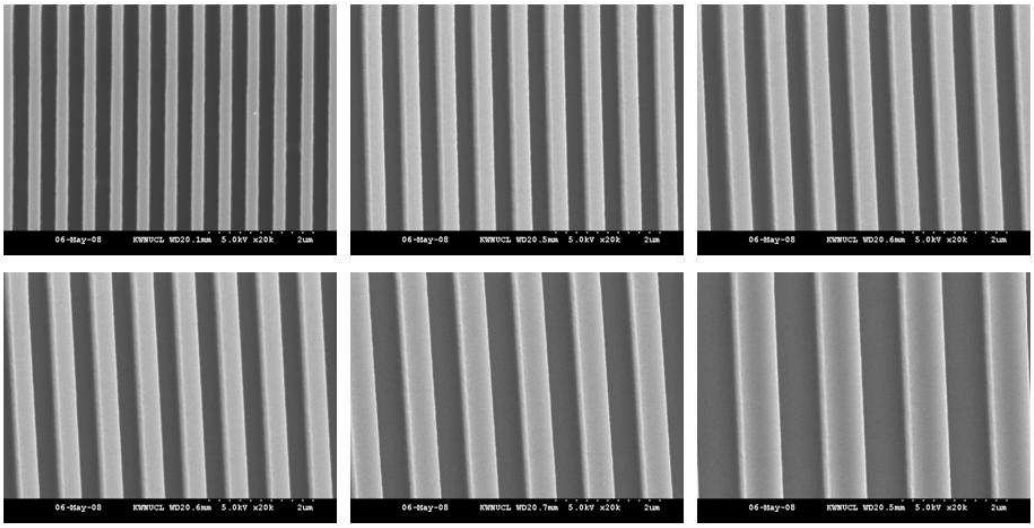

Figure 3.11: The SEM images of polymer molds having different half-pitches with (a) 250 nm, (b) 350 nm, (c) 400 nm, (d) 450 nm, (e) 600 nm, and (f) 800 nm, respectively.

**2. LC cell fabricated with in-cell nanoscale optical films**

For measurement of the optical anisotropic, the phase retardation and the aligning capability, LC cells were fabricated with imprinted optical film and with the rubbed polyimide (PI) layers. Nanostructures were produced on the LCP layer for spontaneously aligning, planar aligned (PA) or homeotropic aligned (HA), of LC molecules without using an alignment layer by taking the Berreman approach. By producing LC cell having the imprinted LCP layer as alignment layer, we also examined imprinted LCP

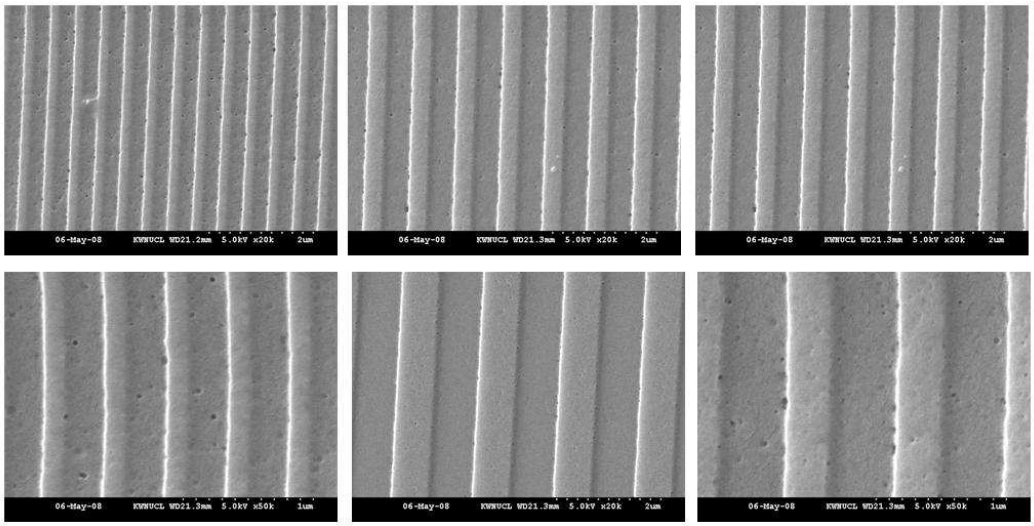

Figure 3.12: The SEM images of polymer molds having different half-pitches with (a) 250 nm, (b) 350 nm, (c) 400 nm, (d) 450 nm, (e) 600 nm, and (f) 800 nm, respectively.

layer for their aligning capability. It is composed of crossed polarizers and our LC cell was made using two glass substrates and in-cell imprinted LCP layer on the lower glass substrate with no extra-coated alignment layer for LCP alignment and/or LC molecular ordering. PI, JALS 146-R50 or JALS 684 (JSR co., Japan), was coated on the upper glass substrate for the respective PA or HA LC molecules and baked at 160°C for 1 hour. For LC molecular layer has the same optical anisotropic value as that of QWP, the cell thickness was maintained 1.6 $\mu$m and 2.6 $\mu$m thickness using glass spacers in the PA and the HA LC cells, respectively. The LC material used

MLC-6012 and MJ-96758 (E. Merck), which were injected into the cells by capillary action at room temperature.

### 3. Results

Figures 3.11 and 3.12 show the SEM images of nanostructures of PDMS mold and transferred on the LCP layers based the PDMS molds by using NIL. In this NIL process, the half-pitches of the PDMS mold were 250, 350, 400, 450, 600, and 800 nm, respectively as shown in Fig. 3.11. Parts of the nanostructures on the PDMS mold possessed shapes of lines, and the width ratio of the resulting lines and the space between them was 1. The depths of the mold patterns for preparing fixed about 500 nm. As shown in Fig. 3.12, the SEM images of the imprinted LCP layer after separation from the mold of the PDMS pattern of LS prepared under low temperature and a low pressure condition. Comparison of the patterns on the PDMS mold and imprinted LCP layer revealed that the patterns of nanostructures were successfully transferred from the PDMS mold onto the LCP layer. In imprinting process, polymer mold requires rigidity to prevent the collapse of microstructure, and at the same time, it should be sufficiently soft to release the transferred polymer layer. Taking these into account, PDMS is a suitable material to be employed as a template for manufacturing microscale

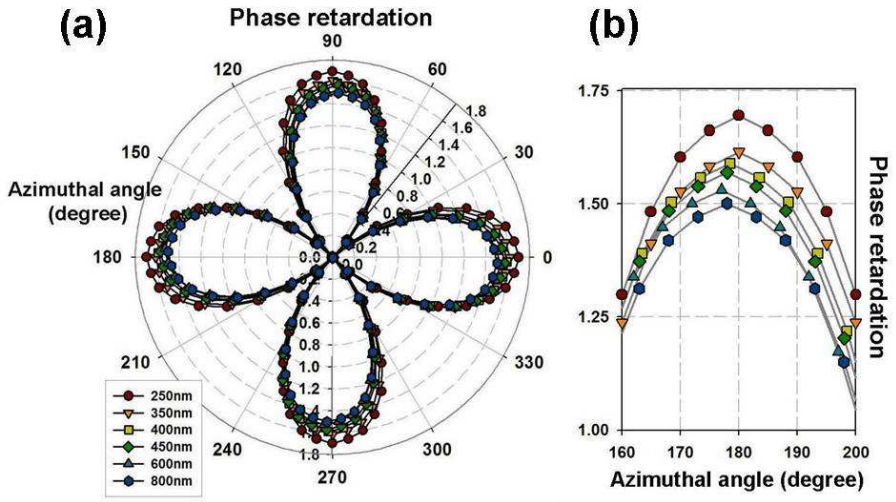


Figure 3.13: The measured PEM results of nanoscale imprinted optical films.

polymer structures. However, there are typically three above mentioned failures when nano-patterns are fabricated by NIL. Therefore, it was induced lower adhesion energy that fluorine-based SAM produced between PDMS mold and LCP layer. Therefore, nanoscale lines were patterned with high regularity at precisely determined nanoscale intervals, strongly indicating that nanostructures could be patterned with high feature density and precision using this NIL technique using PDMS mold.

Figure 3.13 shows optical retardation of the imprinted LCP films prepared with different pattern sizes measured as a function of azimuthal angle by the PEM technique. The different half-pitches of the imprinted LCP

films were from 250 nm to 800 nm with 1 in line/space ratio and about 500 nm in depth. The symbols, such as circles, inverse triangles, rectangles, diamonds, triangle, and sexangles, denote the measured optical retardation results through the imprinted LCP films with different half-pitches, respectively.

### 3.3.4 Thermal patterning (different phase states)

We used a patterned retarder based on a LCP, RMS 03-001C (E. Merck). The patterned retarder has two different phase states, an anisotropic state and an isotropic state, respectively. The optical retardation of the anisotropic region and that of the isotropic region correspond to a half waveplate (HWP) and a dummy layer, respectively. The optical axis of the HWP makes an angle of 45° with respect to the direction of the polarizer. Figure 3.14 shows fabrication process of inner patterned retarder by two-step UV treatments. As shown in Fig.3.14(a), first UV exposure on the coated LCP layer during imprint process using metal mask through metal-mask for crosslinking and second UV exposure in the non-exposed (uncrosslinked) region preserved imprint process during heating at 200°C as shown in Fig.3.14(b).

As shown in Fig. 3.14(a), single directional LS patterns of PDMS mold

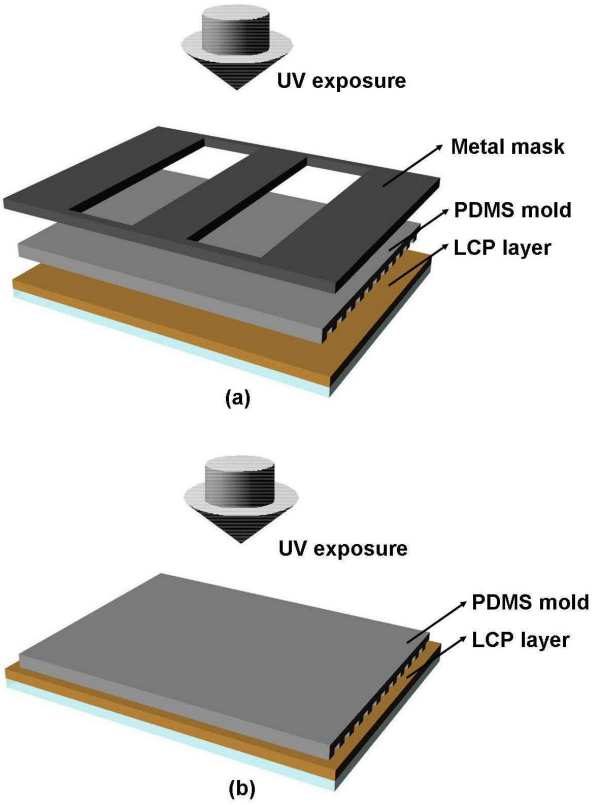


Figure 3.14: Fabrication process of inner patterned retarder by two-step UV treatments. (a) First UV exposure on the coated LCP layer during imprint process using metal mask through metal-mask for crosslinking. (b) Second UV exposure in the non-exposed (uncrosslinked) region during heating.

were used for fabricating a patterned retarder with $\lambda/2$ and 0 retardation. The patterned retarder was subsequently crosslinked by UV light in the first irradiation region through a metal-mask under $N_2$ atmosphere at room temperature. The retardation of $\lambda/2$ was then produced. As shown in Fig. 3.14(b), during heating about 200 °C the patterned retarder became isotropic in the non-exposed (uncrosslinked) region. The isotropic was then crosslinked by the second UV exposure.

Figure 3.15 shows microscopic textures of the patterned retarder with multi-domain on the ITO glass substrate observed at an angle of 45° and 0° between the rubbing and that of one of crossed polarizers using a POM. The patterned LCP retarder has anisotropic and isotropic domains, as shown in Figs. 3.15(a),(c) and 3.15(b),(c). The isotropic region shows the dark state in any direction of the optical axis. In contrast, the anisotropic region shows bright and dark states depending on the direction of the polarizer. Here, I and A coincide with an isotropic state and an anisotropic state, respectively.

The optical retardation, $2\pi d\Delta n/\lambda$, of the retarder was measured as a function of azimuthal angle by the PEM technique. Here, $d$, $\Delta n$, and $\lambda$ represent the thickness, the optical anisotropy of the retarder, and the wavelength of the light used, respectively. The measured results are shown in Fig. 4.13. The open circles and the open triangles denote the patterned

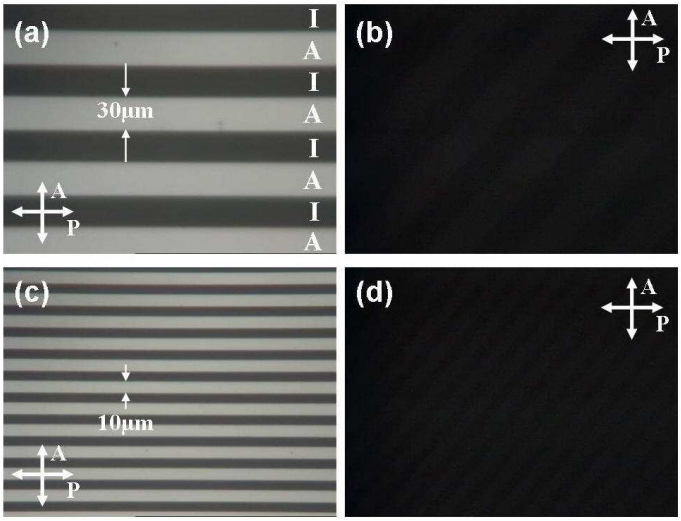


Figure 3.15: The microscopic textures of the inner patterned retarder based on LCP molecules observed under crossed polarizers: (a),(c) an angle of 0° and (b),(d) 45° between the direction of retarder and the rear polarizer. The isotropic region shows the dark state in any direction of the optical axis and the anisotropic region shows bright and dark states depending on the direction of the polarizer. Here, I and A coincide with an isotropic state and an anisotropic state, respectively.

retarder with an anisotropic state and an isotropic state, respectively. The maximum phase retardation was about 1.6 in the anisotropic region, which corresponds to $\lambda/4$ for $\lambda = 632.8$ nm. In contrast, the retardation in the isotropic region was only 0.06 [102].

### Dielectric measurement

The dielectric measurements have been performed by Impedance/gain phase analyzer (4192A, Hewlett-Packard). The sandwitched type of capacitor sample, metal-insulator-metal (MIM), is used for dielectric measurements. For fabricating MIM sample, electrode metal (Au) was deposited onto the surface of a patterned retarder with different phase state on the ITO glass

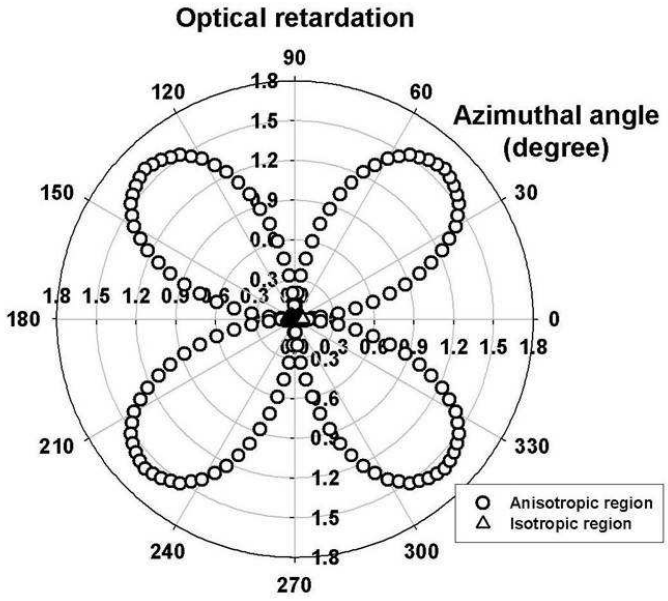


Figure 3.16: The optical retardation of the retarder was measured as a function of azimuthal angle by the PEM technique. The open circles and the open triangles denote the patterned retarder with an anisotropic state and an isotropic state, respectively.

substrate. The dielectric measurements have been done both in anisotropic region and isotropic region. The values of capacitance will directly give the value of real part of permittivity of the sample using following equation,

$$\varepsilon_r \varepsilon_0 = C \cdot \frac{d}{A} \tag{3.21}$$

where $C$, $d$, and $A$ are the capacitance, thickness of retarder, and square measure of the sample. For accurate measurement, seven samples fabricated in the same condition was measured and searched average value. The average capacitances and permittivities were $C_{iso} = 1.326 \times 10^{-2}$ F in the isotropic state region and $C_{ani} = 6.517 \times 10^{-3}$ F in the anisotropic state region at the frequency of 1 kHz and the relative permittivities, $\epsilon_r = \epsilon/\epsilon_o$, in both anisotropic and isotropic regions were $\epsilon_{iso} = 14.97$ F/m in the isotropic state region and $\epsilon_{ani} = 7.36$ F/m in the anisotropic state region, respectively. Here, $C_{iso}$, $C_{ani}$, $\epsilon_{iso}$, and $\epsilon_{ani}$ are respectively capacitances and permittivities in both isotropic state and anisotropic state regions and vacuum permittivity is $8.85 \times 10^{-12}$ $C^2/N{\cdot}m^2$. [102].

### 3.3.5 Dual patterning (twisted retarders)

Coated twisted retarders are well known as compensators for LCDs. Since the twist angle in such a layer changes linearly with the layer thickness, the

production of twisted retarders requires extreme coating thickness accuracy if the twist angle has be controlled even within a few degrees.

If different azimuthal alignment directions of twisted retarder are defined by dual surface grooves, one is alignment layer on the substrate and the other is a microstructure of PDMS mold, a twist deformation can be induced without any chiral dopant. Rather than controlling the twist by an intrinsic helical twisting power, the twist angle is defined by the two azimuthal alignment directions and therefore the twist angle is not sensitive to thickness variations. This certainly offers a big advantage in production since extremely high precision coating is not required to realize a well defined twist angle.

Moreover, there is no helical sense defined by chiral dopants, thus the volume imprinting-induced twist angles can be locally different. In particular, a pattern of left- and right handed twisted retarders can be realized. Figure 3.17 shows a surface aligned 5 $\mu$m thick twisted retarder was generated. The ordering direction of the alignment layer was uniform, whereas photopolymerization using imprinting technique with UV exposure, which is used polymer mold with the LS pattern direction at +45° and -45° relative to the alignment direction of the lower substrate.

Perfect achromatic behaviour is achieved if the Mauguin condition is

satisfied. However, to satisfy the Mauguin condition, the layers become very thick with the consequence of high material consumption and high exposure energies required for alignment. On the other hand, a compromise can be made like in the case of TN-cells, which are not perfectly achromatic, but since they exhibit a high degree of achromaticity they are quasi achromatic. Therefore, for a 90° twist angle, the first minimum condition could for example be adjusted, which requires $\Delta nd$ to be roughly 0.48 $\mu$m, where $\Delta n$ is the optical anisotropy of the material and d the thickness of the layer. For lower twist angles the optimum value of $\Delta nd$ increases, whereas it decreases for twist angles above 90°. Typical $\Delta n$ values of LCP materials range from 0.1 to 0.25. Therefore, typical layer thicknesses for such quasi achromatic rotators are in the range from 2 $\mu$m to 5 $\mu$m, depending on the $\Delta n$ of the material. Figure 3.18 shows the measured results of wavelength dependence of HWP.

If the conditions for wave guiding are fulfilled, twisted retarders work as achromatic rotators, which rotate the polarization of light according to the twist angle induced in the individual areas. Such properties are for example requested for 3D-LCDs to encode the polarization information individually for the viewer's left and right eye. It is well known that a 3D-impression from a display can be obtained when the left and right eye receive simi-

lar images that are slightly shifted in position with respect to each other. One of the methods of achieving this is to provide one of the images in one polarization state and the other image in the second polarization state. The information for both eyes is simultaneously present on the screen. The viewer needs glasses provided having two polarizers with orthogonal polarization directions to select the information for each of the eyes. The system is shown in Fig. 3.19.

The twisted retarder can be used to display the information in the de-

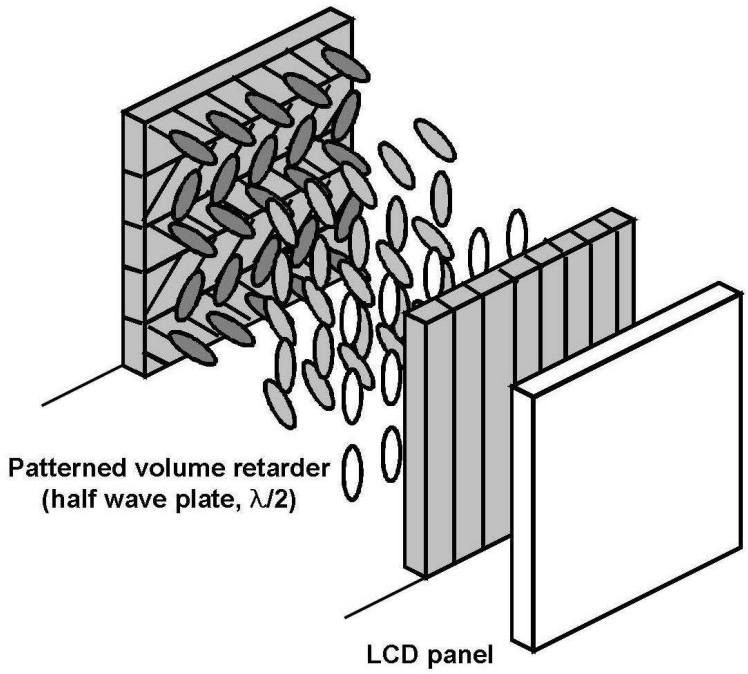


Figure 3.17: Configuration of a patterned, volume twisted retarder with areas of left- and right handed twist.

sired polarization. The display has to be provided with a polarizer to be able to generate polarized light. In case of an LCD this polarizer is always present. We have shown earlier that it is possible to pattern a nematic LCP film with areas that do not rotate the polarization of light and areas that rotate the polarization over 90°. When for example the odd data lines are provided with the parts of the retarder that rotate the polarization by 90°, and the even data lines are provided with the parts of the retarder that do not rotate the polarization of light, half of the display can be used to provide the information for one eye and the second half for the other eye.

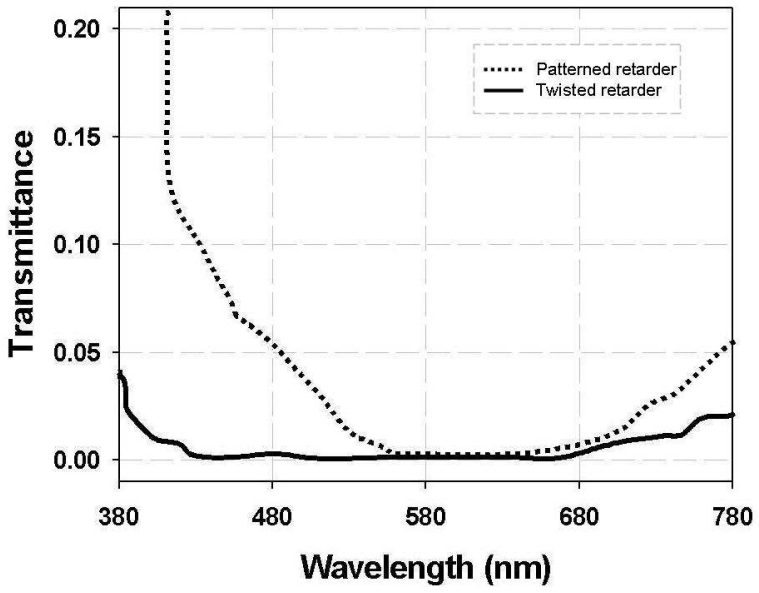


Figure 3.18: Wavelength dependence of QWP such as A-plate and twisted retarder.

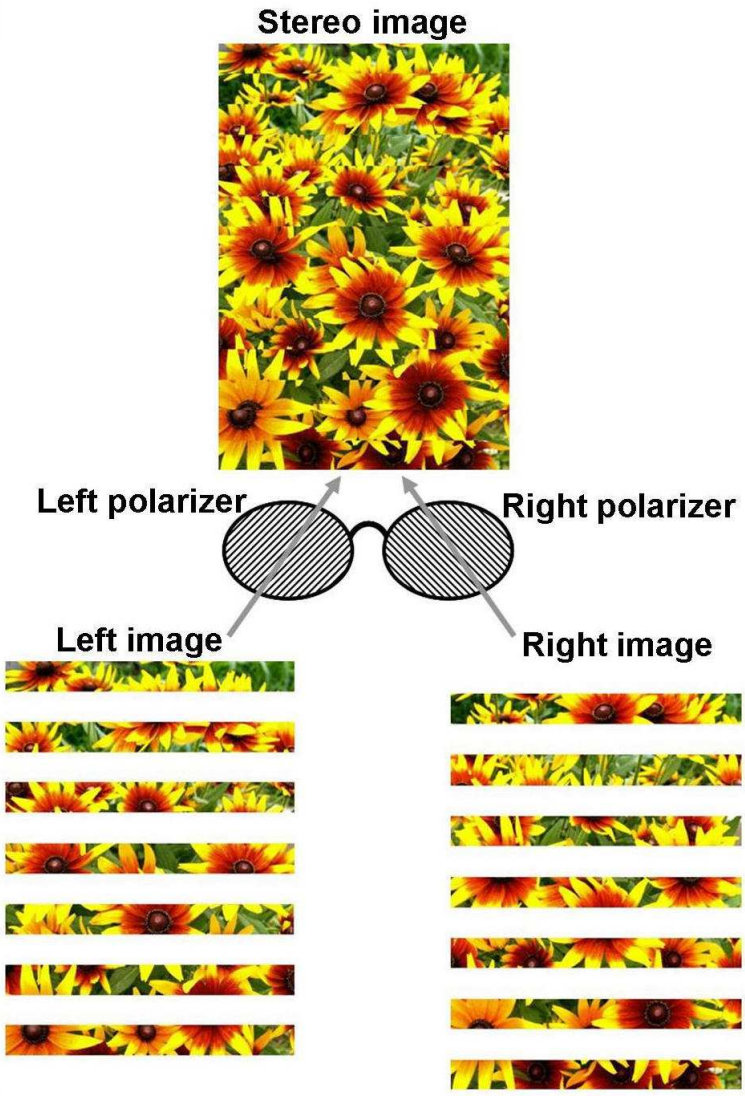


Figure 3.19: Principles of polarization encoded stereoscopic vision

The here-described method is earlier than the currently used systems based on photolithographic structuring of the polarizer.

## 3.4 Self-aligning capability of LCs

### 3.4.1 The LC alignment on a patterned LCP film

Using the Berreman concept, microgrooves were prepared on the LCP film to explore the possibility of aligning the LC molecules without using any surface treatment or an extra alignment layer. An imprinted, patterned LCP film was implemented into a LC cell to examine two-fold functionality of an alignment layer and an in-cell phase retarder. Our LC cell have a patterned QWP LCP film on the lower glass substrate and a polyimide (PI) alignment layer of JALS 146-R50 (JSR co., Japan) on the upper glass substrate for the planar LC alignment. The LC cell was placed between crossed polarizers such that one of the optic axes was at 45° with respect to the direction of the rubbing direction on the PI layer. The cell thickness was maintained 3.2 $\mu$m thickness using glass spacers so that the LC layer corresponds to the QWP. The LC material used was MLC-6012 (E. Merck) and injected into the cell by capillary action at room temperature.

Through the imprinting process, an optically anisotropic optical film was

fabricated on the inner side of glass substrate. Using the Berreman concept [24], the microgrooves were prepared on the surface of the anisotropic optical film to provide the spontaneous alignment of LC molecules on the imprinted optical film without using any surface treatment or an extra alignment layer. To verify a self-aligning capability of LCs, PEM results and azimuthal anchoring energy were measured using planar aligned (PA) and TN LC cell configurations.

As shown in Fig.3.21, the optical retardation, $2\pi\Delta nd/\lambda$, through the imprinted LCP film at the wavelength of 632.8 nm was measured as about

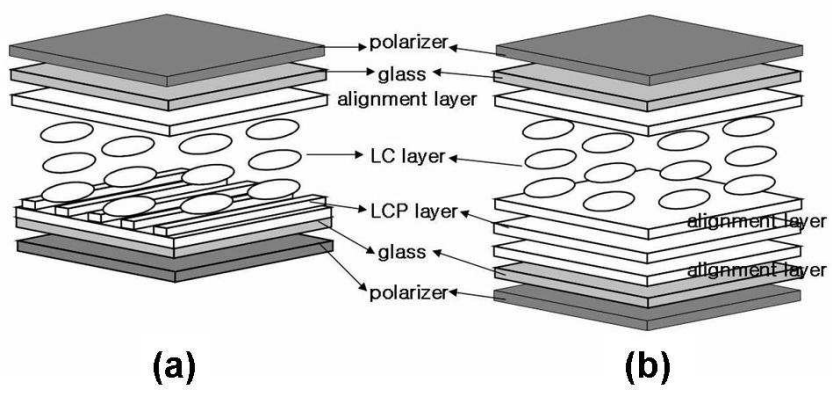


Figure 3.20: The LC cell configuration with (a) the imprinted LCP film behaving as both an in-cell retarder and an alignment layer and (b) phase retardation layer having two alignment layers for aligning LC layer and LCP layer.

Table 3.5: The material constants of MLC-6012.

| parameters | values |
|---|---|
| $K_1$ | $11.6 \times 10^{-12}$ N |
| $K_2$ | $5.5 \times 10^{-12}$ N |
| $K_3$ | $16.1 \times 10^{-12}$ N |
| $\Delta\varepsilon$ | 8.2 † |
| $\varepsilon_\perp$ | 3.9 † |
| $n_o$ | $1.4620 + 5682/\lambda^2$ ‡ |
| $n_e$ | $1.5525 + 9523/\lambda^2$ ‡ |

† $\varepsilon$ is measured at 1 kHz.

‡ $\lambda$ is a wavelength of incident light in nm.

$\pi/2$ (open circles) by using a PEM method. This optical retardation of $\pi/2$ corresponds to that of a QWP. It is then concluded that our imprinting technique is very powerful method of fabrication various patterned optical films. We also examined the patterned LCP film for their aligning capability. The optical retardation through the LC molecular layer on the patterned LCP film was measured as about $\pi$ (open triangles) by using a PEM method. This optical retardation of $\pi$ corresponds to that of two QWP and we found that the LC molecules on the patterned LCP film had a better alignment.

This result suggests that microgroove surfaces of the patterned LCP film can induce the alignment ability of LC molecules. The measured azimuthal anchoring energy, generated from the microgrooves, proved the possibility of aligning LC molecules by a TN LC cell implemented an imprinted optical film. Our LC cell have an imprinted optical film, which optical retardation is equal to that of a QWP, on the lower glass substrate and a PI alignment

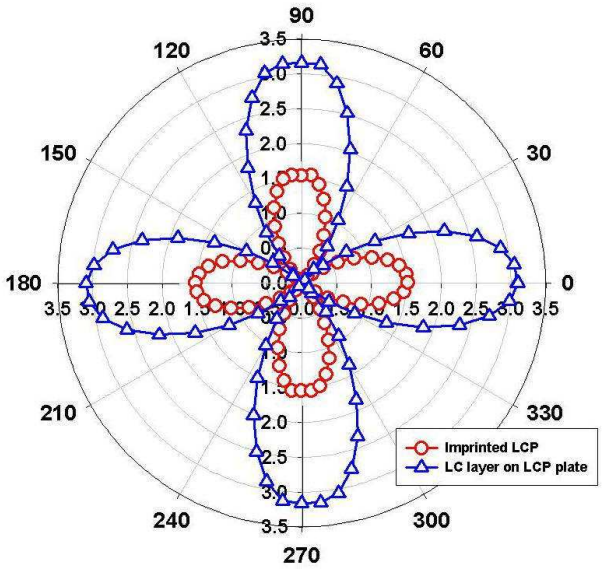


Figure 3.21: The optical retardation of the imprinted LCPs and aligned LCs on the imprinted LCP plate by using PEM technique measured as a function of the azimuthal rotation angle. Red open circles and blue open triangles denote optical retardations of the imprinted LCPs and aligned LCs on the imprinted LCP plate, respectively [100].

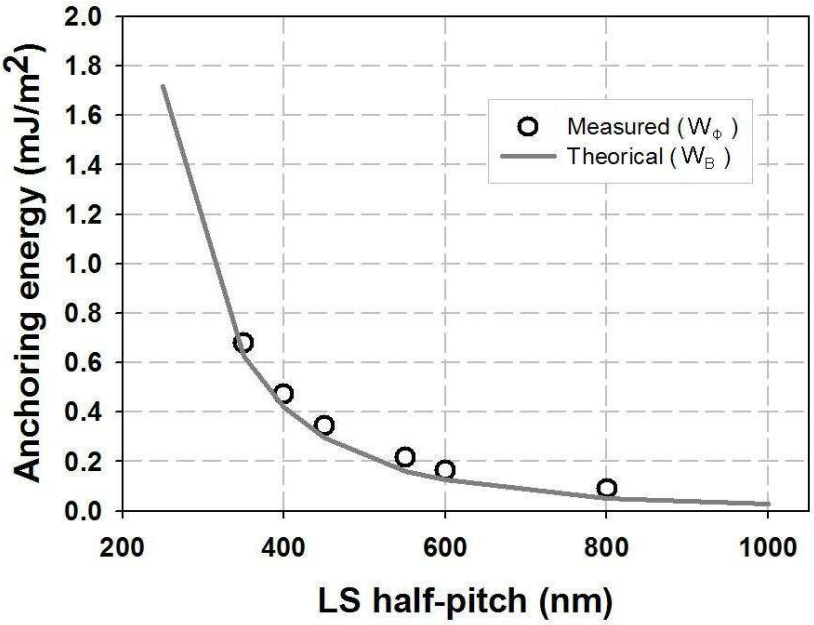


Figure 3.22: The azimuthal anchoring energy of nanoscale optical films having different half-pitches from 250 nm to 800 nm.

layer of JALS 146-R50 (JSR co., Japan) on the upper glass substrate. For fabricating TN LC alignment, the direction of micro-scale LS grooves of imprinted optical film is perpendicularly aligned that of rubbing of the PI alignment layer. The cell thickness (d) was maintained 5 $\mu$m thickness using glass spacers and the used LC material was MLC-6012 and injected into the TN LC cell by capillary action at room temperature. The azimuthal anchoring energy was measured using the cell rotation method for the TN

cell [103]. The azimuthal anchoring energy can be written as

$$W_\phi = 2K_2\phi/d \sin 2\phi \tag{3.22}$$

where $K_2$, d, and $\phi$ denote the twist elastic constant, the cell gap of the LC cell, and twist angle, respectively. Using the literature value of $K_2 = 5.5 \times 10$ pN. In the microgrooves of the imprinted optical films having the half-pitch of 2.0 $\mu$m with the LS ratio of 1, an azimuthal anchoring energy ($W_\phi$) was 8.43 $\times 10^{-6}$ J/m$^2$. From the theoretical point of view, within the Berreman formalism [104], the azimuthal anchoring energy is written as $W_B = 2\pi 3a^2K/\lambda^3$, where a, $\lambda$, and K represent the amplitude, the pitch of each microgroove in a sinusoidal shape, and the mean value of the splay and bend elastic constants. Based on the parameters we used for our TN LC cell, the amplitude a = 500 nm, the half-pitches ($\lambda/2$) from 250 nm to 800 nm, and the mean elastic constant $K = (K_1 + K_3)/2 = 13.9 \times 10^{-12}$ N, the theoretical value of the azimuthal anchoring energy is then predicted as from 0.1 $\times 10^{-3}$ J/m$^2$ (800 nm) to 0.7 $\times 10^{-3}$ J/m$^2$ (250 nm) as shown in Fig. 3.22. Comparing the measured result with the theoretical prediction, the measured value is fairly large due to the surface chemical effect of the aligned LCP molecules of the imprinted optical film. It should be noted that the magnitude of the azimuthal anchoring energy generated by the

microgrooves, on the order of about $10^{-4}$ J/m$^2$, is sufficient for aligning LCs over the film surface area.

Water contact angles were measured by the sessile drop technique using a Phoenix 300 surface angle analyzer (Surface Electro Optics, Korea) and analyze with ImagePro 300 software. Contact angle measurements provide a gauge of the relationship between a liquid and the surface characteristics of a solid on which the liquid is placed. The water contact angles were measured nanoscale optical films having different half-pitches from 250 nm to 1.5 $\mu$m. As shown in Fig. 3.23, the water contact angles were measured to be approximately from 110° (1.5 $\mu$m) to 130° (250 nm), respectively.

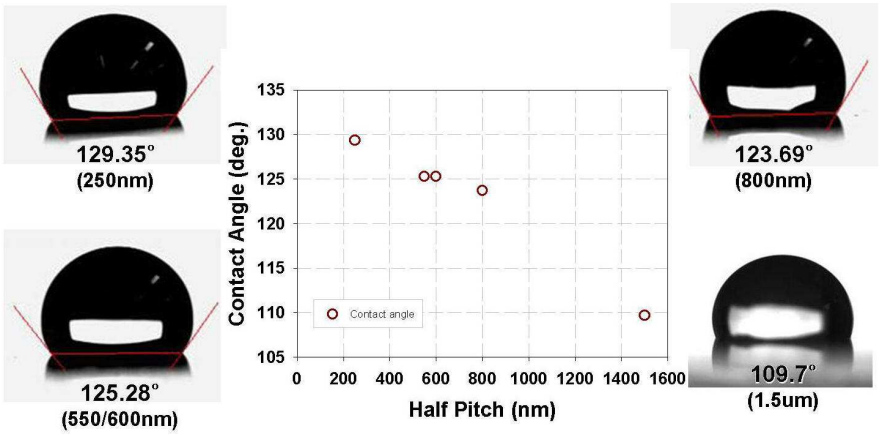


Figure 3.23: Contact angle measurements of a DI-water droplet on nanoscale optical films having different half-pitches from 250 nm to 800 1.5 $\mu$m.

### 3.4.2 Imprinted optical films with periodic multi-axes

We developed a novel optical film with multi-optic axes, fabricated based on LCP material using an imprinting technique [84, 105]. It is extremely important to produce an imprinted optical film (IOF) which can be used as both an anisotropic LCP retarder and a self-aligning capability of introduced LC molecules onto the IOF. In addition, it allows for a complementary layer (CL) of LC which is electrically tunable. Consequently, these imply that a simple and versatile fabrication of an in-cell patterned optical element, such as a voltage-dependent optical retardation modulator, can be achieved. Moreover, this imprinting technique, having only one-step process, produces multi-optical arrays of microstructures embossed on the LCP layer.

#### 1. Imprinting technique and replicated patterns

We used a PDMS mold with multi-directional micro-patterns and a commercial LCP material, RMS 03-001C (E. Merck) [106], to fabricate an anisotropic IOF. As shown as Fig. 3.24(a), the LCP material was spin-coated on an indium-tin oxide (ITO) glass substrate at the spinning rate of 3000 rpm for 30 seconds without any surface treatment and/or a pre-coated alignment layer, giving the layer thickness of 1.2 $\mu$m, and baked subsequently at 65 °C for 5 minutes. Figure 3.24(b) and (c) show schematic

diagrams of producing a patterned LCP film with multi-optic axes through an imprinting process which utilizes our PDMS mold with thickness of 5 cm. To prevent the PDMS mold from adhering to the patterned LCP film during the imprinting process, the surface of the PDMS mold was treated with vacuum evaporation of a silane agent, (tridecafluoro-1, 1, 2, 2,-tetrahydrooctyl)-1-1-trichlorosilane, for 1 minute [108]. By pressing the

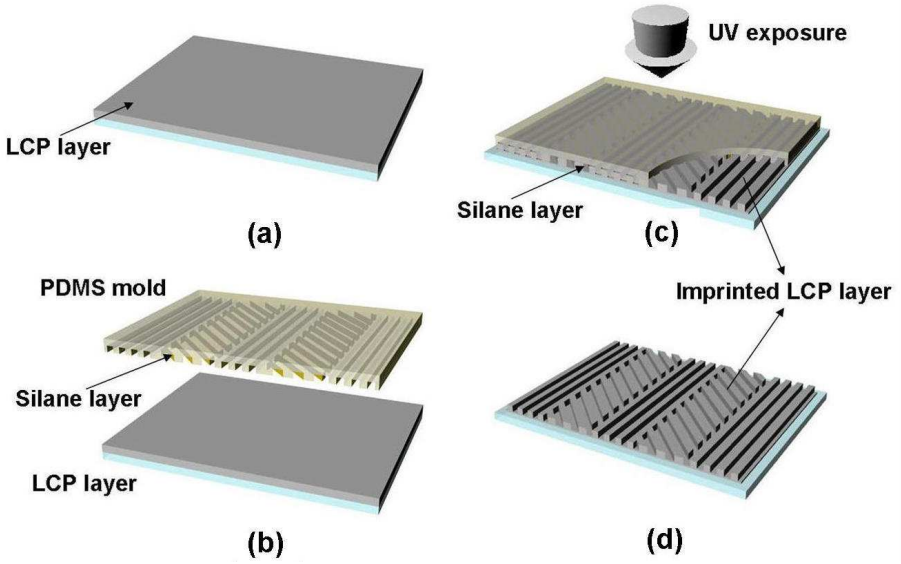


Figure 3.24: The schematic diagram showing the fabrication of a LCP based IOF with multi-optic axes. (a) Spin-coated LCP material onto ITO glass substrate. (b), (c) Patterned structure transferred from a PDMS mold to a LCP-coated substrate using imprinting technique. (d) IOF with multi-optic axes [107].

PDMS mold onto the prepared LCP layer, micro-patterns of the mold were replicated on the surface of the LCP layer. The patterns of the PDMS mold were well transferred to the LCP layer. After the patterns were formed on the LCP layer, the LCP layer was exposed to the UV light at the intensity of a 40 mW/cm$^2$ for 300 seconds under a $N_2$ atmosphere so as to preserve the shapes of micro-patterns. The IOF was then peeled off from the PDMS mold. Figure 3.25 show the SEM and FESEM images of microstructures produced on PDMS mold and those transferred on the LCP layer from the mold. As shown as the SEM image in Fig. 3.25(a), the PDMS mold consists of multi-domains with different directions, -45° and 0°, of LS of PDMS

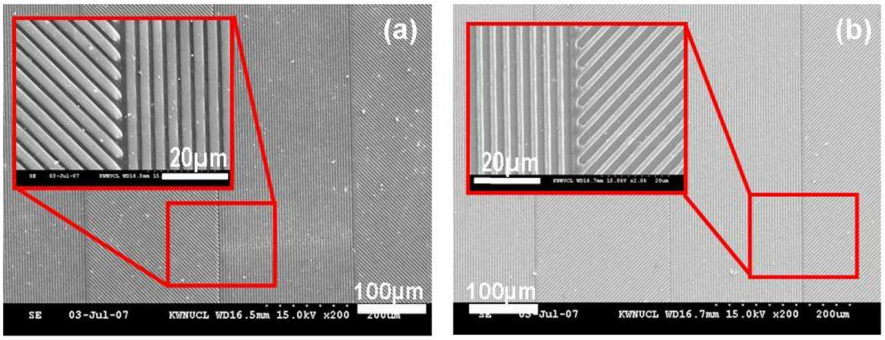


Figure 3.25: The SEM image of (a) a PDMS mold and (b) an imprinted LCP layer consist of multi-domains. In each domain, the pitch and the ratio of LS were 4.0 $\mu$m and 1 with different directions of LS. Enlarged images using FESEM show in a red-colored boxes [107].

mold and widths of an individual domain were varied from 10 $\mu$m to 100 $\mu$m. The half-pitch of the LS pattern was 2.0 $\mu$m in the LS ratio 1 and the depth was fixed as 300 nm. The feature sizes were determined using a SEM and the enlarged images using a FESEM show in the red-colored boxes. During the imprinting process, the PDMS mold served as a confinement for the rodlike LCP molecules and so imprinted LCP film with multi-domains of different optic axes, 0°, 45°, was induced. Figure 3.25(b) shows the SEM image of the imprinted LCP film corresponding to the negative LS shapes of the PDMS mold.

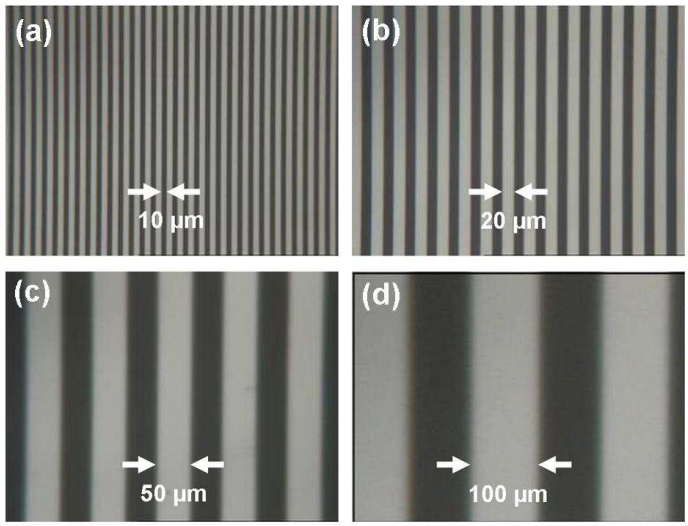


Figure 3.26: The POM images of the IOFs having different domain widths of (a) 10 $\mu$m, (b) 20 $\mu$m, (c) 50 $\mu$m, and (d) 100 $\mu$m, respectively [107].

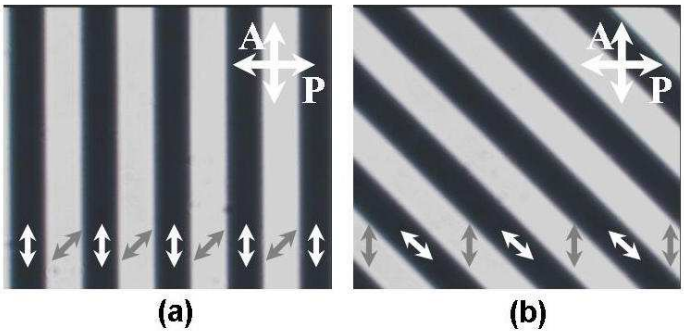


Figure 3.27: The microscopic textures of IOF with multi-axes observed under crossed polarizers (a) an angle of 0° and (b) 45° between the domain direction of IOF and the rear polarizer. Small white and gray arrows coincide with multi-domains with the directions of 45° and 0° aligned LS patterns, respectively.

Figure 3.26 show the POM images of microstructures transferred on the LCP layer from the PDMS molds with various widths of separated domain. The POM images shown from Fig. 3.26(a) to Fig. 3.26(d) correspond to IOFs having the domain widths of 10 $\mu$m, 20 $\mu$m, 50 $\mu$m, and 100 $\mu$m, respectively. As shown in Fig. 3.26, the IOF, the half-pitch of which was 2 $\mu$m with the LS ratio 1, shows bright and dark states along the directions of 45° and 0° between the direction of LS patterns in multi-domain and that of the rear polarizer. The patterns of IOF through an imprinting process which utilizes PDMS molds with multi-domains were well transferred to

the surface of LCP layer and thus, the POM images with different domain widths show well defined IOF with multi-optic axes. Note that the PDMS mold is soft enough to release the LCP film, and at the same time, it has nearly sufficient rigidity to prevent the broken of microstructures after the PDMS mold was peeled off [100]. Using our imprinting process combined with a UV exposure, micro-scale lines will be patterned with high regularity at precisely determined micro-scale intervals, strongly indicating that mi-

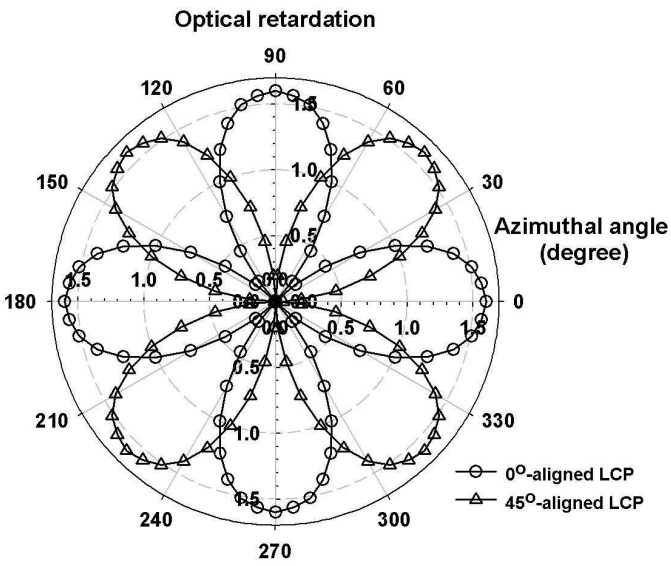


Figure 3.28: The optical retardation of the IOF measured as a function of azimuthal angle by the PEM technique. The open circles and the open triangles denote the IOF with multi-domains with the directions of 0° and 45° aligned LS patterns, respectively [107].

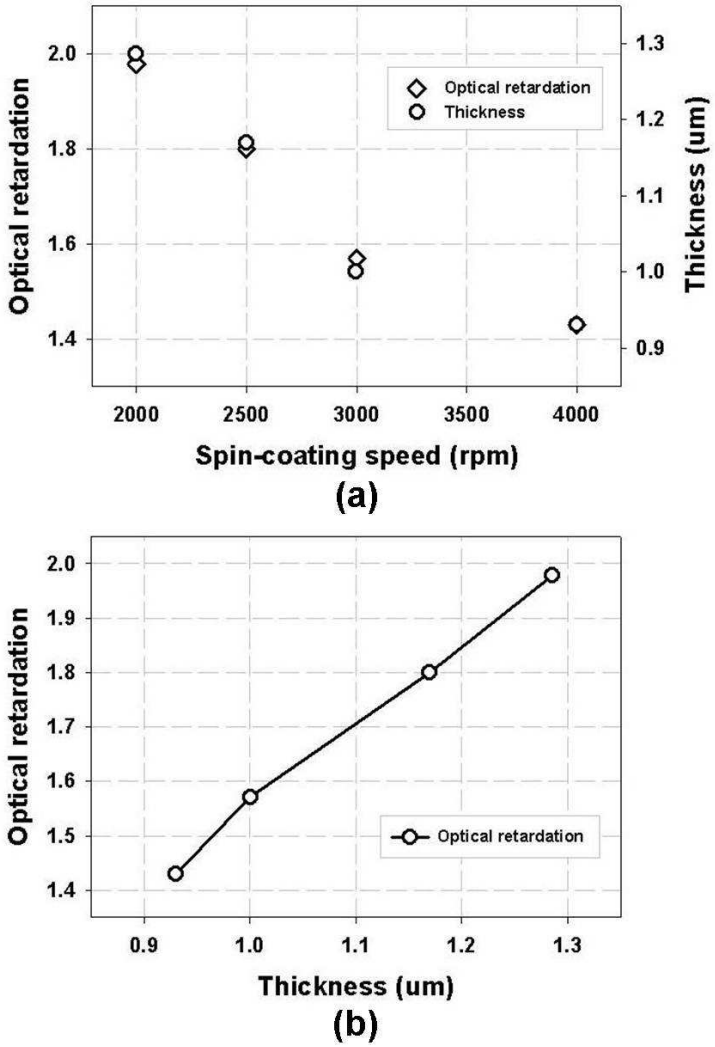


Figure 3.29: Optical retardations dependent spin-coating speed and thickness.

crostructures can be patterned with high feature density and precision. The micro-patterns of the PDMS mold were well transferred to the surface of the LCP layer under an imprinting pressure resulting from just above a gravitational force of the PDMS mold. After the micro-patterns were formed on the IOF, the film was exposed to UV light under a nitrogen atmosphere so as to preserve the shapes of the micro-patterns. The IOF with multi-patterned domains was then peeled off from the PDMS mold and resulting micro-patterns were preserved while the mold was released from the IOF.

Figures 3.27(a) and (b) show microscopic textures of IOF with multi-domains on the ITO glass substrate observed at an angle of 45° and 0° between the optic axes of the IOF and that of one of crossed polarizers using a POM. Two directions of LS pattern in the PDMS mold with multi-domains give rise to the multi-optic axes of the IOF. As shown in Fig. 3.27(a), the IOF shows bright and dark states along the directions of 45° and 0° between the optic axes of the IOF as an optical retarder and the rear polarizer. Small white and gray arrows coincide with multi-domains with the directions of 45° and 0° aligned LS patterns, respectively. Figure 3.27(b) shows microscopic texture when the IOF with multi-optic axes was rotated by an angle of 45° with respect to Fig. 3.27(a). In this case, the bright and dark states were reversed. This is direct evidence demonstrating that the

imprinting technique is capable of ordering LCP molecules and patterning LCP layer with multi-domains. As shown in Fig. 3.28, the measured optical retardation of the IOF using the PEM technique was about $\pi/2$ corresponds approximately to QWP ($\lambda/4$) of the wavelength used. A He-Ne laser of 632.8 nm was used as a light source. The optical retardation of the IOF could be controlled from $\pi/2$ to $\pi$ by spinning rate and/or content of liquid crystalline molecules in a LCP mixture as shown in Fig. 3.29.

**2. Thermal stability**

The thermal stability was monitored in terms of the retardation change in time at 150 °C and 200 °C. Note that the two temperatures correspond to the baking temperature of the LC alignment layer and the deposition temperature of metal electrodes. Figure 3.30 shows the measured thermal stability of the imprinted optical films in time dependence at 150 °C and 200 °C, which temperatures correspond to the baking temperature of the LC alignment layer and the deposition temperature of metal electrodes fabricated onto the optical films. The initial phase retardation of the LCP film was about 1.978 and the measured optical retardations of the imprinted film with curing times of 10 minutes were about 1.9159 at 150 °C and about 1.884 at 200 °C after heating for 6 hours, respectively. In conclusion, reductions

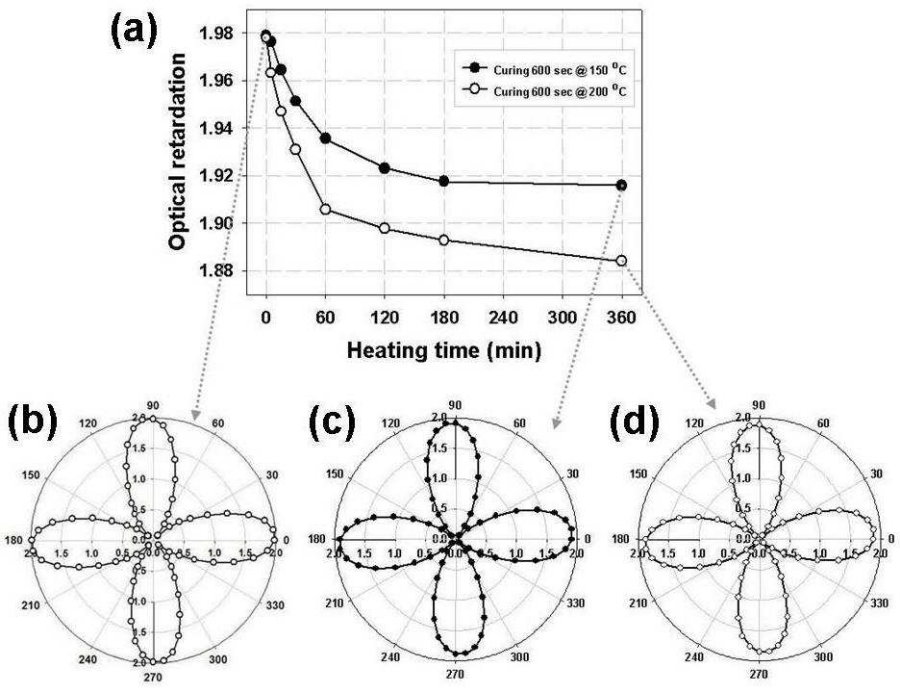


Figure 3.30: (a) The high stability of an imprinted optical film measured at 150 °C and 200 °C after 6 hours. (b) Initial optical retardation of the optical film. The optical retardation of the optical film at (c) 150 °C and (d) 200 °C after 6 hours [101].

of the phase retardation of the imprinted film at different heating temperatures were observed about 3 % and under 5 %, respectively. The measured results with adequate curing time, over 10 minutes, are on the high stable level with those of the photo-alignment induced LCP optical film (20 % reduction ratio) and the rubbing-induced LCP optical film (10 % reduction

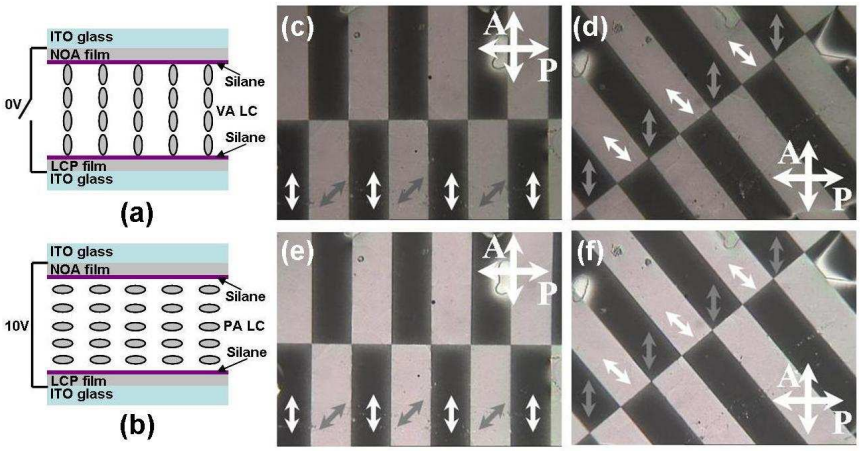


Figure 3.31: In-cell ETR fabricated with IOFs. The ETR configurations in (a) the absence of an applied voltage (0 V) and (b) the existence of an applied voltage (10 V). The microscopic textures of the retarder observed under crossed polarizers (c) an angle of 0° and (d) 45° between the direction of IOF and the rear polarizer in the absence of an applied voltage (0 V) and (e) an angle of 0° and (d) 45° between the direction of IOF and the rear polarizer in the existence of an applied voltage (10 V). Small white and gray arrows coincide with multi-optic axes, 45° and 0° aligned LS patterns, respectively [107].

ratio). Consequently, our imprinted multi-axes optical LCP film has enough thermal stability and lower degradation of optical efficiency.

### 3. Electrically tunable retarder (ETR)

This imprinting technique, having only one-step process, produces an IOF with multi-array of microstructures embossed on the LCP layer. Moreover, it was achieved that transferred completely LCP film with multi-optic axes, the difference of which is a 45° between at both domains. The optical anisotropy of IOF was observed with a POM and the optical retardation of the IOF was measured using a PEM method and the self-aligning capa-

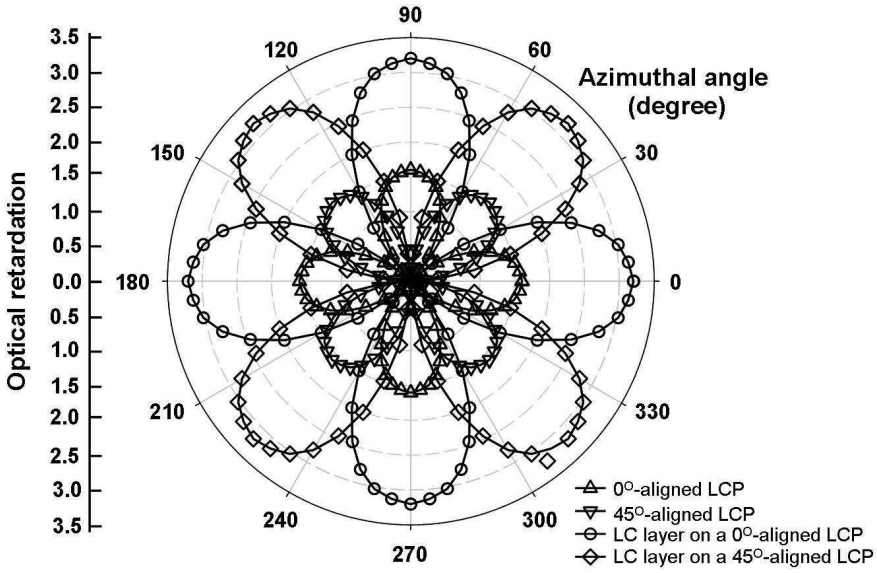


Figure 3.32: The optical retardation of the IOF measured as a function of azimuthal angle by the PEM technique. The open circles and the open triangles denote the IOF with multi-domains with the directions of 0° and 45° aligned LS patterns, respectively [107].

bility of LCs and effect of silane treatment on the IOF were observed with a POM and measured using a contact angles measurement, PEM method, azimuthal anchoring energy measurement. Finally, structures and optical properties of an in-cell ETR fabricated using the IOF were introduced in section. Through the imprinting process, an optically anisotropic IOF was fabricated on the inner side of glass substrate. Using the Berreman concept, the microgrooves were prepared on the surface of the anisotropic IOF to provide the spontaneous alignment of LC molecules on the IOF without using any surface treatment or an extra alignment layer. The measured azimuthal anchoring energy, generated from the microgrooves, proved the possibility of aligning LC molecules by a TN LC cell implemented an IOF. Our LC cell have an IOF, which optical retardation is equal to that of a QWP, on the lower glass substrate and a PI alignment layer of JALS 146-R50 on the upper glass substrate. For fabricating TN LC alignment, the direction of micro-scale LS grooves of IOF is perpendicularly aligned that of rubbing of the PI alignment layer. The cell thickness ($d$) was maintained 5 $\mu$m thickness using glass spacers and the used LC material was MLC-6012 and injected into the TN LC cell by capillary action at room temperature. The azimuthal anchoring energy was measured using the cell rotation method for the TN cell. The azimuthal anchoring energy can be written as $W_\phi$

$= 2K_2\phi/d\sin^2\phi$ where $K_2$, $d$, and $\phi$ denote the twist elastic constant, the cell gap of the LC cell, and twist angle, respectively. Using the literature value of $K_2 = 5.5 \times 10^{-12}$ N. In the microgrooves of the IOFs having the half-pitch of 2.0 $\mu$m with the LS ratio of 1, an azimuthal anchoring energy ($W_\phi$) was 8.43 $\times 10^{-6}$ J/m$^2$. From the theoretical point of view, within the Berreman formalism, the azimuthal anchoring energy is written as $W_B = 2\pi^3 a^2 K/\lambda^3$, where $a$, $\lambda$, and $K$ represent the amplitude, the pitch of each microgroove in a sinusoidal shape, and the mean value of the splay and bend elastic constants. Based on the parameters we used for our TN LC cell, the amplitude $a = 300$ nm, the pitch $\lambda = 4$ $\mu$m, and the mean elastic constant $K = (K_1 + K_3)/2 = 13.9 \times 10^{-12}$ N, the theoretical value of the azimuthal anchoring energy is then predicted as 1.21 $\times 10^{-6}$ J/m$^2$ [101]. Comparing the measured result with the theoretical prediction, the measured value is fairly large due to the surface chemical effect of the aligned LCP molecules of the IOF. It should be noted that the magnitude of the azimuthal anchoring energy generated by the microgrooves, on the order of about $10^{-5}$ J/m$^2$, is sufficient for aligning LCs over the film surface area.

### Contact angle measurement

Water contact angles were measured by the sessile drop technique using a Phoenix 300 surface angle analyzer (Surface Electro Optics, Korea) and analyze with ImagePro 300 software.

When the silane based treatment onto the surface of IOF, the micro-patterns was not only well transferred from the mold but also controlled of the surface wettability. Here, the effect of silane treatment was measured using a measurement of the contact angle. Contact angle measurements provide a gauge of the relationship between a liquid and the surface characteristics of a solid on which the liquid is placed. The water contact an-

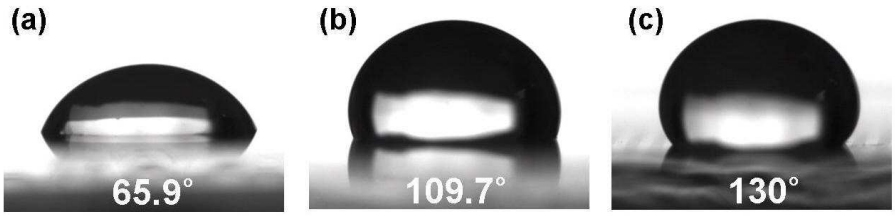


Figure 3.33: Contact angle measurements of a DI-water droplet on several surfaces. (a) Spin-coated LCP layer and (b) Fluorinated with (tridecafluoro-1,1,2,2-tetrahydrooctyl)-1-1-trichlorosilane on the surface of coated LCP layer before curing. (c) Imprinted, patterned LCP film with silane layer after curing by exposure of UV light [107].

gle was measured before and after surface of LCP film was treated with a silane agent, and compared with that of IOF. As shown in Fig. 3.33, the water contact angle of a spin-coated LCP layer before silane treatment was measured to be approximately 65.9°. However, when the silane treated on surface of the IOF, the contact angle increased to 130°. Consequently, the hydrophobic surface of the IOF induces a vertically alignment (VA) of LCs.

## 3.5 In-Cell Polarizers

The most essential passive optical element in LCDs is the polarizer. Polarizers are indispensable for the displaying of the information content and important front-of-screen performance parameters, such as brightness and contrast, are strongly influenced by the performance of the polarizer. Currently, the most widely used polarizers for LCD applications are derivatives of the H-sheet polarizer as invented by E. H. Land [98]. These dichroic polarizers are based on uniaxially stretched poly(vinyl alcohol) that is impregnated with iodine or doped with dichroic dyes. These sheet polarizers show excellent optical performances that can be expressed by the polarization efficiency (PE) in combination with the single-piece transmittance ($T_{sp}$, which means a transmission of unpolarized light through a single polarizer,

as

$$PE = \sqrt{\frac{T_p - T_c}{T_p + T_c}} \times 100\% \tag{3.23}$$

$$T_{sp} = \frac{10^{-A_p} + 10^{-A_c}}{2} \tag{3.24}$$

where $T_p$ and $T_c$ are defined as the transmission of unpolarized light through two polarizers with their transmission axis parallel and perpendicular, respectively, and where $A_p$ and $A_c$ are defined as the absorbance parallel and perpendicular to the average orientation of the long axis of the chromophores, respectively. The polarizer performance can also be expressed by a single parameter; the extinction ratio (ER)

$$ER = \frac{T_p}{T_c} \tag{3.25}$$

For high-end sheet polarizers such as those applied in LCD monitors or flat-panel televisions, the performance exceeds a polarization efficiency (PE) of 99.9 % at a single-piece transmission of 43.5 [109, 110]. Unfortunately, two triacetylcellulose (TAC) layers are needed in conventional polarizers to protect the stretched poly(vinyl alcohol) film on both sides against moisture and to obstruct relaxation effects under influence of heat and/or humidity by which the PE value would deteriorate. Further, an adhesive layer is needed in order to laminate the polarizer to the display. The necessary use

of protective and adhesive layers adds unnecessary use of protective and adhesive layers adds unnecessary thickness to H-sheet polarizers. Finally, these polarizers show limited thermal stability and low resistivity against solvents.

Numerous advantages are foreseen when the traditional sheet polarizers are replaced by ultrathin coatable polarizers situated on the inside of the cell (in-cell). Apart from a significant reduction in display thickness and weight, the positioning of the polarizers inside the cell eliminates all parallax-related issues and is beneficial to the robustness of the display. Furthermore, substrates that otherwise would be rejected because of their birefringence, e.g., thin, low-weight, and strong plastic foils or cheap, low-quality glass substrates, can be used when the polarizers are situated inside the LCD cell. The optimal position of the coatable polarizers inside the LCD cells can vary between the electrodes in order to prevent the need for increased driving voltages of the LCD panels.

One possible approach to obtaining thin, coatable polarizers is based on the use of lyotropic liquid crystalline dyes that form a crystalline polarizer with sub-micrometer film thickness after coating and evaporation of the solvent. [111–113] A few reports are known on patterned polarizers based on the combination of lyotropic dyes and photoalignment layer. [114, 115]

In all cases the polarization performance is insufficient for almost all mainstream LCD applications. Here we report on thin-film polarizers based on highly ordered guest-host systems. These thin-film polarizers hold all of the advantages mentioned above and can meet the polarization performance of traditional sheet polarizers at film thicknesses of only $\sim \mu$m, whereas conventional sheet polarizers have a thickness of approximately 100 $\mu$m.

Our approach towards thin, coatable polarizers utilizes the in- situ photopolymerization of reactive LCs. The low viscosity of the reactive LCs facilitates easy alignment, while the in situ photopolymerization provides freedom in choosing the polymerization temperature and conditions enabling the selection of the optimum phase and molecular order. This technology has been applied in the preparation of numerous optical foils, for example, patterned retarder [116], broadband circular polarizers [33], wide viewing angle films [117], and cholesteric color filters [118].

We utilize this technology for the preparation of guest-host polarizers. Dye molecules with an elongated structure are dissolved in a LCP host together with a small amount of photoinitiator. Upon alignment of the host material, for instance, through means of an alignment layer, the dye molecules are co-aligned, resulting in dichroic absorption of the dye molecules. In situ photopolymerization of the LCPs results in the forma-

tion of a crosslinked network that stabilizes the anisotropic properties of the film.

In order to determine the highest attainable polarization performance of guest-host polarizers based on LCPs, the dichroic ratio for a dichroic dye in the different LCPs has been determined form polarized UV-vis spectroscopy. For this purpose, LCPs were doped with 1 wt.% of the dichroic azo dyes, exhibiting an elongated structure similar to the selected LCPs. LC cells with a 1.2 $\mu$m cell gap and an antiparallel alignment were filled with the dye-doped liquid crystalline compounds at elevated temperatures through capillary forces and were subsequently placed in a hot stage inside an UV-vis spectrometer. Polarized UV-vis absorption measurements under 0° and 90° with respect to the alignment direction were recorded at different temperatures.

### 3.5.1 Fabrication of a dichroic dye-containing polarizer by imprinting technique

We used a commercial dichroic azo dye materials, G-241, G-472, and G-207 (Hayashibara, Japan) [119] to fabricate a thin film dye-polarizer. According to Appendix A, the dichroic dyes have high ordering due to the orienta-

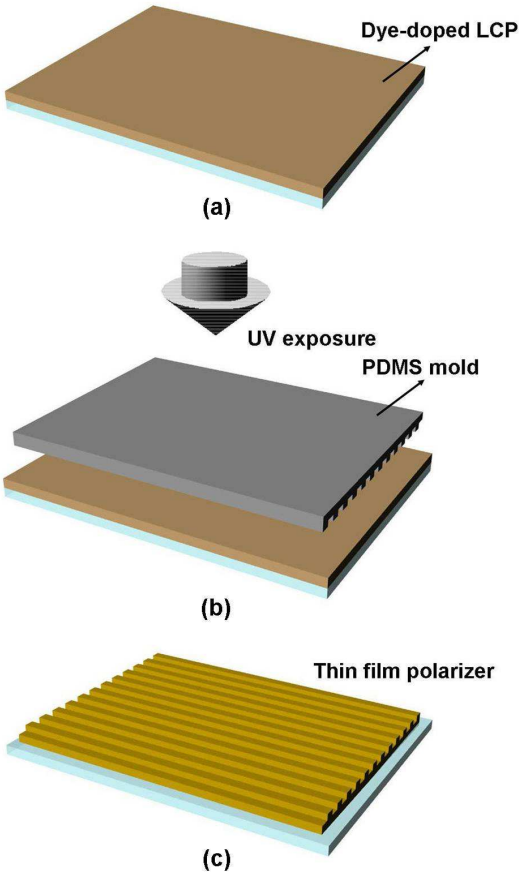


Figure 3.34: The schematic diagram showing the fabrication of a dye-doped LCP based thin film polarizer. (a) Spin-coated dye-doped LCP material onto ITO glass substrate. (b) Patterned structure transferred from a PDMS mold to a dye-doped LCP coated substrate using imprinting technique. (c) Thin film dye-polarizer with microstructure surface.

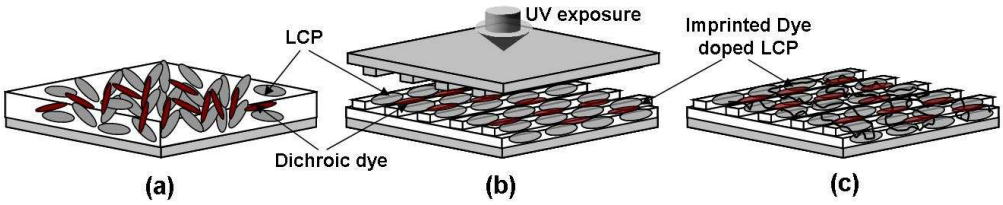


Figure 3.35: The mechanism of dye-polarizer using imprinting process.

tional rigidity induced by the length of five azo groups. Figure 3.34 shows a schematic diagram of producing a dye-polarizer through an imprinting process which utilizes our PDMS polymer mold. The dichroic azo dyes 1 wt.% doped LCP materials were first spin-coated on a glass substrate at the spinning rate of 1000 rpm for 30 seconds, giving the layer thickness of about 2 $\mu$m, and baked subsequently at 65°C for 1 minute. By pressing the PDMS mold onto the prepared dye-doped LCP layer, micro-patterns of the mold were replicated on the dye-doped LCP layer. The micro-patterns of the PDMS mold were well transferred to the surface of the dye-doped LCP layer under an imprinting pressure resulting from just above a gravitational force of the PDMS mold. After the micro-patterns were formed on the dye-doped LCP layer, the dye-doped LCP layer was exposed to the UV light at the intensity of 40 mW/cm$^2$ for 5 minutes under a $N_2$ atmosphere so as to preserve the shapes of the micro-patterns. The imprinted dye-doped LCP

film was then peeled off from the PDMS mold. The optical transmittance and absorption dependent parallel and perpendicular respect to polarized incident light were measured with a UV-vis spectrometer. Non-aligned dye-doped LCP molecules (Fig. 3.35.(a)) were induced by using imprinting process (Fig. 3.35.(b)) and thus, the imprinted dye-doped LCP layer was photocrosslinked by UV exposure during imprinting process (Fig. 3.35.(c)).

### 3.5.2 Results and discussion

These dye-polarizers are based on imprinted LCP material doped dichroic dyes. These thin film polarizers show excellent optical performances that can be expressed by the polarization efficiency (PE) in combination with the single-piece transmittance ($T_{sp}$, which means a transmission of unpolarized light through a single polarizer, where $T_p$ and $T_c$ are defined as the transmission of unpolarized light through two polarizeres with their trnasmission axis parallel and perpendicular, respectively, and where $A_p$ and $A_c$ are defined as the absorbance parallel and perpendicular to the average orientation of the long axis of the chromophores, respectively.

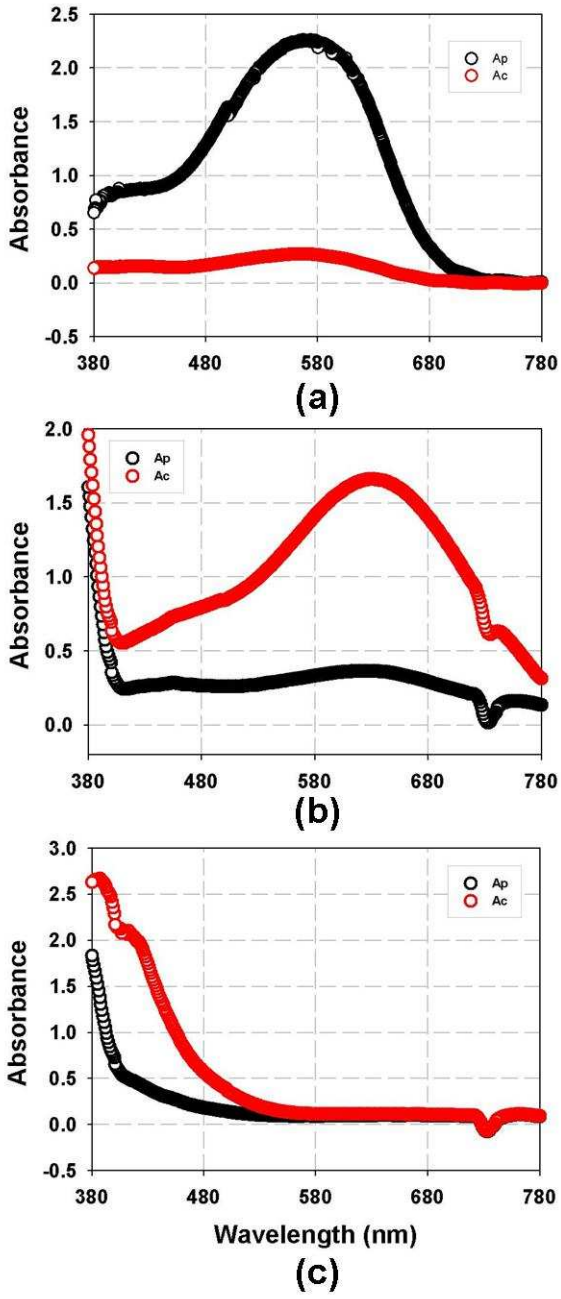


Figure 3.36: The absorption dependent polarization direction of our polarizer doped dichroic dyes such as (a) G-241, (b) G-472, and (c) G-207.

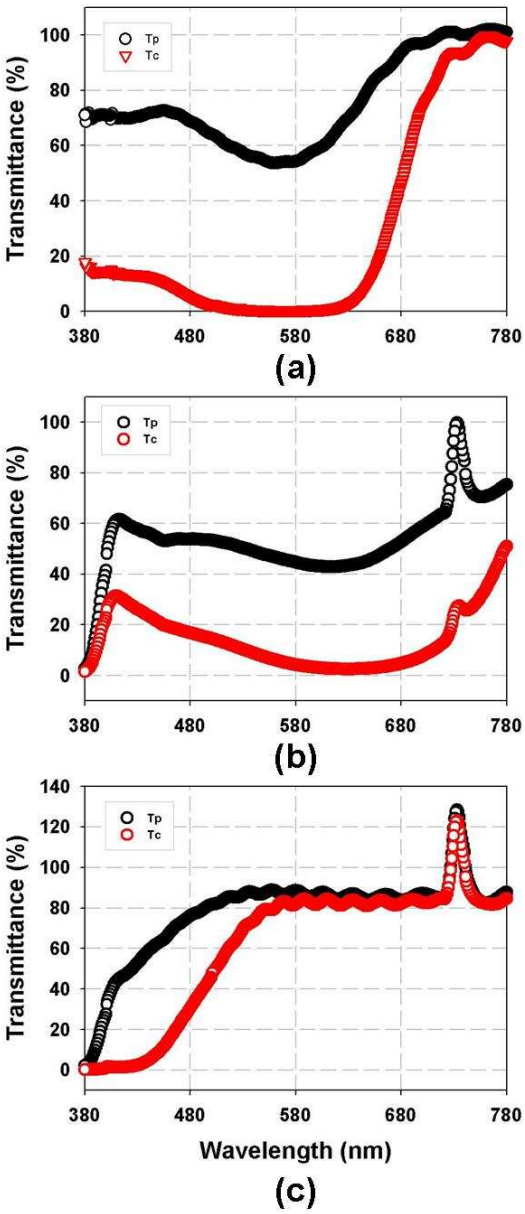


Figure 3.37: The transmission dependent polarization direction of our polarizer doped dichroic dyes such as (a) G-241, (b) G-472, and (c) G-207, respectively.

### 1. Optical properties

The absorption dependent polarization direction of our polarizer doped dichroic dyes. Where $A_p$ and $A_c$ are defined as the absorbance parallel and perpendicular to the average orientation of the long axis of the chromophores, respectively. The maximum absorption wavelengths of the doped dichroic dyes are 554 nm (G-241), 619 nm (G-472), and 425 nm (G-207), respectively. Figures 3.36(a), (b), and (c) show the absorption dependent polarization direction of our polarizer doped dichroic dyes such as G-241, G-472, and G-207, respectively. As shown in respective Figs. 3.36(a), (b), and (c), black and red symbols denote $A_p$ and $A_c$. Those are absorption of polarized light through their sample axis parallel and perpendicular, respectively.

Figure 3.37 shows the transmission dependent polarization direction of our polarizer doped dichroic dyes such as G-241, G-472, and G-207. $T_p$ and $T_c$ are transmission of unpolarized light through two polarizers with their transmission axis parallel and perpendicular, respectively. The maximum absorption wavelengths of the doped dichroic dyes are 554 nm (G-241), 619 nm (G-472), and 425 nm (G-207), respectively. Figures 3.37(a), (b), and (c) show the transmission dependent polarization direction of our polarizer

doped dichroic dyes such as G-241, G-472, and G-207, respectively. As shown in respective Figs. 3.37(a), (b), and (c), black and red symbols denote $T_p$ and $T_c$. Those are transmission of unpolarized light through two polarizers with their transmission axis parallel and perpendicular, respectively.

Figure 3.38 shows the polarization efficiency in combination of the $T_p$ and $T_c$ above shown in Fig. 3.37. According to Eq.3.23 and 3.24, the performance exceeds a PE of over 98 % and a single-piece transmission of 27.4 % at a wavelength from 530 nm to 630 nm as shown in Fig.3.38(a). The performance exceeds a PE of over 95 % and a single-piece transmission of 22.7 % at a wavelength from 580 nm to 680 nm and over 97 % and a single-piece transmission of 19.4 % at a wavelength from 380 nm to 450 nm as shown in Figs.3.38(b) and (c), respectively.

**2. Samples of dye-polarizers**

We utilize this technology for the preparation of dichroic azo dyes doped LCP layer as a guest-host polarizers. Dye molecules with an elongated structure are dissolved in a LCP host together with a small amount of photoinitiator. Upon alignment of the host material, for instance, through means of an alignment layer, the dye molecules are co-aligned, resulting in

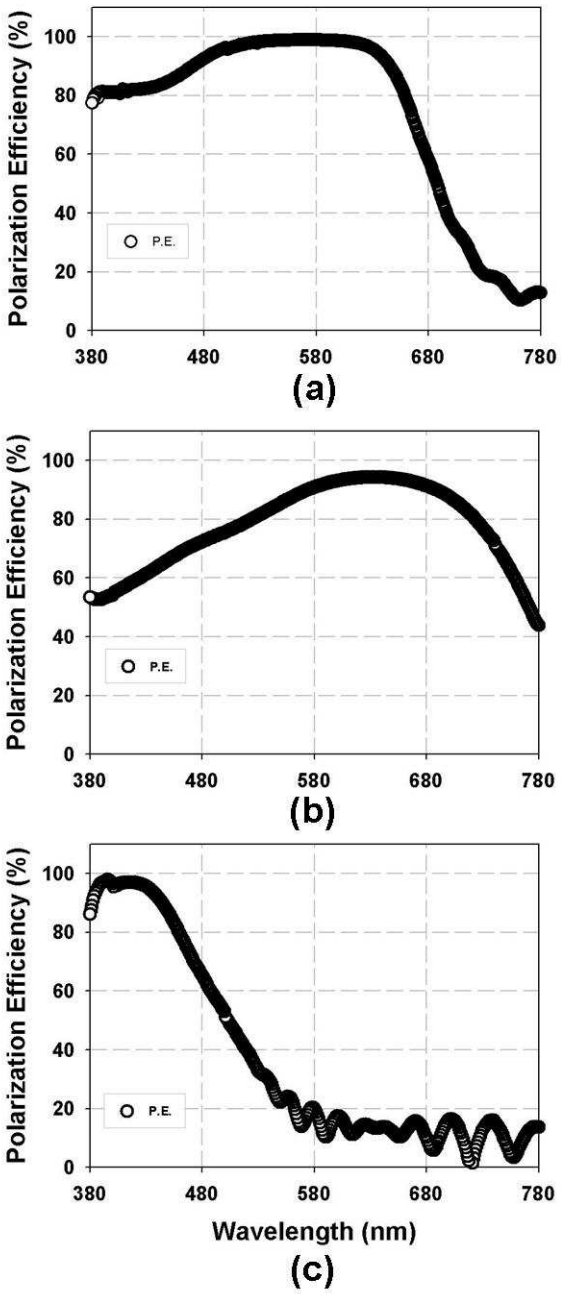


Figure 3.38: The polarization efficiency (PE) of our polarizer doped dichroic dyes such as (a) G-241, (b) G-472, and (c) G-207, respectively.

dichroic absorption of the dye molecules. In photopolymerization of the LCP s results in the formation of a crosslinked network that stabilizes the anisotropic properties of the film.

Figure 3.39 shows the photograph of our polarizer doped dichroic dye such as G-241. Due to imprint lithography, LS pattern direction transferred from PDMS mold to surface of the dichroic dye doped LCP layer. These patterns were preserved by using UV exposure during the imprinting process. As shown in Fig. 3.39(a), our polarizer sample is perpendicular respect to the direction of polarized incident light. The other is parallel respect to the direction of polarized incident light as shown in Fig. 3.39(b).

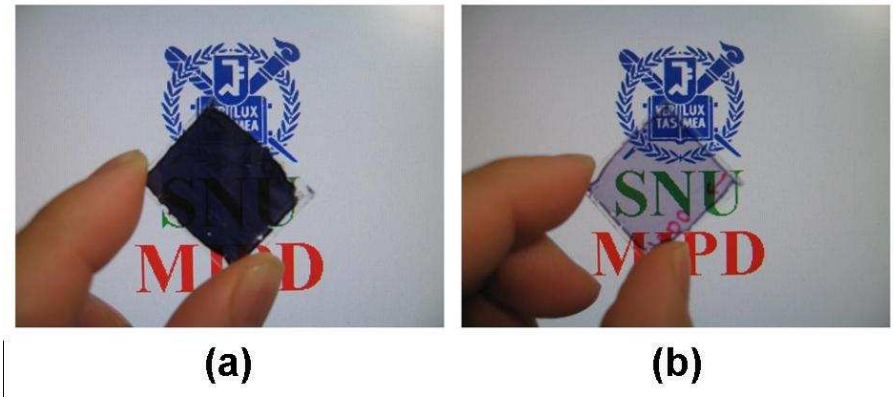


Figure 3.39: Photograph of our polarizer doped dichroic dye such as G-241. (a) Perpendicular and (b) parallel transmission axis in respect to linear polarized light.

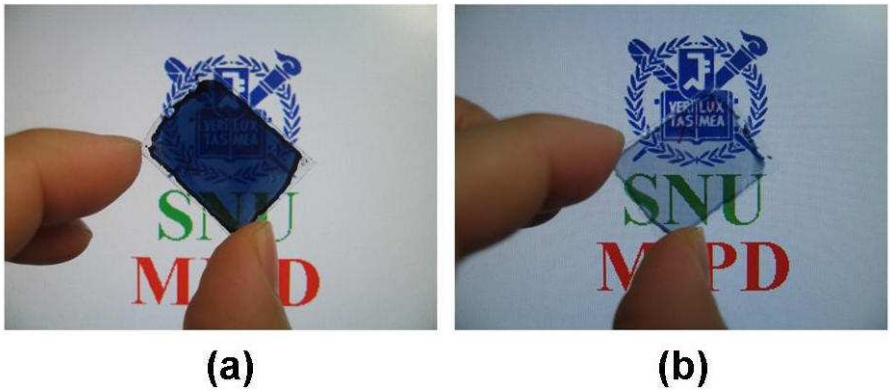


Figure 3.40: Photograph of our polarizer doped dichroic dye such as G-472. (a) Perpendicular and (b) parallel transmission axis in respect to linear polarized light.

According to Eq.3.25, the extinction ratio (ER) of our dichroic dye doped is nearly 100 at about wavelength of 560 nm.

Figure 3.40 shows the photograph of our polarizer doped dichroic dye such as G-472. Due to imprint lithography, LS pattern direction transferred from PDMS mold to surface of the dichroic dye doped LCP layer. These patterns were preserved by using UV exposure during the imprinting process. As shown in Fig. 3.40(a), our polarizer sample is perpendicular respect to the direction of polarized incident light. The other is parallel respect to the direction of polarized incident light as shown in Fig. 3.40(b). According to Eq.3.25, the ER of our dichroic dye doped is nearly 60 at

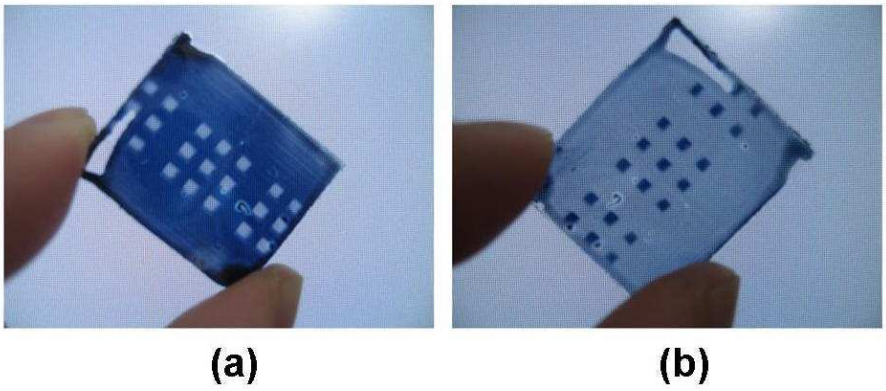


Figure 3.41: Photograph of our patterned polarizer. (a) Perpendicular and (b) parallel transmission axis in respect to linear polarized light.

about wavelength of 620 nm.

The versatility of the guest-host polarizer based on imprinted photopolymerization is demonstrated in Fig. 3.41. A patterned polarizer is obtained by UV curing the dye-doped LCP under $N_2$ atmosphere during imprinting process using PDMS mold with multi-axes. Due to imprinting with multi-axes, Fig. 3.41 shows the photograph of our patterned polarizer. As shown in Fig.3.41(a), multi-optic axes, 0° and 90°, respect to that of polarizer. Figure3.41(b) shows inversion image of the Fig.3.41(a).

### 3. Our thin film polarizer

Figure 3.42 shows our thin film polarizer doped three dichroic dyes. For fabricating our thin film polarizer, three dichroic dyes such as G-241, G-

472, and G-207 doped in the soluble LCP material. These dyes mixed 1 wt.%, respectively. Figure 3.43 shows the absorption dependent polarization direction of our polarizer. As shown in Figs. 3.43(a) and (b), black and red symbols denote $A_p$ and $A_c$. Those are absorption of polarized light through their sample axis parallel and perpendicular, respectively.

Figure 3.44 shows the transmission dependent polarization direction of our polarizer doped dichroic dyes such as G-241, G-472, and G-207. $T_p$ and $T_c$ are transmission of unpolarized light through two polarizers with their transmission axis parallel and perpendicular, respectively. Figure 3.45 shows the polarization efficiency in combination of the $T_p$ and $T_c$ above


Figure 3.42: Photograph of our thin film polarizer doped three dichroic dyes. (a) Perpendicular and (b) parallel transmission axis in respect to linear polarized light.

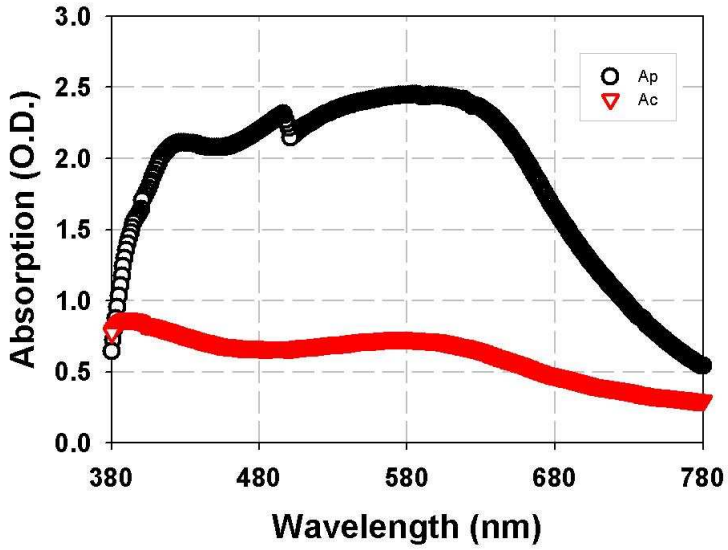


Figure 3.43: The absorption dependent polarization direction of our polarizer doped three dichroic dyes such as G-241, G-472, and G-207.

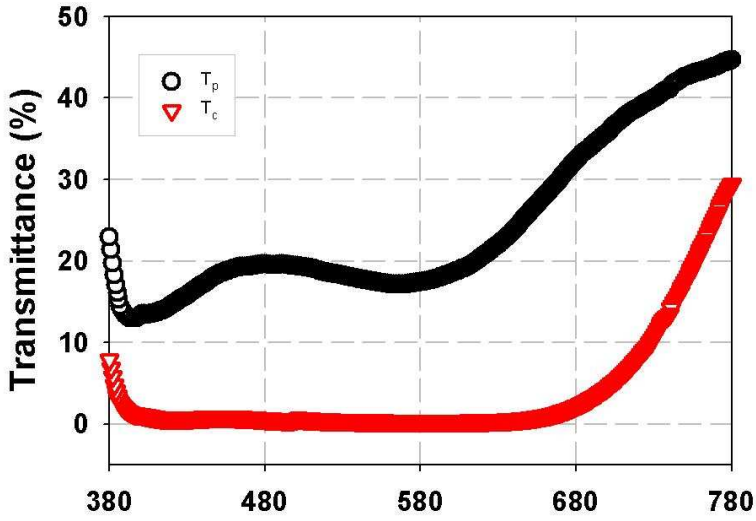


Figure 3.44: The transmission dependent polarization direction of our polarizer doped three dichroic dyes such as G-241, G-472, and G-207.

shown in Fig. 3.45. According to Eq.3.23, the performance exceeds a PE of over 96 % at a wavelength from 400 nm to 680 nm as shown in Fig.3.45.

According to Eq.3.25, the ER of our dichroic dye doped is nearly 60 at about wavelength of 620 nm as shown in Fig.3.46.

In conclusion, we have demonstrated the feasibility of high-contrast, thin-film, guest-host polarizers based on photopolymerization of LCPs doped dichroic dyes by using imprinting technique. During imprinting process, LCP molecules were aligned by microsturctures on the surface of PDMS mold. And thus, dye molecules with an elongated structure are dis-

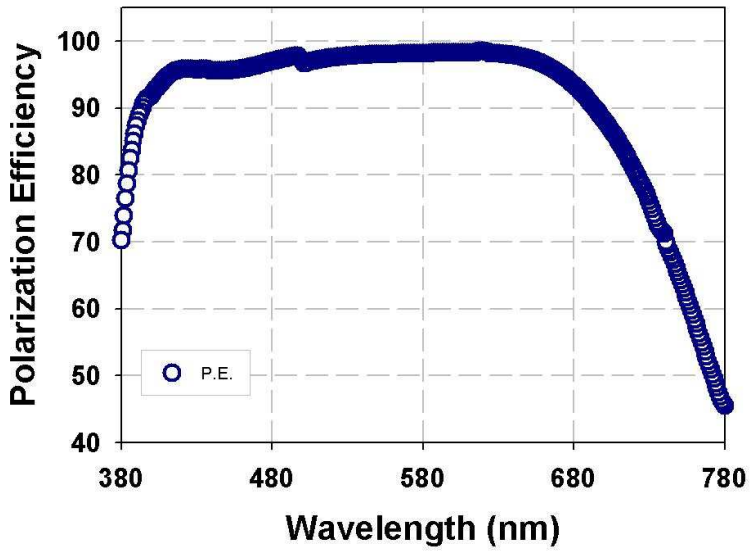


Figure 3.45: The polarization efficiency (PE) of our polarizer doped three dichroic dyes such as G-241, G-472, and G-207.

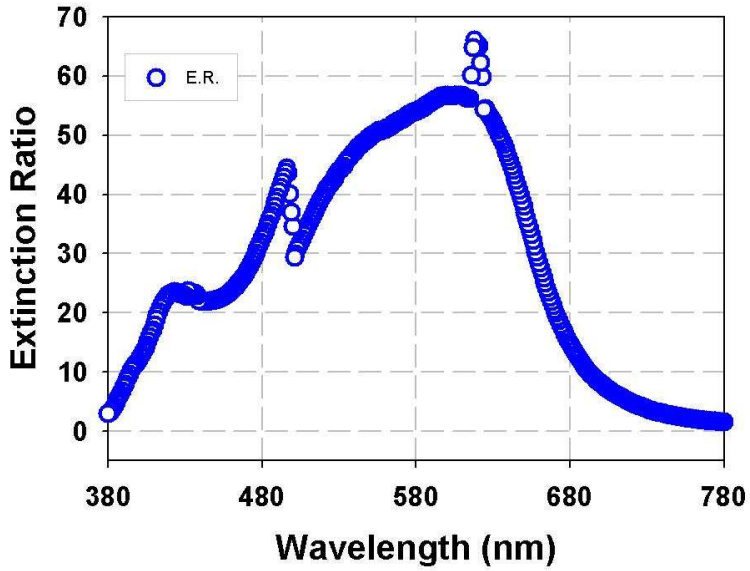


Figure 3.46: The extinction ratio of our thin film polarizer doped three dichroic dyes.

solved in a LCP host together with a small amount of photoinitiator. Upon alignment of the host material, for instance, through means of an alignment layer, the dye molecules are co-aligned, resulting in dichroic absorption of the dye molecules. In situ photopolymerization of the LCPs results in the formation of a crosslinked network that stabilizes the anisotropic properties of the film. Within the absorption band of the dye, the polarization performance of these guest-host polarizers exceeds the performance of other thin film polarizer technologies and equals that of state of the art sheet polarizers. Further optimization of dichroic dye mixture is required in order to

obtain high-performance, color-neutral, guest-host polarizers. In our view, guest-host polarizers offer numerous advantages over traditional sheet polarizers as they have reduced thickness and weight, can be applied in-cell, and can be patterned. Therefore, we believe that the presented thin-film polarizer technology based on LCPs is highly promising and may prove to be an attractive alternative for traditional sheet polarizers in LCD applications such as transflective LCD.

### 3.5.3 Application of in-cell polarizer

We developed an organic light emitting diode (OLED) embedded an in-cell polarizer. The in-cell polarizer, fabricated inside device by an imprinting process, has multi-functionality of light emission with polarization selectivity and highly efficient luminance. Accordingly, this configuration of OLED is expected to be applied as an efficient light source application in liquid crystal displays.

#### Introduction

Recently, the application of the OLED [120] devices as an efficient light source is attracting much attention due to low power consumption and the potentials for large area planar light sources. In addition to the interest on

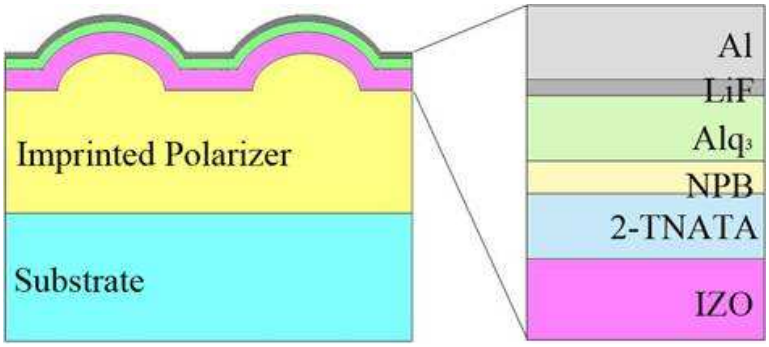


Figure 3.47: The schematic of the proposed OLED device with in-cell imprinted polarizer.

white OLEDs (WOLEDs) for interior lightings, many approaches to utilize OLEDs as back light units (BLUs) in LCDs have been proposed for the efficient power consumption and the compactness of devices. The majority of such researches have tried to produce linearly polarized emission, which is required due to the intrinsic characteristics of the LCDs, directly from the OLED by the surface treatment of active area such as rubbing [121] or the friction-transfer methods [122]. However, their polarizing efficiencies were far from the sufficient level for the practical use, and the emission characteristics also decreased due to the damage and/or contamination on active layer. Here, we propose an OLED embedding an imprinted in-cell polarizer 3.47. By employing the in-cell polarizer, we can efficiently produce polarized emission without any direct treatment on the active area, and

moreover, the microstructures produced during the imprinting process can significantly improve the luminance efficiency of the device.

In addition, imprinted thin polarizer with microstructures situated on the inside of the cell (in-cell). Apart from a significant reduction in display thickness and weight, the positioning of the polarizers inside the cell eliminates all parallax-related issues and is beneficial to the robustness of the display, especially flexible devices.

**Experiments**

We utilize imprinting technique for the preparation of guest-host polarizers. Dye molecules with an elongated structure are dissolved in a LCP host together with a small amount of photo-initiator. Upon alignment of the host material during imprinting process, for instance, through means of micro-patterns of PDMS mold, the dye molecules are co-aligned, resulting in dichroic absorption of the dye molecules. In situ photopolymerization of the LCPs results in the formation of a crosslinked network that stabilizes the anisotropic properties of the film.

Our method used to fabricate in-cell polarizer is very similar with the Berreman approach which has been used for the alignment of LC molecules. By imprinting LCP layer using microstructured stamp, the alignment of

dye-doped LCP was induced due to the azimuthal anchoring energy of the microstructures. The fabricated LCP layer had an anisotropic light absorption due to the dichroic characteristic of the azo-dye, which results to a linear polarization of the emission light. Figure 3.47 schematically shows a cross-sectional structure of the proposed device fabricated by such imprinting process. As shown in Fig. 1, the doped LCP layer having microstructures were produced between the substrate and the transparent anode as an in-cell polarizer. The microstructured polydimethylsiloxane (PDMS) stamp was prepared to have reverse replica patterns of the master mold, which was formed on a glass substrate by conventional photolithography and thermal reflow processes [123]. Each pattern in one-dimensional periodic microstructures has the width of 3 $\mu$m, the height of 1.1 $\mu$m and the pitch of 6 $\mu$m. The LCP, RMS03-001C (E. Merck) layer doped with the dichroic dye, G-472 (Hayashibara Inc., Japan) with a concentration of 1 wt.% was spin-coated on the glass substrate, and was then imprinted using the PDMS stamp. After cross-linking the LCP layer under the UV irradiation in $N_2$ environments, the well-defined microstructures of LCP layer, an in-cell polarizer, was obtained. To fabricate the OLED device, a transparent indium zinc oxide (IZO) anode was sputtered on the polymer layer with the thickness of 300 nm. Organic layers were then consecutively deposited

in vacuum, in a pixel area of 4 $mm^2$. The organic materials used were 2-TNATA as a hole injection layer, NPB as a hole transport layer, Alq3 as an emissive and an electron transport layers. Then LiF/Al was deposited as a metallic cathode. The optimized thickness of each layer was 60 nm for 2-TNATA, 20 nm for NPB, 60 nm for $Alq_3$, 1 nm/200 nm for LiF/Al.

**Results and Discussion**

To evaluate the polarization characteristics of an imprinted in-cell polarizer, the electroluminescence (EL) spectra of the devices with the in-cell polarizer were measured with assistance of the conventional sheet polarizer. Figure 3.48(a) indicates the compared results measured with the sheet polarizer placed parallel and crossed to the long axis of the in-cell polarizer. In Fig. 3.48(b), the calculated extinction ratio is illustrated. Note that the ratio exceeds 30 dB in the range of 500 nm to 580 nm, which includes most of the emitting spectra of the fabricated green color OLED device. In the wavelength of 555 nm, which approximately meets with the peak wavelength of the fabricated OLED, the extinction ratio reaches up to about 40 dB. Accordingly, it is proved that the in-cell polarizer has the proper polarization efficiency in a certain color. For the real applications for BLU in LCD, the white color OLED device would be utilized for light emission. In such cases,

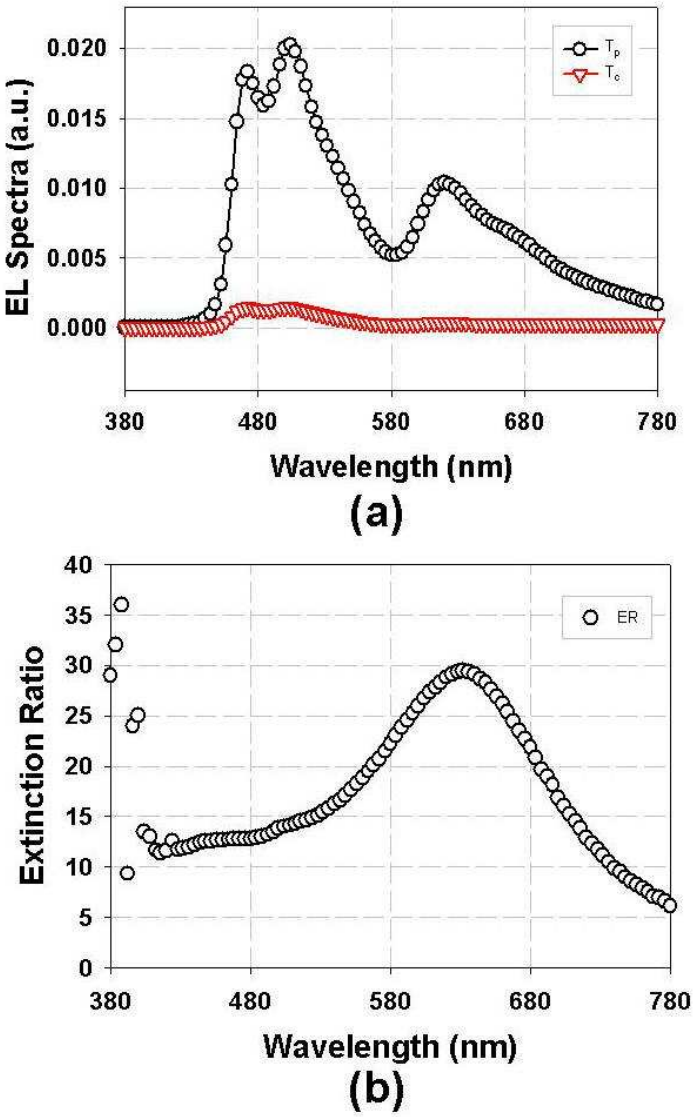


Figure 3.48: (a) The EL spectra of the fabricated OLED measured through a polarizer parallel and crossed to the polarization direction of the in-cell polarizer. (b) The extinction ratio of fabricated device.

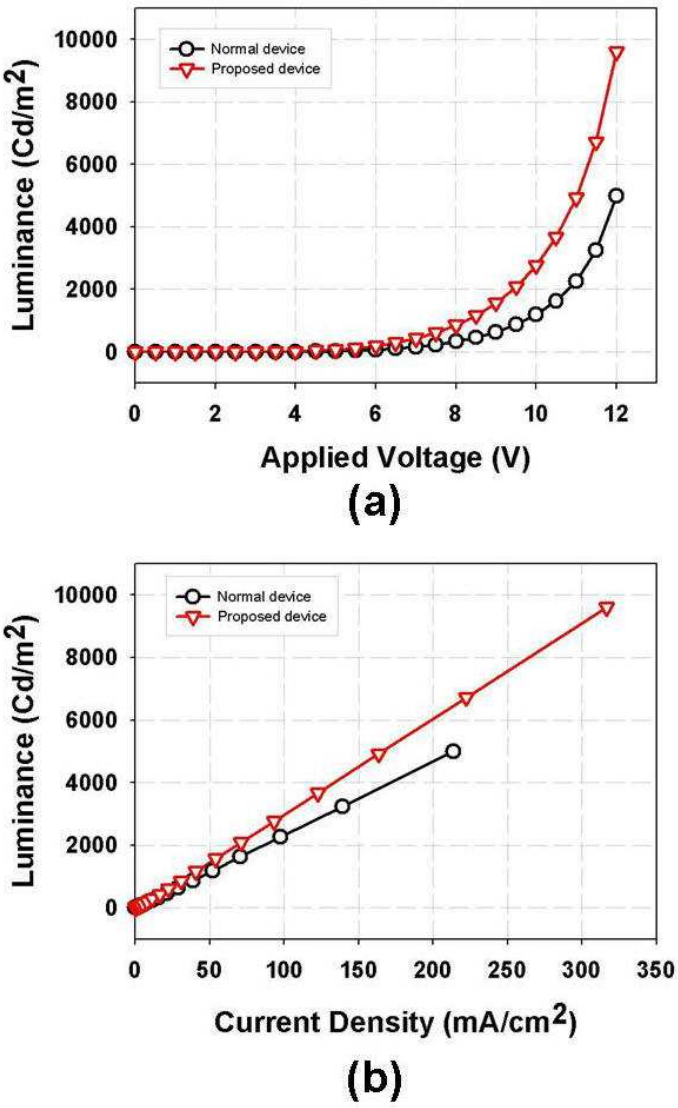


Figure 3.49: The emission characteristics of the normal device with flat structures which employs the conventional sheet polarizer outside the device (normal device), and the OLED with an in-cell imprinted polarizer (proposed device).

the PE should be improved in the wide range of the color, by various approaches such as doping with dyes having higher dichroic ratio in the wider range or changing the geometrical dimensions and/or shapes of imprinted microstructures. It has been known that very small fraction of emission light can reach the LC panel, because the light intensity passing through the polarizer generally decreases in a certain degree. Thus, the sufficient level of light intensity should be also required for the practical application as an efficient light source. In order to clarify the luminance efficiency of the proposed device, two samples were fabricated at the same conditions. Device 1 and 2 is the normal device with flat structures which employs the conventional sheet polarizer outside of the device, and the proposed device with an imprinted in-cell polarizer, respectively. Figure 3.49 depicts the current-voltage-luminance (I-V-L) characteristics. Proposed device shows almost doubled luminance for given applied voltage compared to normal device. This results partly from an enhanced light extraction arising from the microstructures and partly from an increased effective active area. As shown in an inset of Fig. 3.49, the luminance of proposed device is improved compared to normal device at the same current density, which means that the microstructures have improved the light extraction of the OLED device. Thus, it can be concluded that the proposed OLED is suitable for the use

of BLU with highly efficient as well as polarized emission characteristics.

In conclusion, we presented the OLED with an imprinted in-cell polarizer. It is demonstrated that the imprinted dye-doped LCP layer has the proper polarization characteristics and the microstructures significantly increases luminance efficiency. The OLED having in-cell polarizer is expected to be used in practical device application as an efficient light source.

# Chapter 4

# Mobile Display Applications

## 4.1 Transflective Liquid Crystal Displays

### 4.1.1 Introduction

Transmissive LCDs have been widely used in laptop computers, desktop monitors, high-definition televisions (HDTVs) and so on. The most commonly used transmissive 90° TN LCD [124] exhibits a high contrast ratio due to the self phase compensation effect of the orthogonal boundary layers in the voltage-on state. However, its viewing angle is relatively narrow since the LC directors are switched out of the plane and the oblique incident light experiences different phase retardations at different angles. For

TV applications, wide viewing angle is highly desirable. Currently, in-plane switching (IPS) [125] and multi-domain vertical alignment (MVA) [126] are the mainstream approaches for wide-view LCDs. A major drawback of the transmissive LCD is that its backlight source needs to be kept on all the time as long as the display is in use; therefore, the power consumption is relatively high. Moreover, the image of a transmissive LCD is easily washed out by the strong ambient light such as direct sunlight.

Reflective LCD, on the other hand, has no built-in backlight source. Instead, it utilize the ambient light for displaying images. The detailed introduction of available operating modes for reflective LCDs can be found in [127]. In comparison to transmissive LCDs, reflective LCDs have advantages in lower power consumption, lighter weight, and better outdoor readability. However, a reflective LCD relies on the ambient light and thus is inapplicable under low or dark ambient conditions.

In an attempt to overcome the above drawbacks and take advantages of both reflective and transmissive LCDs, transflective LCDs have been developed to use the ambient light when available and the backlight only when necessary. A transflective LCD can display images in both transmissive mode and reflective mode simultaneously or independently. Since LC material itself does not emit light, the transflective LCD must rely on either

ambient light or backlight to display images. Under bright ambient circumstances, the backlight can be turned off to save power and, therefore, the transflective LCD operates in the reflective mode only. Under dark ambient conditions, the backlight is turned on for illumination and the transflective LCD works in the transmissive mode. In the low-to-medium ambient surroundings, the backlight is still necessary. In this case, the transflective LCD runs in both transmissive and reflective modes simultaneously. Therefore, the transflective LCD can accommodate a large dynamic range. Currently, the applications of transflective LCD are mainly targeted to mobile display devices, such as cell phones, digital cameras, camcorders, personal digital assistants (PDAs), pocket personal computers (PCs), and global position systems (GPS), etc.

LCDs rely on an ambient light or backlight to display images. Based on the light modulation mechanisms, transflective LCDs can be classified into four categories: 1) absorption type; 2) scattering type; 3) reflection type; and 4) phase-retardation type. The first three categories do not modulate the phase of the incident light; rather, they absorb, scatter, or reflect light. In some cases, it is possible to use one polarizer or none at all to achieve high brightness. As for the phase-retardation type, two polarizers are usually indispensable in order to make both transmissive and reflective modes work

simultaneously.

### 4.1.2 Cell gap structures

#### A. Dual gap structure

Most of transflective LCDs in the market have dual cell gap structures. A transflective LCD with a dual gap was first proposed by Kubo *et al.* [128] and different types were developed by many researchers [129–131]. Each pixel in the dual gap structure is divided into reflective and transmissive regions, the former is made of aluminium formed on the evenly shaped acrylate resin, and the latter is made of ITO. The average thickness of the acrylic resin is nearly equal to the cell gap in the reflective region. The cell gap in the transmissive region is then twice as thick as that in the reflective region. The LCD panel consists of retardation films, polarizers placed on both sides of the glass substrates, and a homogeneous LC layer. In this structure, the contrast ratio and color gamut were improved compared to a transmissive-type LCD [132]. For better color characteristics, the dual color filter with a scattering layer in dual gap structure of the electrically controllable birefringence (ECB) mode was also proposed [133]. The transflective LCDs in dual cell gap structures have been widely used because of

the simple optical structure and good optical performances. In the dual gap structure, however, the fabrication process is complicated. Moreover, the EO characteristics of transmissive and reflective regions are inevitably different and two driving schemes are needed. Although the transflective LCD with a multi-gap has good optical performances, the multi-gap fabrication process results in high cost and low yield in manufacturing due to this complicated fabrication problems [134].

**B. Single gap structure**

The single cell gap structure has divide into the dual and the single mode depending on the LC mode. Recently, transflective LCDs with a single cell gap structure, having periodically patterned electrodes [129], or two different modes in two subpixel [131, 135]. As an example of a dual mode transflective LC cell, the LC molecules are homogeneously aligned in the transmissive region and hybrid aligned in the reflective region [135]. If a phase retardation through the LC layer in the homogeneously aligned (transmissive) region is $\lambda/2$, the phase retardation in the hybrid aligned (reflective) region is approximately $\lambda/4$, where $\lambda$ denotes the wavelength of the incident light. In both the bright and dark states, the phase retardation on passing through the reflective region twice is then equivalent to that

through the transmissive region [135]. In the intermediate states, the EO properties of the two subpixels differ from each other due to the difference in the threshold behavior between the ECB mode and the hybrid aligned nematic (HAN) mode. In dual mode configuration, the difference in electro-optic responses are essential.

In recent years, single-gap transflective configurations with a single LC mode adopting the in-plane switching (IPS) mode have been proposed [136]. However, the optical efficiency in the IPS cases are limited due to the optical loss from the IPS electrodes. Therefore, the brightness in this case should be enhanced to improve the outdoor readability for practical applications. In section **5.2**, **5.3**, and **5.4**, single-gap designs having in-cell patterned retarder, in-cell patterned polarizer, and wire-grid polarizer will been proposed to improve such weakness of existing transflective LCDs having single mode and single cell gap structure. In such single LC mode, the optical path difference between two regions should be compensated by two separate retardation plates with the identical thickness. For the purpose of low cost and self-alignment, a micro-patterned retarder is required. Up to now, a complicated patterning technique for fabricating a micro-patterned retarder was employed using an UV-polymerizable liquid crystalline material [137]. As discussed in the following sections, we demonstrate a simple fabrication

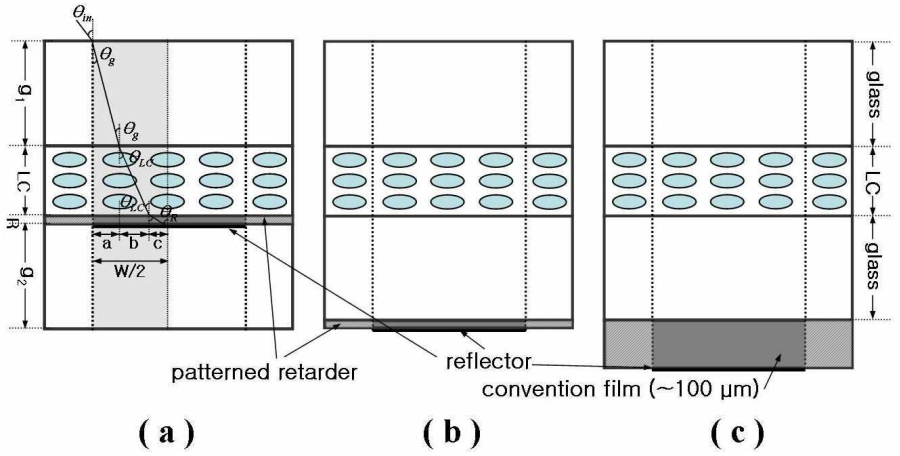


Figure 4.1: Comparison of parallax problems: (a) conventional retardation film (100um thick). (b) out-cell patterned retarder. (c) in-cell patterned retarder (1.2um thick).

process of patterned retarder or patterned polarizer by adopting a single imprinting process and employ a wire-grid polarizer. Consequently, the proposed transflective LCDs have advantages such as the simple fabrication process, the possibility for high performances such as the simultaneously high transmittance and high reflectance simultaneously and wide viewing angle characteristics.

### 4.1.3 In-cell patterned retarder

A disadvantage of common transflective LCDs is that the retardation layer, which is laminated on the exterior of the devices, leads to optical parallax,

and thus severe problems such as lower efficiency and narrow viewing angle are occurred. We adopted a photo-patterned optical compensation layer inside our transflective LC cell. Figure 4.1 shows structure of the transflective LC cell with an in-cell or out-cell patterned retarder and conventional retardation film laminated on the exterior of the display. Utilization of such an in-cell patterned retarder results in a desirable thickening of displays, 1.2 $\mu$ m or under per film, and a solution of parallax problem. The solution produces good viewing angles. Let us evaluate the maximum viewing angles as a function of the incident light angle ($\theta_{\mathrm{in}}$) of transflective LC cells with three types of optical retardation layer using Snell's Law.

$$n_{\mathrm{air}} \cdot \sin\theta_{\mathrm{in}} = n_{\mathrm{g_1}} \cdot \sin\theta_{\mathrm{g_1}} = n_{\mathrm{LC}} \cdot \sin\theta_{\mathrm{LC}} = n_{\mathrm{g_2}} \cdot \sin\theta_{\mathrm{g_2}} = n_{\mathrm{R}} \cdot \sin\theta_{\mathrm{R}} \quad (4.1)$$

In the proposed transflective LC cell with an in-cell patterned retarder, $g$, LC and R are thickness of glass, liquid crystal layer and patterned retarder as shown in Fig. 4.1.

$$a = c = \ g_1 \cdot \tan\theta_{\mathrm{g_1}} = \ g_2 \cdot \tan\theta_{\mathrm{g_2}} \quad (4.2)$$

$$b = LC \cdot \tan\theta_{\mathrm{LC}} \quad (4.3)$$

$$d = R \cdot \tan\theta_{\mathrm{R}} \quad (4.4)$$

In equations 4.2 - 4.4, a, b, c, and d are constants, where a and c are the height component of tangent plane in the glass and b and d can be obtained in the LC layer and retarder layer by solving same methods. Referring to Figure 4.1, we now consider a subpixel (R or G or B pixel) of finite size W. For the estimate of maximum incident viewing angle, the height component of optical path length of incidence light fix a half of width (W/2).

$$W/2 = a + b + d$$
$$= g_1 \cdot \frac{\frac{2}{3}\sin\theta_{\text{in}}}{\sqrt{1 - \frac{4}{9}\sin^2\theta_{\text{in}}}} + LC \cdot \frac{\frac{1}{n_{\text{eff}}}\sin\theta_{\text{in}}}{\sqrt{1 - \frac{1}{n_{\text{eff}}^2}\sin^2\theta_{\text{in}}}} + R \cdot \frac{\frac{1}{n_{\text{R}}}\sin\theta_{\text{in}}}{\sqrt{1 - \frac{1}{n_{\text{R}}^2}\sin^2\theta_{\text{in}}}} \tag{4.5}$$

$$\frac{1}{n_{\text{eff}}^2} = \frac{\sin^2\theta_{\text{LC}}}{n_{\text{e}}^2} + \frac{\cos^2\theta_{\text{LC}}}{n_{\text{o}}^2} \tag{4.6}$$

where R = 1.2 $\mu$m, LC and $n_{\text{eff}}$ are our transflective LC cell gap, 2.4 $\mu$m, and effective refractive index of LC layer, respectively. We further studied the pixel size effect on the EO performance.

Figure 4.2 plots incident viewing angles of the transflective LC cell with different three types of patterned retarder at two types of pixel size. At pixel size 3W = 510 $\mu$m, the incident viewing angles of transflective LC cell with out-cell retarder or conventional retardation film laminated on the exterior of the display are only changed from 1.8° at 2 mm to about 11° at

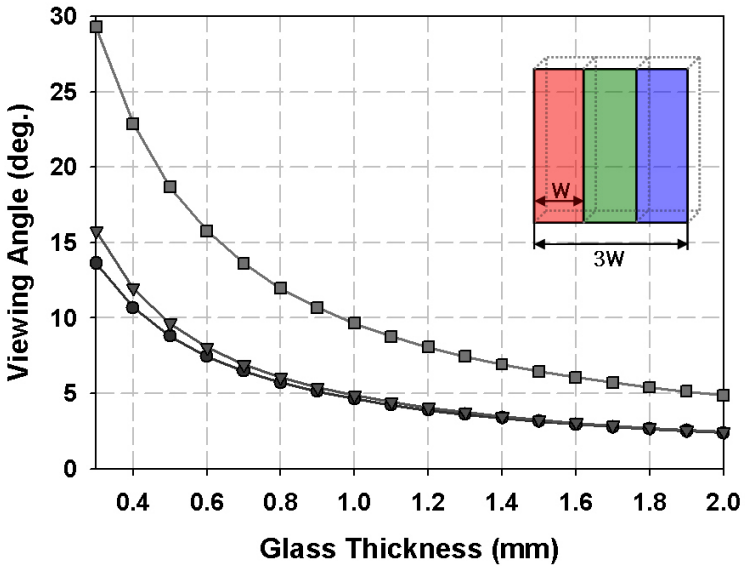


Figure 4.2: Incident viewing angles of the transflective LC cell with different three types of patterned retarder at the pixel size 3W, 510 $\mu m$.

0.3 mm glass thickness. But, the incident viewing angles of transflective LC cell with in-cell patterned retarder is changed from 3.6° to 23° under same conditions. Also, if the pixel size 3W is 510 $\mu m$, the incident viewing angles of transflective LC cell with out-cell retarder or conventional retardation film laminated on the exterior of the display are only changed from 2.4° at 2 mm to about 15° at 0.3 mm glass thickness. But, the incident viewing angles of transflective LC cell with in-cell patterned retarder is changed from 5° to 30° under same conditions. The incident viewing angle of transflective LC cell with in-cell patterned retarder is considerably improved twice as

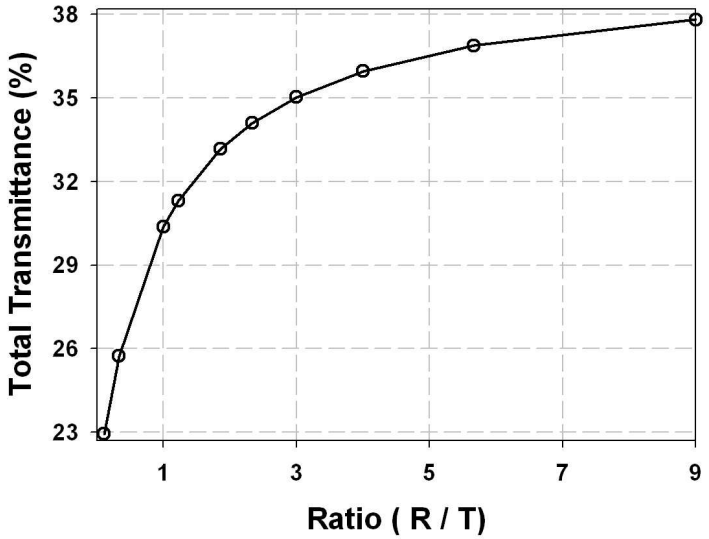


Figure 4.3: The ratio (reflective/transmissive) dependence of total transmittance in our transflective LC cell.

much as that of transflective LC cell with out-cell retarder or conventional retardation film.

### 4.1.4 Reflective/transmissive part Ratio

In the improved our transflective LC cell, the periodically patterned reflector is onto a lower ITO glass substrate. Design of the ratio of the R-part and the T-part looks for optimum condition of maximum light efficiency. We first fix the rest cell parameters and investigate the impact of width of R-part and that of T-part on light efficiency. In order to improve the optical

performance of R-part to increase the backlight utilization efficiency while still keeping the ambient light efficiency unchanged, we set the area of the R-part larger than that of the T-part with the width ratio of R and T changed from 1:10 to 9:1.

Figure 4.3 shows the R/T part ratio dependent total transmittance. Since the R/T part ratio changes substantially from 1/1 to 3/1, the total light efficiency is more 30% and 35%, respectively. In reality, the R-part shows better light efficiency and wider viewing angle than the T-part. Moreover, the maximum light efficiency in the T-part makes possible using a developed backlight unit.

In this chapter, we demonstrate a high optical efficient transflective LCD with single LC mode in a single cell gap. The individual pixels in a transflective LCD are normally divided into two regions, transmissive and reflective regions. A way of compensating the optical path difference between the two regions must be compensated by the use of an in-cell patterned retarder (section **5.2**), an in-cell polarizer (section **5.3**), and wire-grid polarizer (section **5.4**).

## 4.2 Transflective LCD Having an In-Cell Patterned Retarder

We demonstrate a novel design of a transflective LC cell using an inverse twisted nematic (ITN) mode and embedded optical layers in a single gap configuration [138]. To overcome several disadvantages in the TN and electrically controlled birefringence (ECB) modes, the ITN mode based on a homeotropic to twisted planar (HTP) transition is proposed for our transflective LC cell [139]. The embedded films in the LC cell were aligned and patterned by an imprinting technique using silane treated polymer mold [84, 141]. The IOFs can be used function as an in-cell patterned retarder or a viewing angle enhancement film. In addition, the geometrically generated microstructures of the surface of IOFs have a self-aligning capability of LCs due to Berreman effect and thus, the inverse nematic LC layer undergoes a vertical to 90°-TN state in the transmissive part and a vertical to 45°-TN state in the reflective part during operation. Moreover, it achieves compensation of optical path difference (OPD) between both parts and possesses higher transmission, wider viewing, and achromatic characteristics. This device is expected to have high transmittance and high reflectance simultaneously. Moreover, an imprinting technique, using a photopolymerizable

LCP material, is a a simple and versatile technique for fabricating micro-patterned optical films with multi-array.

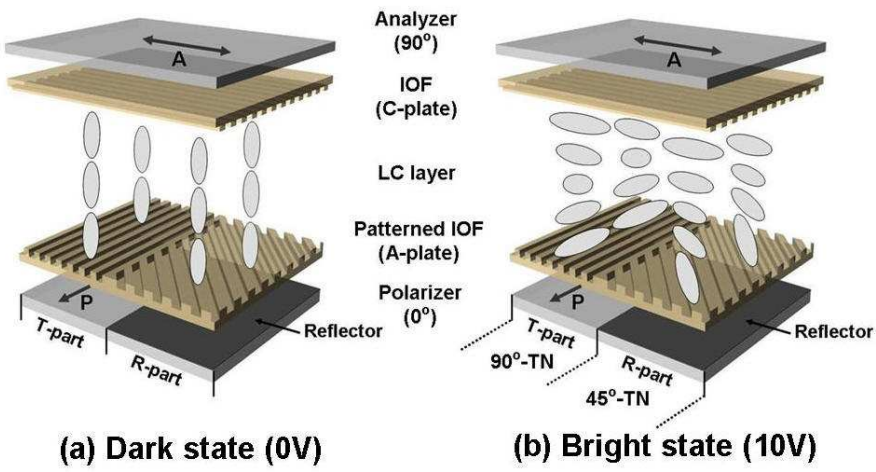


Figure 4.4: The schematic diagram and the operation principle of our ITN transflective LC cell : (a) under no applied electric field (a dark state) and (b) under an applied electric field (a bright state).

### 4.2.1 Device configuration

Figure 4.4 shows the schematic diagram and the operation principles for achieving a dark state and a bright state of the proposed our ITN transflective LC cell. The LC cell is composed of two IOFs, patterned A-plate and C-plate, on the inside of glass substrates in both crossed polarizers. The phase retardation of an in-cell patterned retarder in both two parts is a

$\lambda/4$, which value corresponds to that of a QWP, and these optic axes have different aligned direction each other. One patterned retarder (A-plate) on the lower glass substrate has multi-domain with the directions of 45° and 0° aligned LS patterns, respectively. The other IOF (C-plate) on the upper glass substrate with an array of metal reflectors has only one directional LS patterns in the whole region. Though the other IOF is a C-plate with microstructure, the phase retardation of the homeotropic aligned LCP film has zero. According to introduce LC molecules between both IOFs with microstructures, ITN mode was induced without any alignment layer, for instance, polyimide layer.

### 4.2.2 Operating principles

When no external voltage is applied, LC molecules in the two parts are aligned vertically and no phase retardation occurs in both T and R parts as shown in Fig. 4.4(a). In the transmissive part, the linearly polarized light, passing through the LC cell, experience no phase retardation and thus the polarization state of the incident light is maintained. Under crossed polarizers, the propagating light is completely blocked. In the reflective part, the incident light, passes through the imprinted retarder with phase retardation as same as a QWP and a LC layer with no phase retardation,

changes circularly polarization state. And then the reflective light from a metal reflector returns to the former linearly polarized by the QWP and thus completely blocked by a single polarizer. As shown in Fig. 4.4(b), when an electrical field is applied, the LC layer occur a 90°-TN state in the transmissive part and a 45°-TN state in the R part due to the HTP transition, using a nematic LC with an negative dielectric anisotropy. In the transmissive part, the linearly polarized light passing through TN LC layer is rotated by 90° and thus optical transmission is produced. In such situation, the TN LC layer has waveguiding effect. In the reflective part, the linearly polarized light is rotated 45° for incidence and is reversely rotated -45° for reflectance and thus optical reflection is achieved.

For achieving reflective or transflective LCDs without loss of optical efficiency, it is well known that QWP must be introduced in the LC cell. These QWP and/or a patterned retarder can be fabricated by using an imprinting technique published the results of our previous research work [142]. Figure 4.5(a) and (b) show microscopic textures of a patterned A-plate, based on RMS 03-001C, on the ITO glass substrate observed at an angle of 45° and 0° using a POM. Two directions of LS in the patterned A-plate give rise to different optic axes of the QWP. One IOF was fabricated on the upper substrate by an imprinting process of fabricating using a LCP

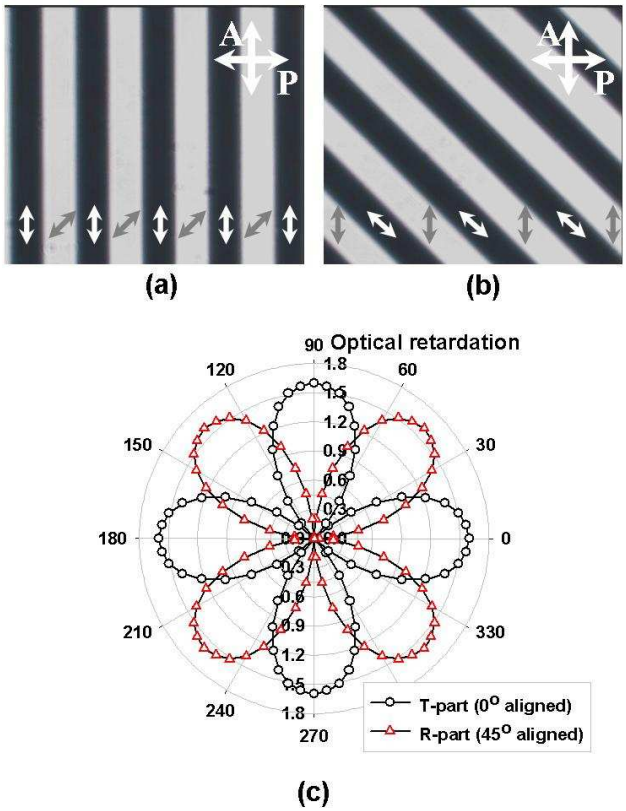


Figure 4.5: The microscopic textures of IOFs, such as a patterned A-plate, observed under crossed polarizers (a) 0°, (b) 45° between the direction of IOF with multi-axes and that of the polarizer. Small white and gray arrows coincide with multi-domains with the directions of 45° and 0° aligned LS patterns, respectively. (c) The optical retardation of the patterned IOF measured as a function of azimuthal angle by the PEM technique. The open circles and the open triangles denote the IOF with the directions of 0° and 45° aligned LS patterns, respectively.

with with negative dielectric anisotropy such as RMS 03-015. Figs. 4.6(a) and (b) show microscopic textures of the IOF with function of wide viewing angle enhancement. The hydrophobic surface wettability of used mold was induced the homeotropic aligned LCP molecules and the microstructure was transferred on the LCP layer from the mold. The homeotropic aligned IOF shows the dark state in any direction of optic axis. And thus, the IOF achieved wider viewing characteristics preserved microstructure on the surface of the LCP film.

On the other hand, another IOF was fabricated by a same imprinting process of fabricating the above mentioned C-plate using another LCP with positive dielectric anisotropy such as RMS 03-001C instead of LCP with

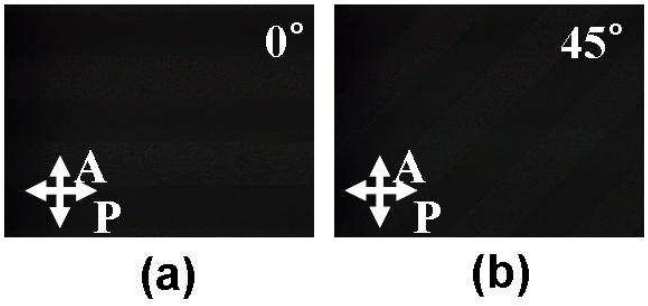


Figure 4.6: The microscopic textures of IOFs, such as a C-plate, observed under crossed polarizers (a) 0° and (b) 45° between the direction of IOF with multi-axes and that of the polarizer.

negative dielectric anisotropy such as RMS 03-015. As shown in Fig. 4.5, the patterned IOF shows bright and dark states along the LS patterns and small white and gray arrows coincide with the directions of 45° and 0° aligned LS multi-domains, respectively. As shown in Fig. 4.5(b), microscopic textures of the patterned IOF was rotated by an angle of 45° with respect to Fig. 4.5(a). In this case, the bright and dark states were reversed. Figure 4.5(c) shows phase retardation of the patterned IOF measured as a function of azimuthal angle by a PEM technique. The phase retardations of the IOFs with parallel (0°) direction and 45°-aligned direction respect to that of polarizer are about 1.6, respectively. The value was about $\pi/2$ corresponds approximately to $\lambda/4$ of the wavelength, $\lambda = 632.8$ nm, used. Also, directions of the maximum retardation results are same as that of the LS patterns in the multi-domains of the IOF.

For an important matter, the microstructures were prepared on the surface of the anisotropic IOFs to provide the spontaneous alignment of LC molecules on the IOF without an extra alignment layer using the Berreman concept. The azimuthal anchoring energy was measured using the cell rotation method. The azimuthal anchoring energy was $8.43 \times 10^{-6}$ J/m$^2$, respectively. The result generated by the microstructure of IOFs is sufficient for aligning LCs [101].

Table 4.1: The material constants of MJ-96758.

| parameters | values |
|---|---|
| $K_1$ | $11.6 \times 10^{-12}$ N |
| $K_2$ | $5.5 \times 10^{-12}$ N |
| $K_3$ | $16.1 \times 10^{-12}$ N |
| $\Delta\varepsilon$ | 8.2 † |
| $\varepsilon_\perp$ | 3.9 † |
| $n_o$ | $1.4620 + 5682/\lambda^2$ ‡ |
| $n_e$ | $1.5525 + 9523/\lambda^2$ ‡ |

† $\varepsilon$ is measured at 1 kHz.

‡ $\lambda$ is a wavelength of incident light in nm.

### 4.2.3 Theoretical description

We first performed numerical simulations to obtain the EO characteristics of several transflective LC cells using the Extended Jones matrix formulation. The profile of LC director as a function of applied voltage was also simulated based on the Oseen and Frank's continuum theory. To calculate the reflectance and the transmittance curves, the nematic LC material used in our transflective LC cell was MJ-96758 (E. Merck). The material parameters used for numerical simulations were the elastic constants, $K_1 = 13.0$

pN, $K_2 = 7.0$ pN, $K_3 = 15.0$ pN, the ordinary refractive index $n_o = 1.4582 + 5558/\lambda^2$, the extraordinary refractive index $n_e = 1.5323 + 7784/\lambda^2$, the dielectric anisotropy $\Delta\varepsilon$ = -4.9, and the rotational viscosity $\gamma = 0.148$ Pa·sec. Here, $\lambda$ is the wavelength of the incident light in nanometer. It is well known that the wave equation for light propagation in helical structure along the helical axis has an exact solution. The vector of electric field follows the twisted director structure of the TN cell. This wave-guiding effect occurs if the thickness of the TN cell d satisfies the Mauguin condition written as $u \gg 1$, where $u = \pi d\Delta n/\lambda\theta$ is the Mauguin parameter, and $\theta$ is the angle of total twist. To analyze the Mauguin condition quantitatively, one can calculate the transmittance $T$ of the TN cell placed between a polarizer oriented along the director at the entrance plate and an analyzer oriented perpendicularly to the director at the exit plate

$$T = \frac{1}{2}\frac{\sin^2[\theta\sqrt{1+u^2}]}{1+u^2} \tag{4.7}$$

where we used $\phi = \pi/2$ as the twist angle, u is the Mauguin parameter given by

$$u = \frac{\Gamma}{2\phi} = 2d\frac{\Delta n}{\lambda} \tag{4.8}$$

The transmittance $T$ vs. the Mauguin parameter $u$ calculated using

Eq.4.7 for 90° and 45° TN cells. As expected, for a large $u$ that corresponds to the Mauguin regime, the transmittance decreases nonmonotonously, through the series of decreasing maxima and zeros. The amplitudes of maxima depend only on $u$ whereas the positions of maxima and zeros depend on both $u$ and $\theta$. One can consider that the cell performs in the Mauguin regime when $T < 1$ % and, therefore, when $u \geq 2$ $\mu$ m with a nematic material of typical birefringence $\Delta n = 0.0905$, the cell thickness was maintained 4 $\mu$ m thick using glass spacers so that the LC material injected into the cell by capillary action at room temperature.

### 4.2.4 Results and discussion

Figure 4.7(a) shows the experimental EO results and those of numerical simulations for our transflective LC cell as function of the applied voltages. The transmittance and the reflectance are the ratio of output intensity to input intensity and the transmittance and the reflectance were 0.42 and 0.41, respectively. The symbols and the lines denote the experimental results and the numerical simulations of the transmittance and the reflectance, respectively. The experimental EO results agree well simulation results. Figure 4.7(b) shows the measured EO response times in our transflective LC cell. The the open circles, the open triangles, and solid line line are

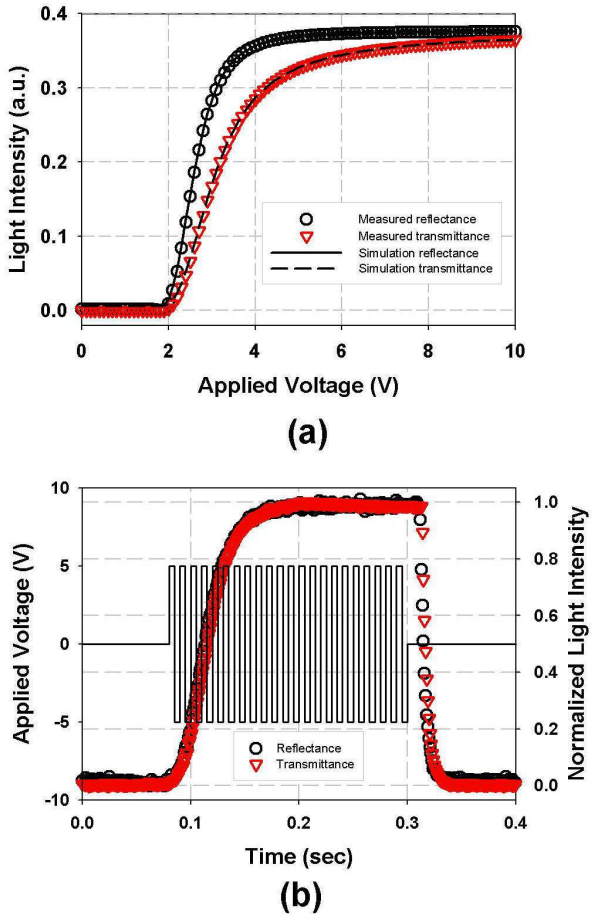


Figure 4.7: (a) The EO characteristics of our transflective ITN LC cell. The open circles, the open triangles and solid lines denote the experimental results of the reflectance, the transmittance, and numerical simulations of the reflectance and transmittance, respectively. (b) The measured EO response times in our transflective LC cell. The the open circles, the open triangles, and solid line line are the normalized EO response times in the T part and the R part and the pulse input, respectively.

the normalized EO response times in both two parts and the pulse input, respectively. The measured rising time and falling time were 5.2 msec and 18.1 msec, respectively.

### 4.2.5 Wide viewing characteristic

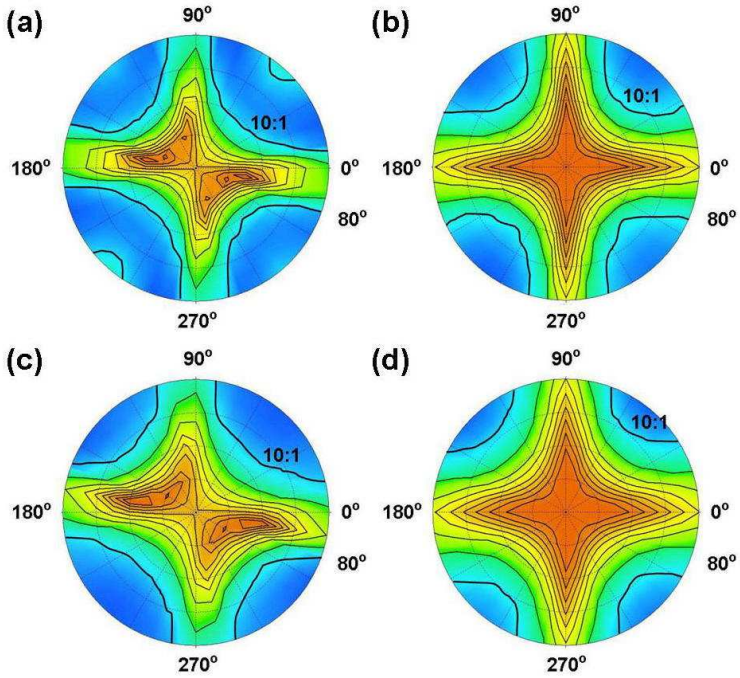


Figure 4.8: Isocontrast plots in (a) the T part, (b) the R part of the existing transflective LC cell without C-plate, in (c) the T part, and (d) the R part of the proposed our transflective LC cell with C-plate, respectively.

Figure 4.8 shows the iso-contrast contour characteristics of the ITN LC layer induced by microstructures of the embedded IOFs. Particulary, due

to the viewing angle enhancement effect of a C-plate onto the upper glass substrate, the T part shows an inherently wide viewing angle with its contrast ratio (CR) > 10:1 viewing cone over 60° at all directions from Fig. 4.8(c). For the R part, although a small leakage at V = 0 exists, as Fig. 4.7 shows, its viewing angle is also quite wide, as observed from Fig. 4.8(d). The CR of 10:1 contour spans over the 50° viewing cone. These results show wider 10 degrees than the viewing angles of the existing transflective LCD without a C-plate.

In conclusion, we have demonstrated an ITN transflective LC cell employing two IOFs with aligning capability of LCs. In addition, the IOFs used in our work behave as an in-cell patterned retarder with multi-optic axes in the upper glass substrate and a viewing angle enhancement film in the lower glass substrate. Moreover, we developed an imprinting technique to produce two type of IOFs. One is a patterned retarder with homogeneous aligned LCP and the other is a viewing angle enhancement film with homeotropic aligned LCP. The patterned homogeneous aligned and homeotropic aligned LCP optical films can be used as both an in-cell functional optical film and an alignment layer of the LC molecules. Consequently, Our proposed transflective LCD shows high transmittance and high reflectance simultaneously and it achieves wider viewing characteristic.

## 4.3 Transflective LCD Having an In-Cell Dye-Polarizer

We proposed a single cell gap transflective LCD using multi-TN based LC cell and embedded patterned dye-polarizer which functions as a polarization direction dependent polarizer to avoid the need of any patterned retarder. For fabricating multi-TN LC mode, the LC cell is composed of both a patterned dye-polarization film and an imprinted QWP with unique alignment direction inside glass substrates. In addition, the geometrically generated microstructures of the surface of two in-cell functional films have a self-aligning capability of LCs due to Berreman effect. This device is expected to have high transmittance and high reflectance simultaneously. Moreover, an imprinting technique, using a photopolymerizable LCP material without and with dichroic dye, is a simple and versatile technique for fabricating micro-patterned optical films with multi-array and unique alignment direction.

### 4.3.1 Device configuration

Figure 4.9 shows the schematic diagram and the operation principles for achieving a dark state and a bright state of the proposed our transflective

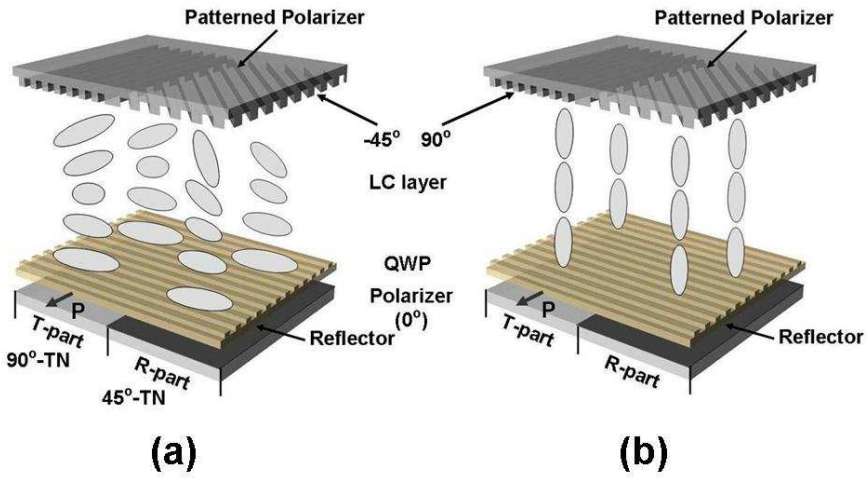


Figure 4.9: The schematic diagram and the operation principle of our transflective LC cell having in-cell dye-polarizer: (a) under no applied electric field (a dark state) and (b) under an applied electric field (a bright state).

LC cell. Our transflective LC cell has a patterned metal (Al) array, which used a reflector for reflective part, on the lower glass substrate. The LC cell is composed of two imprinted optical films, patterned dye-polarizer with multi-optic axes (upper side) and QWP with unique optic axis (lower side), on the inside of glass substrates.

The PE and ER of patterned polarizer researched in previous **Ch. 3** are over 95 % at wavelength from 420 nm to 680 nm and near 60 %, respectively and optic axes of the patterned polarizer are 0° and -45° aligned in the transmissive part and the reflective part, respectively. The phase retardation of

a patterned retarder in both two parts is a $\lambda/4$, which value corresponds to that of a QWP, and this optic axe has unique aligned direction in the whole part. Both imprinted optical films, patterned polarizer and QWP, have microstructure on the surface of the films. According to introduce LC molecules between both imprinted optical films with microstructures, multi-TN mode was induced without any alignment layer, for instance, PI layer.

### 4.3.2 Operating principles

When no external voltage is applied, the LC layer occur a 90°-TN state in the transmissive part and a 45°-TN state in the R part, respectively as shown in Fig. 4.9(a). In the transmissive part, the linearly polarized light passing through TN LC layer is rotated by 90° and thus optical transmission is produced. In such situation, the TN LC layer has waveguiding effect. In the reflective part, the linearly polarized light is rotated 45° for incidence and is reversely rotated -45° for reflectance and thus optical reflection is achieved.

As shown in Fig. 4.9(b), when an electrical field is applied, LC molecules in the two parts are aligned vertically and no phase retardation occurs in both transmissive and reflective parts. In the transmissive part, the linearly

polarized light, passing through the LC cell, experience no phase retardation and thus the polarization state of the incident light is maintained. Under crossed polarizers, the propagating light is completely blocked. In the reflective part, the incident light, passes through the imprinted retarder with phase retardation as same as a QWP and a LC layer with no phase retardation, changes circularly polarization state. And then the reflective light from a metal reflector returns to the former linearly polarized by the QWP and thus completely blocked by a single polarizer.

### 4.3.3 Results and discussion

Figure 4.10(a) shows the experimental EO results and those of numerical simulations for our transflective LC cell as function of the applied voltages. The transmittance and the reflectance are the ratio of output intensity to input intensity and the transmittance and the reflectance were simultaneously 0.37. The symbols and the lines denote the experimental results and the numerical simulations of the transmittance and the reflectance, respectively. The experimental EO results agree well simulation results. Figure 4.10(b) shows the measured EO response times in our transflective LC cell.

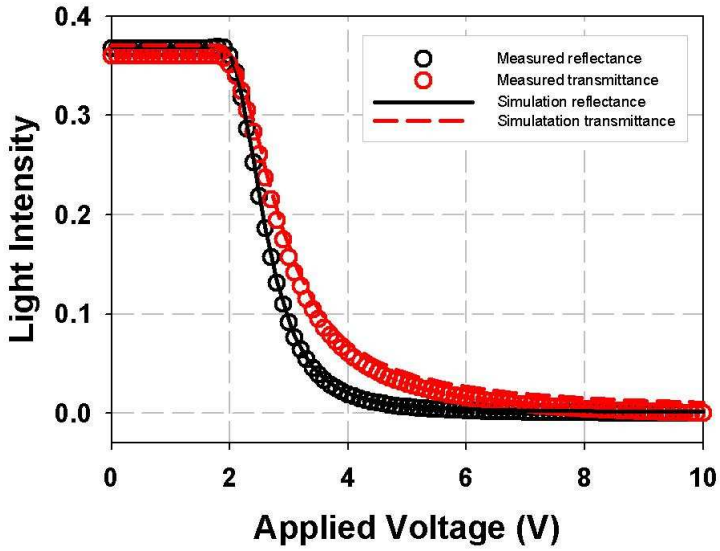


Figure 4.10: The EO characteristics of our transflective LC cell having in-cell patterned dye-polarizer. The open circles, the open triangles and solid lines denote the experimental results of the reflectance, the transmittance, and numerical simulations of the reflectance and transmittance, respectively.

## 4.4 Transflective LCDs Having a Wire-Grid Polarizer

We demonstrate a new design of a single LC mode transflective LCD having a wire grid polarizer (WGP) and an inner patterned retarder in a single gap configuration [102]. In 2006, S. T. Wu et. al had documented high efficient transflective LC cell having a WGP, which was patterned in the reflective part for using only reflector [140]. But, in our research, the WGP is served as a polarizer in the transmissive (T) region and a reflector in the reflective (R) region. This device is expected to have high transmittance and high reflectance simultaneously. Moreover, the patterned retarder has two domains, i.e., an anisotropic part and an isotropic part, that are placed in the T and the R regions, respectively. The patterned retarder based on LCP material can be fabricated on the inner side of lower glass substrate. Due to different liquid crystalline phases of the patterned LCP layer between the two regions, two induced optical properties of the LCP layer in the transmissive region and the reflective region were different in dielectric constant, respectively. As well be discussed later, the appearance of the different dielectric constants is essential to significantly reduce the EO disparity between the transmissive and the reflective region.

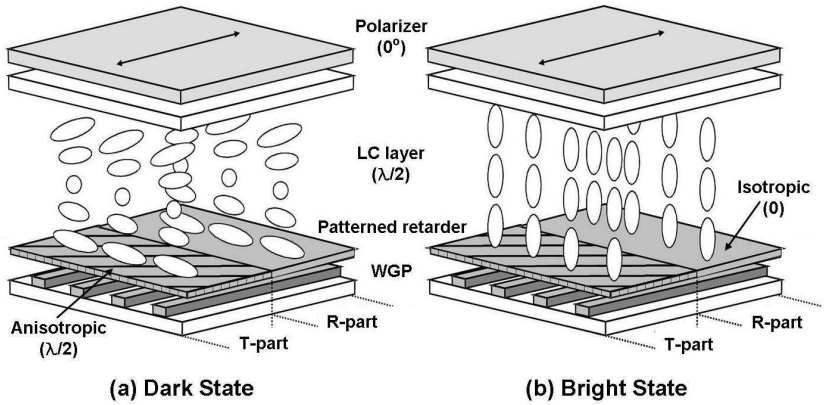


Figure 4.11: The operation principle of our transflective LC cell having a WGP and an inner patterned retarder in a single gap configuration : (a) under no applied electric field (a dark state) and (b) under an applied electric field (a bright state).

### 4.4.1 Device configuration

Figure 4.11 shows a schematic diagram of our transflective LC cell with single cell gap in a single mode configuration. In this single mode transflective LC cell, the LC cell is composed of the upper polarizer, a TN LC layer, a patterned retarder, and a WGP. The optic axis of the polarizer and the direction of wire grids of the WGP are crossed to each other. The structure of a WGP where metal, e.g. aluminum (Al), ribs are periodically formed on the ITO glass substrate. For an unpolarized incident light, the light component whose electric field vector is parallel to the wire grids will be

almost fully reflected by the WGP. Conversely, most of the light with electric field vector perpendicular to the wire grids will transmit through the WGP. For fabricating a TN LC cell, JALS 146-R50 (JSR co., Japan) was spin-coated onto the upper ITO glass substrate and the patterned retarder on the lower ITO glass substrate having WGP and thus, baked at 160 °C for 1 hr. The inner surfaces were rubbed unidirectionally. The two glass substrates were assembled using glass spacers of 5.4 $\mu$m thickness, the LC was filled into the cell at room temperature so that the phase retardation of the TN aligned LC layer corresponds approximately to $\lambda/2$ of the wavelength used. A He-Ne laser of 632.8 nm was used as a light source. All the measurements were carried out at room temperature. Having a single LC mode in our transflective LC cell, the phase retardation on passing through the transmissive part twice is then equivalent to that through the reflective part. In the intermediate states, the EO properties of the two subpixels differ from each other.

In contrast to use a patterned retarder having a same retardation with different optic axes, the patterned retarder with different phase retardation influences the LC director profiles in our transfletive LC cell. The patterned retarder has two domains, i.e., an anisotropic part and an isotropic part, that are placed in the T and the R parts, respectively. The optical re-

tardation of the anisotropic part and that of the isotropic part correspond to a HWP and a dummy layer, respectively. In the reflective part, the LC molecules have same LC profiles irrespective of the novel patterned retarder. In transmissive part, however, it was found that the EO property through the LC layer decreases slowly with increasing the applied voltage in the low voltage regime because of the lower dielectric anisotropic constant. As a consequence, the EO disparity between the transmittance and the reflectance is significantly reduced.

### 4.4.2 In-Cell patterned retarder using thermal patterning

We used a patterned retarder based on a LCP, RMS 03-001C, to realize a single LC mode in a single gap configuration. The patterned retarder has two different phase states, an anisotropic state and an isotropic state, that are placed in the T and the R parts, respectively. The optical retardation of the anisotropic region and that of the isotropic region correspond to a HWP and a dummy layer, respectively. The optical axis of the HWP makes an angle of 45° with respect to the direction of the polarizer. If a phase retardation through the LC layer and a patterned retarder in the T-part

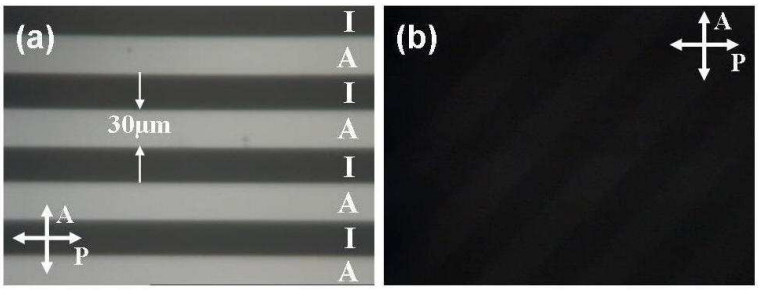


Figure 4.12: The microscopic textures of the inner patterned retarder based on LCP molecules observed under crossed polarizers: (a) an angle of 0° and (b) 45° between the direction of retarder and the rear polarizer. The isotropic region shows the dark state in any direction of the optical axis and the anisotropic region shows bright and dark states depending on the direction of the polarizer. Here, I, A, and R coincide with an isotropic state, an anisotropic state, and rubbing direction, respectively.

is $\lambda$, the phase retardation in the R-part is approximately $\lambda/2$, where $\lambda$ denotes the wavelength of the incident light. In both the bright and dark states, the phase retardation on passing through the T-part twice is then equivalent to that through the R-part. The R-part area relative to the T-part area depends solely on the aperture ratio of the metal-mask. Figure 4.12(a) and (b) show microscopic textures of the patterned retarder with multi-domain on the ITO glass substrate observed at an angle of 45° and 0° between the rubbing and that of one of crossed polarizers using a POM. The

patterned LCP retarder has anisotropic and isotropic domains, as shown in Figs. 4.12(a) and 4.12(b). The isotropic region shows the dark state in any direction of the optical axis. In contrast, the anisotropic region shows bright and dark states depending on the direction of the polarizer. Here, I, A, and R coincide with an isotropic state, an anisotropic state, and rubbing direction, respectively. The optical retardation, $2\pi d\Delta n/\lambda$, of the retarder was measured as a function of azimuthal angle by the PEM technique. Here, $d$, $\Delta n$, and $\lambda$ represent the thickness, the optical anisotropy of the

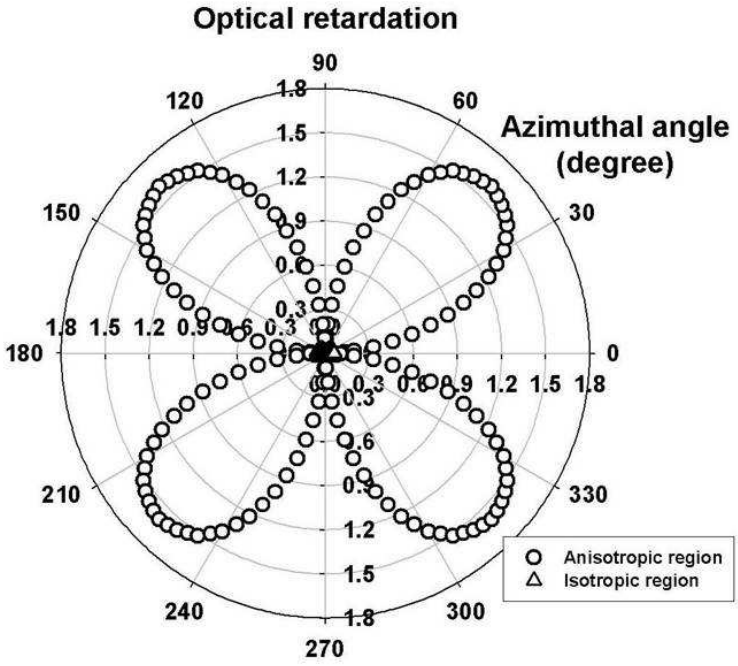


Figure 4.13: The optical retardation of the retarder measured as a function of azimuthal angle by the PEM technique.

retarder, and the wavelength of the light used, respectively. The measured results are shown in Fig. 4.13 and The open circles and the open triangles denote the patterned retarder with an anisotropic state and an isotropic state, respectively. The maximum phase retardation was about 1.6 in the anisotropic region, which corresponds to $\lambda/4$ for $\lambda = 632.8$ nm. In contrast, the retardation in the isotropic region was only 0.06.

The dielectric measurements have been performed by Impedance/gain phase analyzer (4192A, Hewlett-Packard) [1]. The sandwitched type of capacitor sample, metal-insulator-metal (MIM), is used for dielectric measurements. For fabricating MIM sample, electrode metal (Au) was deposited onto the surface of a patterned retarder with different phase state on the ITO glass substrate. The dielectric measurements have been done both in anisotropic region and isotropic region. The values of capacitance will directly give the value of real part of permittivity of the sample using following equation, $\epsilon = \epsilon_0\epsilon_r = C \cdot d/A$, where $C$, $d$, and $A$ are the capacitance, thickness of retarder, and square measure of the sample. For accurate measurement, seven samples fabricated in the same condition was measured and searched average value. The average capacitances and permittivities were $C_{iso} = 1.326 \times 10^{-2}$ and $\epsilon_{iso} = 14.97$ in the isotropic region and $C_p$ $(C_\perp) = 6.517 \times 10^{-3}$ and $\epsilon_p$ $(\epsilon_\perp) = 7.36$ in the anisotropic region at the fre-

quency of 1kHz. Here, $C_{iso}$, $C_p$ ($C_\perp$), $\epsilon_{iso}$, and $\epsilon_p$ ($\epsilon_\perp$) are capacitances and permittivities in both isotropic and anisotropic regions, respectively [102].

### 4.4.3 Results and discussion

The nematic LC material used in this work was MLC-6012 of E. Merck. The extraordinary and ordinary refractive indices of MLC-6012 are $n_{\rm e} = 1.5525 + 9523/\lambda^2$ and $n_{\rm o} = 1.4620 + 5682/\lambda^2$, respectively. Here, $\lambda$ is the wavelength of the incident light in nanometers. The dielectric anisotropy and the elastic constants are $\Delta\epsilon = 8.2$, $K_1 = 11.6 \times 10^{-12}$ N, $K_2 = 5.5 \times 10^{-12}$ N, and $K_3 = 16.1 \times 10^{-12}$ N, respectively.

The transmitted and the reflected intensities in our transflective LC cells are shown as a function of the applied voltage in Fig. 4.14. The open circles and the open circles denote the experimental results of the transmitted and the reflected intensities, respectively. As shown in Figs. 4.14(a) and (b), there is no appreciable difference in the transmittance between the case of a patterned retarder with different optic axes and that of a patterned retarder with different phase states. The reflectance and the transmittance are the ratio of output intensity to input intensity and the reflectance and the transmittance were 0.46. In fact, above patterned retarder with different phase states, the reflectance curve coincides well with the transmittance

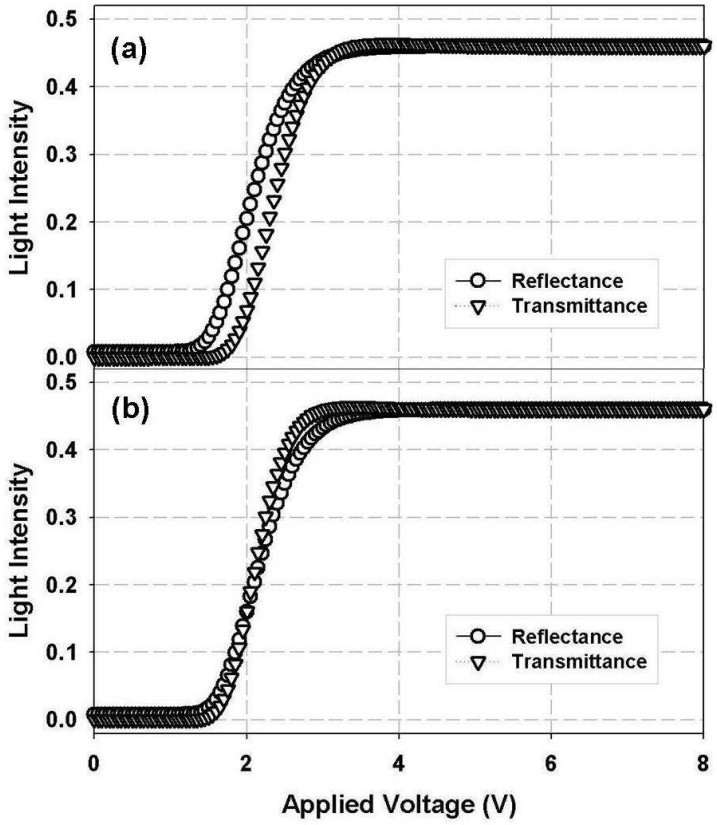


Figure 4.14: The operation principles of our transflective LC cell having a WGP : (a) with an inner patterned retarder and (b) without an inner patterned retarder.

curve due to the presence of different optical anisotropy in the LC cell as shown in Fig. 4.14(b). Clearly, the EO disparity between the transmissive and the reflective parts was significantly reduced by introducing the patterned retarder with multi-domains into the LC cell.

The WGP used in our work behaves as a polarizer in the transmissive region and a polarization-dependent reflector in the reflective region. The WGP completely reflects light with its polarization parallel to the wire grids and transmits light with its polarization perpendicular to the wire grids. Our proposed transflective LC display with a WGP as both a polarizer in the transmissive region and a reflector in the reflective region show high transmittance and high reflectance simultaneously. Moreover, the EO disparity between the transmissive and reflective parts was significantly reduced by the adopting the patterned retarder with different phase state in both parts.

# Chapter 5

# Conclusion Remarks

In recent years, Organic and polymeric materials have attracted great interest for a long time since their excellent performances in the optical and electronic devices and fundamental success of molecular engineering in creating a new class of materials with appropriate physical and optical properties. Particularly, liquid crystals (LCs) and liquid crystalline polymers (LCPs) are very useful in several key areas of electronic and optical devices. Moreover, the multi-ordered LC systems have attracted great interest and have been widely studied because of the importance of the fundamental research and their potential for device applications to the optical systems including displays. Recently, organic functional materials, offering far greater fabrication flexibility and processing simplicity than current inorganic optical

materials, have extensively studied for the use as electrically active materials having the properties of conductivity and/or light-emission. With increasing the demands of mobile devices in the digital multimedia broadcasting environments, all organic displays where all the elements consisting of the display are made of the organic materials, have attracted much attention since several advantages such as low-power consumption and simple fabrication processes. In addition, optical elements, such as optical retardation plates, color filters, polarization converters, and interference filters, based on LCPs are one of the classes that have been widely used for the advancement of LC displays (LCDs) that provide improved optical performances such as high light efficiency, wider viewing angle properties, and complicated optical functions. In such cases, it is not only necessary to produce the LCP into an optically anisotropic film structure being divided into multi-domains. Thus, the employment of these structures as alignment layers is in need of ordering and patterning for organic materials.

In this thesis, we have investigated the mechanism of imprinting technique and proposed to fabricate functional optical elements and/or non-display and/or display applications having the functional optical elements. In addition, nano- or microstructures on the surface of functional optical elements induce self-aligning capability of introduced LC molecules. Also, the

novel optical element concepts of the in-cell dye-polarizer and the wire-grid polarizers (WGPs) using an imprinting technique and a thermal deposition or coating of nanoparticles on the imprinted polymeric nanoscale structures and display applications with the novel optical elements for high device performances are proposed and demonstrated.

In **Chap. 1**, the physical properties of the LCs and the need of novel aligning and/or patterning technique used in this thesis was briefly introduced. The motivation of this research on the imprinted surface-controlled structures for the optical and electronic elements and/or devices was also introduced in this chapter.

In **Chap. 2**, we have investigated the mechanism of imprinting technique and proposed to fabricate functional optical elements and/or non-display and/or display applications having the functional optical elements. In addition, nano- or microstructures on the surface of functional optical elements induce self-aligning capability of introduced LC molecules.

In **Chap. 3**, the novel optical element concepts of the in-cell dye-polarizer and the WGPs using an imprinting technique and a thermal deposition or coating of nanoparticles on the imprinted polymeric nanoscale structures.

In **Chap. 4**, we demonstrate a high optical efficient transflective LCD

with single LC mode in a single cell gap. The individual pixels in a transflective LCD are normally divided into two regions, transmissive and reflective regions. A way of compensating the optical path difference between the two regions must be compensated by the use of an in-cell patterned retarder, an in-cell polarizer, and wire-grid polarizer.

In **Chap. 5**, throughout this thesis, patterning and aligning the organic functional materials by imprinting technique with self-aligning capability of imprinted surface structures for injected LC molecules has been extensively explored from the viewpoints of scientific researches and device applications. Basically, almost optical and electronic elements and/or applications can be practically realized in the functional organic passive and active systems produced. Moreover, theoretical description and several device concepts, such as patterned metal electrodes using thermal deposition on the patterned polymer mold or nanoparticles, introduced here may be a foundation for the future scientific researches and applications.

# Bibliography


[1] L. M. Blinov and V. G. Chigrinov, *Electrooptic Effects in Liquid Crystal Materials* (Springer-Verlag Inc., New York, 1994).

[2] P. G. de Gennes and J. Prost, *The Physics of Liquid Crystals*, 3rd ed. (Oxford University Press, New York, 1993).

[3] I. C. Khoo and F. Simoni, *Physics of Liquid Crystalline Materials* (Gordon and Breach Science Publishers, Philadelphia, 1991).

[4] S. Elston and R. Sambles, *The Optics of Thermotropic Liquid Crystals* (Tayor and Francis, Padstow, 1998).

[5] J.-H. Park, J.-H. Lee, and S.-D. Lee, Mol. Cryst. Liq. Cryst. **367**, 801 (2001).

[6] T.-Y. Yoon, J.-H. Park, J. Sim, and S.-D. Lee, Appl. Phys. Lett. **81**, 2361 (2002).

[7] J. S. Patel, M. A. Saifi, D. W. Berreman, C. Lin, N. Andreadakis, and S.-D. Lee, Appl. Phys. Lett. **57**, 1718 (1990).

[8] J.-H. Lee, H.-R. Kim, and S.-D. Lee, Appl. Phys. Lett. **75**, 859 (1999).

[9] J. S. Patel and K. Rastani, Opt. Lett. **16**, 532 (1991).

[10] J.-H. Park, C.-J. Yu, J. Kim, S.-Y. Chung, and S.-D. Lee, Appl. Phys. Lett. **83**, 1918 (2003).

[11] V. K. Gupta, J. J. Skaife, T. B. Dubrovsky, and N. L. Abbott, Science **279**, 2077 (1998).

[12] Y. Choi, Y. Lee, H. Kwon, and S.-D. Lee, Mater. Sci. Eng. C **24**, 237 (2004).

[13] H. J. Cantow, Adv. Polym. Sci., 59 (1984).

[14] H. Finkelmann, Angew. Chem. **99**, 840 (1987).

[15] H. Ringsdorf, B. Schlarb, J. Venzmer, Angew. Chem. **100**, 117 (1988).

[16] B. Reck, H. Ringsdorf, Makromol. Chem. Rapid Commun. **6** 291 (1985).

[17] Data provided by WIKIPEDIA (http://wikimediafoundation.org) website.

[18] L. M. Blinov and V. G. Chigrinov, *Electrooptic Effects in Liquid Crystal Materials* (Springer-Verlag, New York, 1993).

[19] T. J. Slukin and Poniewierski, *Fluid Interfacial Phenomena*, (Wiley, Chichester, 1986).

[20] A. K. Sen and D. E. Sullivan, Phys. Rev. E **35**, 1391 (1987).

[21] P. I. C. Teixeira, Phys. Rev. E **55**, 2876 (1997).

[22] D.-H. Chung, Ph. D. Thesis, Tokyo Institute of Technology, Tokyo (2003).

[23] M. Hasegawa, EKISHO **3**, 3 (1999).

[24] D. W. Berreman, Phys. Rev. Lett. **28**, 1683 (1972).

[25] J. L. Janning, Appl. Phys. Lett. **21**, 173 (1972).

[26] P. Chaudhari, Nature **72**, 127 (1981).

[27] A. J. Pidduck, S. D. Haslam, G. P. Bryan-Brown, R. Bannister, and I. D. Kitely, Appl. Phys. Lett. **71**,2907 (1997).

[28] J. H. Kim, M. Yoneay, J. Yamanoto, and H. Yokoyama, Appl. Phys. Lett. **78**,3055 (2001).

[29] W. Gibbons, P. J. Shannon, S. T. Sun, and B. J. Swetlin, Nature **351**,49 (1991).

[30] M. Schadt, K. Schmitt, V. Koznikov, and V. Chigrinov, Jpn. J. Appl. Phys. **31**,2155 (1992).

[31] V. N. Raja and J.-C. Lee, Liq. Cryst. **28**, 1723 (2001).

[32] J. Kim, Y.-W. Lim, and S.-D. Lee, Jpn. J. Appl. Phys. **45**, 810 (2006).

[33] D. J. Broer, J. Lub, and G. N. Mol, Nature **378**, 467 (1995).

[34] B. M. I. van der Zande, C. Doornkamp, S. J. Roosendaal, J. Steenbakkers, A. Op't Hoong, J. T. M. Osenga, J. J. Van Glabbeek, L. Stofmeel, J. Lub, M. Shibazaki, K. Asahara, T. Inada, M. Yoshiga, and S. Kawata, J. SID **13/8**, 627 (2005).

[35] V. G. Chigrinov and V. M. Kozenkov, Proc. of Intern. Conf. "Liquid Crystal Materials, DEvices and Displays", 241 (1995).

[36] S. Kobayashi, Workshops on Information Display, 1 (1995).

[37] T. Uchida and H. Seki, *Liquid Crystals Applications and Uses*, (World Scientific, Singapore, 1991).

[38] L. M. Blinov, E. I. Kats, and A. A. Sonin, Uspekihi Fiz. Nauk **152**, 449 (1987).

[39] , B. Myrvold and K. Kondo, Liq. Cryst. **18**, 271 (1995).

[40] K. Y. Han and T. Uchida, Mol. Cryst. Liq. Cryst. **262**, 45 (1995).

[41] J. K. Song, K. Y. Han, and V. G. Chigrinov, IDW'96, 407 (1996).

[42] M. Schadt, et al. Jpn. J. Appl. Phys. **34**, 764 (1995).

[43] K. Y. Han, et al., Proc. of SID'97, 81 (1997).

[44] S. Faetti, *Physics of Liquid crystalline Materials*, edited by I.-C. Khoo and F. Simoni (Gordon and Breach Publishers, 1988).

[45] G. Barbero, N. V. Madhusudana, and G. Durand, J. Phys. Lett. **45**, L613 (1984).

[46] G. Ryschenkow and M. Lleman, J. Chem. Phys. **64**, 404 (1976).

[47] S. Naemura, Appl. Phys. Lett. **33**, 1 (1978).

[48] H. Yokoyama and H. A. van Sprang, J. Appl. Phys. **57**, 4520 (1985).

[49] Y. A. Nastishin, R. D. Polark, S. V. Shiyanovskii, V. H. Bodnar, and O. D. Lavrentovich, J. Appl. Phys. **86**, 4199 (1999).

[50] A. Lien and H. Takano, J. Appl. Phys. **69**, 1304 (1991).

[51] H. S. Kwok, J. Appl. Phys. **80**, 3687 (1996).

[52] K. Sumiyoshi and Y. Hatada, Liq. Cryst. **22**, 327 (1997).

[53] Y. C. Araujo, P. G. Toledo, V. Leon, and H. Y. Gonzalez, Colloid Interface Sci. **176**, 485 (1995).

[54] A. M. Almanza-Wokrman, S. Raghavan, P. Deymier, D. J. Monk, and R. Roop, J. Electrochem. Soc. **149**, H6 (2002).

[55] R. Colorado and T. R. Lee, Langmuir **19**, 3288 (2003).

[56] T. M. Chapman and K. G. Marra, Macromolecules **28**, 2081 (1995).

[57] J. Marchand-Brynaert, G. Pantano, and O. Noiset, Polymer **38**, 1387 (1997).

[58] J. Davies, C. S. Nunnerley, A. C. Brisley, R. F. Sunderland, J. C. Edwards, P. Kruger, R. Knes, A. J. Paul, and S. Hibbert, Colloids Surf. A **174**, 287 (2000).

[59] S. Guruvenketa, G. M. Raoa, M. Komath, and A. M. Raichur, Appl. Surf. Sci. **236**, 278 (2004).

[60] R. W. Paynter, Surf. Interface Anal. **26**, 674 (1998).

[61] J. Larrieu, B. Held, F. Clement, N. Soulem, and D. Dubois, Eur. Phys. J. Appl. Phys. **26**, 113 (2004).

[62] A. Athanassiou, M. I. Lygeraki, D. Pisignano, K. Lakiotaki, M. Varda, E. Mele, C. Fotakis, R. Cingolani, and S. H. Anastasiadis, Langmuir **22**, 2329 (2006).

[63] K. Ichimura, S. K. Oh, and M. Nakagawa, Science **288**, 1624 (2000).

[64] C. Raduge, G. Papastavrou, D. G. Kurth, and H. Motschmann, Eur. Phys. J. E **10**, 103 (2003).

[65] C. D. W. Wilkinson and M. O. Riehle, Nano Lett. **5**, 2097 (2005).

[66] J. T. Han, Y. Zheng, J. H. Cho, X. Xu, and K. Cho, J. Phys. Chem. B **109**, 20773 (2005).

[67] W. Barthlott and C. Neinhuis, Planta **202**, 1 (1997).

[68] K. Autumn, Y. A. Liang, S. Tonia Hsieh, W. Zesch, W. P. Chan, T. W. Kenny, R. Fearing, and R. J. Full, Nature **405**, 681 (2000).

[69] A. R. Parker and C. R. Lawrence, Nature **414**, 33 (2001).

[70] Y. Li, W. Cai, B. Cao, G. Duan, F. Sun, S. Li, and L. Jia, Nanotechnology **17**, 238 (2006).

[71] L. Zhai, F. Cebeci, R. Cohen, and M. Rubner, Nano Lett. **4**, 1349 (2004).

[72] H. E. Jeong, S. H. Lee, J. K. Kim, and K. Y. Suh, Langmuir **22**, 1640 (2006).

[73] E. Bormashenko, T. Stein, G. Whyman, Y. Bormashenko, and R. Pogreb, Langmuir **22**, 9982 (2006).

[74] H. Liu, L. Feng, J. Zhai, L. Jiang, and D. B. Zhu, Langmuir **20**, 5659 (2004).

[75] H. Gau, S. Herminghaus, P. Lenz, and R. Lipowsky, Science **283**, 46 (1999).

[76] M. Morita, T. Koga, H. Otsuka, and A. Takahara, Langmuir **21**, 911 (2005).

[77] S. Brandon, N. Haimovich, E. Yegar, and A. Marmur, J. Colloid Interface Sci. **263**, 237 (2003).

[78] M. Gleiche, L. F. Chi, and H. Fuchs, Nature **403**, 173 (2000).

[79] A. M. Higgins and R. A. L. Jones, Nature **404**, 476 (2000).

[80] L. Ionov, N. Houbenov, A. Sidorenko, M. Stamm, S. Minko, Adv. Funct. Mater. **16**, 1153 (2006).

[81] A. D. Sommers and A. M. Jacobi, J. Micromech. Microeng. **16**, 1571 (2006).

[82] L. Feng, S. Li, Y. Lim, H. Li, L. Zhong, J. Zhai, Y. Song, A. Liu, L. Jiang, and D. Zhu, Adv. Mater. **14**, 1857 (2002).

[83] Y. Chen, B. He, J. Lee, and N. A. Patankar, J. Colloid Interface Sci. **281**, 458 (2005).

[84] S. Y. Chou, P. R. Krauss, and P. J. Renstrom, Appl. Phys. Lett. **67**, 3114 (1995).

[85] P.-S. Hong, Ph. D. Thesis, Seoul National University, Seoul (2006).

[86] N. Kurata, Digest of Technical Papers of 1998 Society for Information Display International Symposium, 43 (1998).

[87] S. D. Jacobs, K. A. Cerqua, K. L. Marshall, A. Schmid, M. J. Guardalben, and K. J. Skerrett, J. Opt. Soc. Am. B **5**, 1962 (1988).

[88] D. W. Craig and J. Staromlynska, IEEE J. Quantum Electron **26**, 1440 (1990).

[89] G. R. Bird and M. Parrish Jr., J. Opt. Soc. Am. **50**, 886 (1960).

[90] D. Demus, J. W. Goodby, G. W. Gray, H.-W. Spiess, and V. Vill, *Handbook of Liquid Crystals* (Wiley, New York, 1997).

[91] P. G. de Gennes, *The Physics of Liquid Crystals* (Oxford Univ. Press, London, 1974).

[92] U. Finkenzeller, Kontakte **2**, 7 (1988).

[93] R. Eidenschink, D. Erdmann, J. Krause, and L. Pohl, Angew. Chem. **89**, 103 (1977).

[94] P. Chatelain, Bull. Soc. Fr. Mineral Cristalog. **77**, 353 (1954).

[95] J.-H. Lee, C.-J. Yu, and S.-D. Lee, Mol. Cryst. Liq. Cryst. **321**, 317 (1998).

[96] J. C. Kemp, Hinds International Inc. (1987).

[97] S. Chandrasekhar, Contemp. Phys. **29**, 527 (1988).

[98] E. H. Land, J. Opt. Soc. Am. **41**, 957 (1951).

[99] Data provided by GE Silicon (http:/gesilicon.com) Company.

[100] Y.-W. Lim, C.-H. Kwak, and S.-D. Lee, J. Nanosci. Nanotechnol. 8, 4775 (2008).

[101] Y.-W. Lim, C.-H. Kwak, W. Lee, and S.-D. Lee, Mol. Cryst. Liq. Cryst. was accepted (2008).

[102] Y.-W. Lim, C.-H. Kwak, W. Lee, and S.-D. Lee (unpublished).

[103] T. Akahane, H. Kaneko, M. Kimura, Jpn. J. Appl. Phys. **35**, 4434 (1996).

[104] C. J. Newsome, M. O'Neill, R. J. Farley, G. P. Bryan-Brown, Appl. Phys. Lett. **72**, 2078 (1998).

[105] Y. Xia and G. M. Whitesides, J. Mater. Chem. **7(7)**, 1069 (1997). (1995).

[106] Data provided by E. Merck Company. The material parameters are almost same as that of the RMS 03-001 material.

[107] Y.-W. Lim, D.-W. Kim, C.-H. Kwak, and S.-D. Lee (unpublished).

[108] Y. S. Kim, N. Y. Lee, J. R. Lim, M. J. Lee, and S. Park, Chem. Mater. **17**, 5867 (2005).

[109] N. Kawatsuki, R. Tsutsumi, A. Hiraiwa, H. Takatsuka, T. Sakai, J. Polymer Sci.: Part A: Polymer Chem. **46**, 4712 (2008).

[110] W. C. Yip, H. S. Kwok, V. M. Kozenkov, V. G. Chigrinov, Displays **22**, 27 (2001).

[111] L. Ignatov, P. Lazarev, and N. Ovchinnikova, SID Symp. Dig. **31**, 834 (2000).

[112] Y. Bobrov, C. Cobb, P. Lazarev, P. Box, D. Bryant, and H. Wonderly, SID Symp. Dig. **31**, 1102 (2000).

[113] I. G. Khan, S. V. Belyaev, N. V. Malimonenko, M. L. Kukushkina, E. Y. Shishkina, N. N. Masanova, and G. N. Vorozhtsov, Proc. of the 9th Int. Display Workshops (IDW'02), Society for Information Display, Santa Ana, CA, 541 (2002).

[114] D. Matsunaga, T. Tamaki, H. Akiyama, and K. Ichimura, Adv. Mater. **14**, 1477 (2002).

[115] W. C. Yip, H. S. Kwok, V. M. Kozenkov, and V. G. Chigrinov, Displays **22**, 27 (2001).

[116] B. M. I. van der Zande, S. J. Roosendaal, C. Doornkamp, J. Steenbakkers, and J. Lub, Adv. Funct. Mater. **16**, 791 (2006).

[117] P. van de Witte, J. Tuijtelaars, J. A. M. M. van Haaren, S. Stallinga, and J. Lub, Jpn. J. Appl. Phys. Part 1 **38**, 748 (1999).

[118] J. Lub, P. van de Witte, C. Doornkamp, J. P. A. Vogels, and R. T. Wegh, Adv. Mater. **15**, 1420 (2003).

[119] Data provided by Hayashibara Company (Japan).

[120] C. W. Tang and S. A. VanSlyke, Appl. Phys. Lett. **51**, 913 (1987).

[121] M. Jandke, P. Strohriegl, J. Gmeiner, W. Brutting, and M. Schworer, Adv. Mater. **11**, 1518 (1999).

[122] M. Misaki, Y. Ueda, S. Nagamatsu, M. Chikamatsu, Y. Yoshida, N. Tanigaki, and K. Yase, Appl. Phys. Lett. **87**, 243503 (2008).

[123] H. Yang, C.-K. Chao, M.-K. Wei, and C.-P. Lin, J. Micromech. Microeng. **14**, 1197 (2004).

[124] M. Schadt and W. Helfrich, Appl. Phys. Lett. **18**, 127 (1971).

[125] M. Oh-e and K. Kondo, Appl. Phys. Lett. **67**, 3895 (1995).

[126] K. Ohmuro, S. Kataoka, T. Sasaki, and Y. Koike, Digest of Technical Papers of 2003 Society for Information Display International Symposium (Society for Information Display, Boston, 1997), pp. 845.

[127] S. T. Wu and D. K. Yang, *Reflective Liquid Crystal Displays* (Wiley, New York, 2001).

[128] M. Kubo, S. Fujioka, T. Ochi, Y. Narutaki, T. Shinomiya, Y. Ishii, and F. Funada, in Proc. 6th Int. Display Workshop, 183 (1999).

[129] T. B. Jung, J. C. Kim, and S. H. Lee, Jpn. J. Appl. Phys. **42**, L464 (2003).

[130] K. Fujimori, Y. Narutaki, Y. Itoh, N. Kimura, S. Mizushima, Y. Ishii, and M. Hijikigawa, in SID Tech. Digest, 1382 (2002).

[131] S. H. Lee, K.-H. Park, J. S. Gwag, T.-H. Yoon, and J. C. Kim, Jpn. J. Appl. Phys. **42**, 5127 (2003).

[132] P. A. Kossyrev, J. Qi, N, V. Priezjev, R. A. Pelcovits, and G. P. Crawford, Appl. Phys. Lett. **81**, 2986 (2002).

[133] K.-J. Kim, J.-S. Lim, T.-Y. Jung, C. Nam, and B.-C. Ahn, Proc. 9th Int. Display Workshop, 433 (2002).

[134] S.-G. Kang, S.-H. Kim, S.-C. Song, W.0S. Park, and C. Yi, SID Tech. Digest, 31 (2004).

[135] C.-J. Yu, D.-W. Kim, and S.-D. Lee, Appl. Phys. Lett. **85**, 5146 (2004).

[136] K.-H. Park, J.-C. Kim, and T.-H. Yoon, Jpn. J. Appl. Phys. **43**, 7536 (2004).

[137] D. J. Broer, J. Lub, G. N. Mol, Macromolecules **34**, 1736 (1993).

[138] Y.-W. Lim, D.-W. Kim, C.-H. Kwak, and S.-D. Lee (unpublished).

[139] S.-W. Suh, S. T. Shin, and S.-D. Lee, Appl. Phys. Lett. **68**, 2819 (1996).

[140] Z. Ge, X. Zhu, S. T. Wu, J. Display. Technol **2**, 102 (2006).

[141] Y.-W. Lim and S.-D. Lee (unpublished).

[142] Y.-W. Lim, C.-H. Kwak, and S.-D. Lee, J. Nanosci. Nanotechnol. **8**, 4775 (2008).

[143] S. Bernhard, W. Georg, and P. Ludwig, "Liquid-crystal guest-host systems", US patent 4935160 (1990).

# 국문 초록

기능성 유기물에 대한 연구는 고성능 광학 소자 및 전자 소자의 개발과 함께 분자 공학의 눈부신 발전에 힘입어 다양한 연구 분야에서 주목받고 있다. 특히, 액정에 대한 연구는 평판 디스플레이 산업의 비약적인 성장과 광소자 응용에 대한 활발한 연구로 현대 산업사회의 중심 연구분야로 발돋움 했다. 특히, 다중 정렬된 액정 구조는 다중 배향에 대한 기초 연구 뿐만 아니라 다양한 소자로 응용할 수 있어 관심이 집중되고 있다. 최근 들어, 무기물보다 우수한 공정성과 가공성을 지닌 유연성을 가진 기능성 유기물 특히, 액정과 더불어 경화성 액정 폴리머를 이용하여 전기광학 소자를 개발하기 위한 연구가 활발하게 이루어지고 있다. 특히, 액정 및 경화성 액정 폴리머를 이용한 또한, 유비쿼터스와 디지털 멀티미디어 방송의 보급에 따라 휴대 가능한 디스플레이에 대한 요구가 증가함에 따라 전력 소비량이 낮고 고품질의 영상 정보를 구현할 수 있는 전유기 디스플레이에 대한 관심도 높아지고 있다. 전유기 디스플레이는 디스플레이

를 구성하는 모든 부품소자를 유기물로 대체한 새로운 개념의 디스플레이 구조이다.

본 논문에서는 경화성 액정 폴리머를 이용하여 셀 내에 박막의 고효율 광학 필름을 형성하였다. 높은 광효율, 광시야각 특성 그리고 복잡한 광학 구조를 형성할 필요성이 높아짐에 따라 광학 필름 제조시 다중 배향을 유도하여야 할 필요성이 높아지고 있다. 이러한 다중 배향 구조 형성은 기존의 액정 배향 기술인 접촉 방식 또는 비접촉 방식을 이용하는데, 대표적인 접촉 방식인 러빙은 여러 장점과 더불어 물리적인 결함이나 먼지 분자들의 발생으로 인하여 소자의 성능에 치명적인 결점을 유발할 수 있으며 더불어 다중 구조 유도시 다중 러빙의 해상도가 사용되어진 금속 마스크의 해상도에 좌우됨으로 미세 패턴을 형성할 수 없다는 단점이 있다. 이러한 단점을 보완한 광배향 기술은 수 마이크로 사이즈의 다중 구조를 형성 할 수 있다는 장점이 있는 반면 낮은 표면 에너지에 의하여 그 상부에 주입되는 액정의 배향력이 낮아 안정적인 액정 디스플레이 소자를 만드는 것이 불가능하다. 위에서 언급되어진 단점들을 보완하기 위하여, 본 논문에서는 임프린팅 기술을 도입하여 기능성 수동형 광학 소자의 기능을 하면서 더불어 상부에 주입되어진 액정 분자를 배향하고 전기광학적인 컨트롤에 의한 능동형 광학 소자 및 디스플레이를 제작할 수 있다.

첫번째로, 수평 또는 수직 배향되어지는 경화성 액정 폴리머를 이용하여 폴리머 몰드를 이용하여 임프린팅 프로세서를 통하여 기능성 위상지

연판 또는 시야각 향상 필름을 형성할 수 있다. 이때, 그 다중 구조 광학 필름의 표면에 형성되어진 마이크로 또는 나노 사이즈의 표면 구조에 의하여 이 광학 필름들이 액정 표시장치 셀 내에 형성되었을때, 주입된 액정을 배향하는 다중 기능을 수행한다. 이때, 임프린팅시 폴리머 몰드의 구조물에 의하여 경화성 액정 폴리머내의 액정 폴리머의 배향을 유도하고 유도되어진 상태로 자외선을 조사하여 경화시켜 광학 필름을 제작한다.

두번째로, 위의 동일한 방법으로 이색성 염료를 함유한 경화성 액정 폴리머를 임프린팅 기술을 이용하여 경화성 액정 폴리머의 액정 고분자의 배향을 유도하고 유도되어진 액정 고분자에 의하여 그 사이에 도핑된 이색성 염료를 배향하는 방법으로 셀 내 염료형 편광필름을 형성할 수 있다. 이 또한, 그 표면에 형성되어진 마이크로 또는 나노 사이즈의 표면 구조에 의하여 이 편광필름들이 액정 표시장치 셀 내에 형성되었을때, 주입된 액정을 배향하는 다중 기능을 수행한다. 이러한 마이크로 구조를 가지는 이색성 염료 편광자를 구조물로 가지는 유기 발광 소자를 제작하였을때, 그 마이크로 구조에 의하여 발광소자의 효율을 향상 시킬 수 있고 또한 편광자 기능을 하는 염료형 편광자에 의하여 편광된 광을 발광할 수 있어 박막의 백라이트 유닛을 제작하는데 장점을 가지고 있다.

다음으로, 두 가지의 방법으로 제조한 기능성 액정폴리머 광학 필름또는 편광필름을 도입하여 액정 표시장치를 구현하였다. 이러한 광학필름들은 그 고유 기능 뿐만아니라 다중 구조를 가지는 폴리머 몰드를 이용한

한번의 임프린팅 프로세서를 통하여 다중 구조의 광학 필름을 손쉽게 만들 수 있고, 이러한 다중 구조 광학 필름을 이용하여 서로 다른 광학축을 가지는 다중 구조 위상지연판 또는 다중 구조 편광판을 반투과형 액정 표시장치에 적용하여 반사형 및 투과형 모두에서 소자가 발휘할 수 있는 최대 효율을 얻을 수 있는 액정 표시장치를 제작할 수 있다. 더불어 임프린팅 기술을 이용하여 제작되어지는 70 나노 사이즈의 알루미튬 금속 막대를 주기적으로 가지는 와이어 그리드 편광자를 이용하여 편광 방향에 따른 선택적인 광학 투과 및 반사 필름을 이용하여 한 장의 와이어 그리드 편광자를 이용하여 반투과형 액정 표시장치에서 반사형에서는 반사판으로 투과형에서는 편광자로 이용되어지는 고효율의 단일 셀갭, 단일 모드의 반투과형 액정 표시장치를 구현 할 수 있다.

결론적으로, 본 논문에서는 임프린팅 기술을 도입하여 경화성 액정 폴리머를 배향 또는 다중 배향할 수 있다는 장점이 있다. 이러한 장점은 경화성 액정 폴리머에 이색성 염료를 포함한 경우 동일한 방법으로 박막다중 구조에 의하여 그 상단에 주입되어지는 액정 분자를 정렬할 수 있는 장점이 있다. 이러한 광학 필름들을 유기발광소자, 반투과형 액정 표시장치, 3D 표시장치에 적용하여 그 전기광학적 성능을 향상시키고 플렉서블 표시장치의 가능성을 열었으며 향후 전유기 디스플레이를 포함한 휴대형 액정 표시장치에 적합한 응용 소자 제작에 초석을 제공할 수 있을 것으로 기대된다.

주요어: 액정, 액정 배향, 액정 디스플레이, 임프린팅, 경화성 액정 폴리머, 이색성 염료, 기능성 광학 소자, 염료형 편광자, 반투과형 액정 표시장치.

주요어:

학 번: 2002-23542

# Publication

**[1] International Papers**

1. **Y.-W. Lim**, C.-H. Kwak, W. Lee, S.-D. Lee, "Thermally Stable Binary Optical Films Based on Photocrosslinkable Liquid Crystalline Polymers Containing Azodyes", Mol. Cryst. Liq. Cryst. **489**, 183 (2008).

2. D.-W. Kim, E. Jang, **Y.-W. Lim**, S.-D. Lee, "[Invited Paper] Defect-free deformed helix ferroelectric liquid crystal mode in a vertically aligned configuration", J. SID **16/9**, 947 (2008).

3. **Y.-W. Lim**, C.-H. Kwak, S.-D. Lee, "Anisotropic nano-imprinting technique for fabricating a patterned optical film of a liquid crystalline polymer", J. Nanosci. Nanotechnol. **8**, 4775 (2008).

4. **Y.-W. Lim**, D.-W. Kim, S.-D. Lee, "Polymeric optical films as patterned retarders and alignment layers for transflective liquid crystal

displays", Mol. Cryst. Liq. Cryst. **489**, 183 (2008).

5. **Y.-W. Lim**, J. Kim, S.-D. Lee, "A transflective LCD having a patterned retardation layer for a single driving scheme", Mol. Cryst. Liq. Cryst. **458**, 45 (2006).

6. J. Kim, **Y.-W. Lim**, S.-D. Lee, "Brightness-enhanced transflective liquid crystal display having a single cell gap in a vertically aligned configuration", Jpn. J. Appl. Phys. **45**, 810 (2006).

7. D.-W. Kim, C.-J. Yu, **Y.-W. Lim**, J.-H. Na, S.-D. Lee, "Mechanical stability of a flexible ferroelectric liquid crystal displays with a periodic array of columnar spacers", Appl Phys. Lett. **87**, 051917 (2005).

**[2] Domestic Paper**

1. W. Lee, W. Choi, **Y.-W. Lim**, Y.-J. Na, S.-D. Lee, "A Highly Efficient Organic Light-Emitting Diode with an Imprinted In-Cell Polarizer", J. Inf. Disp., 2008 was accepted.

**[3] International Proceedings**

1. W. Lee, **Y.-W. Lim**, S.-D. Lee, "Out-coupling efficiency enhanced organic light-emitting diodes on the flexible substrate", 15th Int'l Display Workshops (IDW'08, Niigata, Japan, 2008).

2. **Y.-W. Lim**, W. Lee, S.-D. Lee, "Out-coupling efficiency enhanced organic light-emitting diodes on the flexible substrate", 7th Int'l Conference on Nanoimprint and Nanoprint Technology (NNT'08, Kyoto, Japan, 2008).

3. **Y.-W. Lim**, D.-W. Kim, W. Lee, S.-D. Lee, "Transflective liquid crystal display with an in-cell retarder in a self-aligned twisted nematic configuration", 22th Int'l Liq. Cryst. Conference 2008 (ILCC 2008, Jeju, Korea, 2008).

4. **Y.-W. Lim**, C.-H. Kwak, W. Lee, S.-D. Lee, "Binary optical films based on photocrosslinkable polymer liquid crystals doped with azobenzenes", 22th Int'l Liq. Cryst. Conference 2008 (ILCC 2008, Jeju, Korea, 2008).

5. **Y.-W. Lim**, W. Lee, S.-D. Lee, "Technologies to fabricated patterned retarders for a high performance transflective liquid crystal displays", Proc. 12th Int'l Symposium on Advanced Display Materials and Devices (ADMD 2008, Daegu, Korea, 2008).

6. **Y.-W. Lim**, W. Lee, S.-D. Lee, "Optical characteristic and aligning capability of imprinted nanoscale thin films", Proc. 19th Int'l Conference on Molecular Electronics and Devices (IC ME&D, Kyungki,

Korea, 2008).

7. D.-W. Kim, E. Jang, **Y.-W. Lim**, S.-D. Lee, "Fast-response transflective display using a tight-pitch ferroelectric liquid crystal in a single-gap configuration", Tech. Digest 38th Soc. Inform. Display (SID, Los Angeles, USA, 2008).

8. S.-D. Lee, **Y.-W. Lim**, D.-W. Kim, C.-H. Kwak, "[Plenary Talk] An imprinting liquid crystalline polymer film as an in-cell patterned retarder and an alignment layer for transflective liquid crystal displays", Proc. 12th Int'l Topical Meeting on Optics of Liquid Crystals (OLC, Puebla, Mexico, 2007).

9. **Y.-W. Lim**, D.-W. Kim, C.-H. Kwak, S.-D. Lee, "[Invited Talk] High-performance transflective liquid crystal display with a wire grid polarizer", Proc. 11th Int'l Symposium on Advanced Display Materials and Devices (ADMD 2007, Daegu, Korea, 2007), p. 33.

10. **Y.-W. Lim**, D.-W. Kim, C.-H. Kwak, S.-D. Lee, "Novel imprinting for fabricating a patterned optical film of a liquid crystalline polymer", Proc. 18th Int'l Conference on Molecular Electronics and Devices (IC ME&D, Daejeon, Korea, 2007), p. 188.

11. D.-W. Kim, C.-J. Yu, **Y.-W. Lim**, J.-H. Na, S.-D. Lee, "Bending tolerance enhancement of a ferroelectric liquid crystal display using columnar spacers in a vertically aligned configuration", Proc. on ICA 2006(ICA 2006, Jeju, Korea, 2006).

12. S.-D. Lee, **Y.-W. Lim**, J. Kim, D.-W. Kim, "[Invited Talk] Novel transflective liquid crystal display having a single cell gap and a single LC mode combined with an inner-patterned retarder", Proc. 6th Int'l Meeting on Information Display and Int'l Display Manufacturing Conference (IMID IDMC, Daegu, Korea, 2006).

13. **Y.-W. Lim**, J. Kim, D.-W. Kim, S.-D. Lee, "Inner-patterned retarder for a single driving transflective liquid crystal display", 21th Int'l Liq. Cryst. Conference 2006 (ILCC 2006, Colorado, USA, 2006), p. 710.

14. **Y.-W. Lim**, J. Kim, S.-D. Lee, "Single driving transflective liquid crystal display in a single configuration with an inner-patterned retarder", Tech. Digest 37th Soc. Inform. Display (SID, San Francisco, USA, 2006), p. 806.

15. J. Kim, D.-W. Kim, **Y.-W. Lim**, S.-D. Lee, "Brightness improvement of transflective LCD in a unified configuration", Tech. Digest 37th Soc. Inform. Display (SID, San Francisco, USA, 2006), p. 817.

16. **Y.-W. Lim**, J. Kim, S.-D. Lee, "A simple patterning of retardation layer for a single mode transflective liquid crystal display", Korea-Japan Joint Forum 2005 (KJF 2005, Daejeon, Korea, 2005), p. 147.

17. **Y.-W. Lim**, J. Kim, S.-D. Lee, "A transflective LCD having a patterned retardation layer for a single driving scheme", Proc. 10th Int'l Symposium on Advanced Display Materials and Devices (ADMD 2005, Daegu, Korea, 2005).

18. D.-W. Kim, **Y.-W. Lim**, J.-H. Na, C.-J. Yu, S.-D. Lee, "Flexible LCDs with columnar spacers for fast response and wideviewing", Proc. 5th Int'l Meeting Inform. Display (IMID, Seoul, Korea, 2005), p. 407.

19. **Y.-W. Lim**, J. Kim, S.-D. Lee, "A transflective liquid crystal display having a patterned retardation layer", Tech. Digest 36th Soc. Inform. Display (SID, Boston, USA, 2005), p. 1880.

20. D.-W. Kim, **Y.-W. Lim**, J.-H. Na, C.-J. Yu, S.-D. Lee, "Fast flexible display applications of deformed helix ferroelectric liquid crystals", Tech. Digest 36th Soc. Inform. Display (SID, Boston, USA, 2005), p. 678.

**[4] Domestic Proceedings**

1. S.-D. Lee, **Y.-W. Lim**, "[Invited Talk] Anisotropic Optical Films Based On Liquid Crystalline Polymers for Device Applications" (일산 KINTEX, 2007).

2. **Y.-W. Lim**, Chang-Hwan Kwak, S.-D. Lee, "Novel In-cell Retardation Layer for a Spontaneous Aligned Liquid Crystal Displays", 한국물리학회 2007 봄 학술논문발표회, (아주대학교, 2007), JP-022.

3. **Y.-W. Lim**, Dong-Woo Kim, S.-D. Lee, "Photo-control of the Azimuthal Easy Axis for a Patterned Liquid Crystalline Order", 한국물리학회 2006 가을 학술논문발표회, (대구, 2006), IP2-06.

4. **Y.-W. Lim**, D.-W. Kim, S.-D. Lee, "Novel Transflective LCD with an Inner-Patterned Retarder", The 9th Korea Liquid Crystal Conference (9th KLCC, 충남대학교, 2006), p. 133.

5. **Y.-W. Lim**, J. Kim, D.-W. Kim, S.-D. Lee, "Brightness-Enhancement of Transflective LCD having a Unified Configuration", The 9th Korea Liquid Crystal Conference (9th KLCC, 충남대학교, 2006), p. 98.

6. **Y.-W. Lim**, D.-W. Kim, S.-D. Lee, "A Single Mode Transflective Liquid Crystal Display Having an Inner-Patterned Retarder", The

17th Optical Society of Korea Annual Meeting 2006 (17th OSK, 아주대학교, 2006), p. 197.

7. J.-H. Na, D.-W. Kim, **Y.-W. Lim**, C.-J. Yu, S.-D. Lee, "Fast Response Display using Deformed Helix Ferroelectric Liquid Crystal on Plastic Substrate", The 8th Korea Liquid Crystal Conference (8th KLCC, 호서대학교, 2005), p. 131.

8. **Y.-W. Lim**, J. Kim, S.-D. Lee, "A Single Step Patterning of the Retardation Layer for a Transflective LCD with a Single LC Mode", The 8th Korea Liquid Crystal Conference (8th KLCC, 호서대학교, 2005), p. 80.

9. Y. Choi, **Y.-W. Lim**, J.-H. Kim, S.-D. Lee, "Fabrication of Micro-Lens Array with Fast Switching Characteristics using Ferroelectric Liquid Crystals", The 7th Korea Liquid Crystal Conference (7th KLCC, 전북대학교, 2004), p. 133.

**[5] Patents**

1. S.-D. Lee, J. Kim, **Y.-W. Lim**, "Display panel and method for manufacturing the same and display apparatus having the same", KR, US, JP, CN, 2005.

2. S.-D. Lee, **Y.-W. Lim**, "Transflective type liquid crystal display device", KR, 2007.

3. S.-D. Lee, **Y.-W. Lim**, "Optical retarder film and method of manufacturing for the same and display device using the same", KR, 2007.

4. S.-D. Lee, **Y.-W. Lim**, "In-cell thin film dye-polarizer and applications", KR, 2008.